

UNIVERSITÀ
DEGLI STUDI
DI PADOVA

Sede Amministrativa: Università degli Studi di Padova
Dipartimento di Ingegneria Civile, Edile ed Ambientale

SCUOLA DI DOTTORATO: SCIENZE DELL'INGEGNERIA CIVILE E AMBIENTALE
CICLO XXV

ON FLOATING BREAKWATERS EFFICIENCY

A 2DV PARAMETRIC BASED ANALYSIS

Direttore della Scuola: Ch.mo Prof. Stefano Lanzoni

Supervisore: Ch.mo Prof. Piero Ruol

Correlatore: Ch.mo Prof. Peter Frigaard

Controrelatore: Ch.mo Prof. Søren R. K. Nielsen

Dottorando: Paolo Pezzutto

ABSTRACT

In long term evolution numerical models, the interactions of a floating barrier with the wave field is then deputed to some parametrized transfer functions, which mimic wave energy transmission and dissipation in the frequency domain. This thesis provide, as final result, two transfer functions (one for incident waves, one for reflected ones) for a particular class of compact shaped floating breakwaters.

These functions are based on three main parameters, which have been derived on physical model results. The first one (χ) is the ratio between the incoming wave frequency and an approximation of FB heave natural frequency, based on principal FB cross section dimensions. Wave steepness has been considered to be the second variable which helps in describing the amount of dissipated energy. A FB draft to water depth ratio has been identified.

Available algorithms for the decomposition into incident and reflected waves of flume records are mostly Stokes-FFT based. Therefore they suffer some limitations for relatively high wave steepness (Ch. 4). Since the latter is considered as a crucial parameter, a lot of effort has been drawn in solving some conundrums of actual methods.

Two algorithms are proposed. The first one (Ch. 5), based on empirical mode decomposition, did not give satisfactory results. The second one (Ch. 6) is based on linear waves superposition, but, getting rid of linear dispersion relation, detects automatically each phase celerity. The proposed algorithm appears to be effective for relatively shallow water waves, for which the phase modulation approach is more consistent than Stokes formulations. A Stokes 2nd order algorithm has also been implemented.

In Ch. 7 the experimental set up is presented. A second order analysis of trans-

mission and reflection processes is also introduced.

Results are given (and discussed) in Ch. 8. Linear transmission and reflection transfer functions are derived, based on experimental data fitting. These are finally validated with irregular wave test measurements.

It is found that the transmission process mainly depends on frequency (χ) and on FB relative draft. The last parameter does not enter the reflection process, which basically described by χ and wave steepness. In particular, steeper waves loose more energy, and are less reflected. For transmitted waves only, a significant amount of energy transfer from primary to secondary harmonics is observed.

SOMMARIO

Nei modelli numerici per applicazioni costiere, l'implementazione delle opere di difesa galleggianti é generalmente costruita a partire da semplici funzioni di trasferimento. Queste distorcono, nello spazio delle frequenze, il campo d'onda incidente in onde trasmesse a tergo dell'opera. Questa tesi propone due funzioni di trasferimento per una particolare classe di frangiflutti galleggianti (di seguito FB): una per il campo trasmesso, l'altra per quello incidente. Tali espressioni sono funzione di tre parametri principali, ricavati sulla base di risultati sperimentali. Il primo di questi (χ) é costituito dal rapporto tra la frequenza dell'onda incidente e un'approssimazione della frequenza naturale di oscillazione verticale del FB. Un secondo parametro é caratterizzato dalla ripiditá dell'onda incidente, mentre l'ultimo é una variabile adimensionale che caratterizza il pescaggio del FB in relazione alla profonditá d'acqua locale.

Gli algoritmi presenti in letteratura, finalizzati alla decomposizione di misure d'onda in incidenti e riflesse, sono generalmente basati su formulazioni tipo Stokes-FFT. Pertanto, in presenza di ripiditá particolarmente elevate, possono interpretare poco correttamente i dati misurati. Poiché la ripiditá (dell'onda) é considerata un parametro fondamentale per la descrizione dei processi dissipativi, si propongono due algoritmi alternativi per la soluzione di tali criticitá. Il primo di questi si basa su un punto di vista AM-FM, decomponendo le misure attraverso l'empirical mode decomposition (Cap. 5). Il secondo rimane su un'ipotesi di sovrapposizione lineare di onde elementari, ma prescinde dall'equazione di dispersione (Cap. 6). Ciò permette un'interpretazione piú affinata delle celeritá di fase. Con particolari vantaggi in acque basse, laddove l'approccio di modulazione di fase é piú appropriato di un'espansione tipo Stokes.

L'apparato sperimentale é descritto nel Cap. 7, nel quale é proposta anche una procedura di analisi dei risultati affinata al secondo ordine.

Dai risultati (Cap.8) si desume che, dal punto di vista lineare, il processo di trasmissione dipende principalmente dalla frequenza dell'onda incidente e dal pescaggio del FB (relativo al fondale). Per quanto concerne le onde riflesse, queste sono meglio descritte dalla ripiditá dell'onda, nonché dalla frequenza. In particolare, le onde piú ripide sono soggette a maggiori dissipazioni e conseguentemente sono riflesse in misura inferiore. Solamente in riferimento al processo di trasmissione, si notano sensibili trasferimenti di energia dalle componenti principali, a favore delle seconde armoniche.

CONTENTS

1. INTRODUCTION	1
1.1 CONCEPT	2
1.2 PROTOTYPE INSTALLATIONS	8
1.2.1 Commercial FBs	8
1.2.2 MegaFloats	9
1.3 WAVE ENERGY DISSIPATION	10
1.3.1 Dissipative Agents	12
1.4 CONTRIBUTIONS OF PRESENT THESIS	15
1.5 THESIS ORGANIZATION	15
2. EFFICIENCY OF FLOATING BREAKWATERS	17
2.1 LITERATURE REVIEW	17
2.2 OTHER POSSIBLE EFFICIENCY DEFINITIONS	22
2.3 NEEDS FOR A UNIFIED DESCRIPTION	24
3. PARAMETERS IDENTIFICATION	27
3.1 TIME SCALE	27
3.1.1 FB natural frequencies	27
3.1.2 Geometric approximation	29
3.1.3 A Predictive Formula for <i>II-type</i> FBs	32

3.2 WAVE STEEPNESS 34

3.2.1 An experiment (Pezzutto et al., 2012) 35

3.3 RELATIVE WATER DEPTH 38

4. REFLECTION ANALYSIS METHODS 39

4.1 FREQUENCY DOMAIN 39

4.1.1 Deterministic Methods 39

4.1.2 LS Methods 42

4.1.3 Weakly non-linear methods 47

4.2 TIME DOMAIN 51

4.2.1 Deterministic Methods 51

4.2.2 Weakly non-linear methods 56

4.3 ERROR SOURCES AND LIMITATIONS 58

4.3.1 Wave models in reflection analysis 58

4.3.2 Is an approximated hydrodynamic model really needed? 59

4.3.3 Airy monochromatic waves 62

4.3.4 Instrument Noise 66

4.3.5 Weakly non-linear waves (Stokes) 68

4.3.6 Non stationary waves 68

4.3.7 Transient waves 70

4.3.8 Other error sources 72

5. MODULATED WAVES 73

5.1 AM-FM DECOMPOSITION 73

5.1.1 Hilbert Transform 74

5.1.2 Two Important Theorems 74

5.1.3 Finite HT 76

5.1.4 Discrete HT - Implementation 77

5.1.5	HT and Water Waves	78
5.2	EMPIRICAL MODE DECOMPOSITION	79
5.2.1	EMD-likes and Water Waves	81
5.3	REFLECTION OF AN AM-FM WAVE	82
5.4	MODE MIXING ELIMINATION IN EMD (ω EMD)	84
5.4.1	Problem definition	85
5.4.2	Possible choices for ω_0	87
5.4.3	Pattern-search of ω_0	89
5.4.4	Other fundamental choices	90
5.4.5	Performance on numerical wave data	93
5.5	REFLECTION ANALYSIS OF ω EMD DECOMPOSED WAVES	94
6.	ON ANOTHER TIME DOMAIN APPROACH	95
6.1	WAVE MODEL	95
6.2	DKR TIPS AND TRICKS	96
6.2.1	Correct angles reproduction	97
6.2.2	Waves reconstruction	98
6.3	LOCAL TREATMENT	100
6.3.1	Algorithm	100
6.3.2	Gauge Spacing	100
6.3.3	Window Length	101
6.3.4	Implementation Tips	102
6.4	GLOBAL TREATMENT	105
6.4.1	Algorithm	105
6.4.2	Window Shape	106
6.4.3	Window Overlap	107

6.5	PERFORMANCE	108
6.5.1	FDKR	108
6.5.2	WFDKR - Flume data examples	112
6.6	CONCLUDING REMARKS	114
7.	EXPERIMENTAL SET-UP	123
7.1	FACILITIES	123
7.1.1	Wave Generation	123
7.1.2	Wave Measurements	124
7.2	MODELS	124
7.3	TEST CASES	125
7.4	ANALYSIS METHODOLOGIES	126
7.4.1	Pre-Analysis	126
7.4.2	Coefficients Expansion	127
7.4.3	Coefficients definition	130
8.	RESULTS AND DISCUSSION	133
8.1	VERIFICATION OF TARGET INCIDENT WAVES	133
8.1.1	Wave Periods	133
8.1.2	Root Mean Square Heights	133
8.1.3	Heights Distribution	134
8.1.4	Discarded Data	136
8.2	WAVE TRANSMISSION	137
8.2.1	Linear Coefficients	137
8.2.2	Second Order Coefficients	142
8.3	WAVE REFLECTION	145
8.3.1	Linear Coefficients	145
8.3.2	Second Order Coefficients	148

8.4 WAVE ENERGY DISSIPATION 149

8.4.1 Primary Wave Energy Losses 149

8.4.2 Net Energy Losses 151

8.5 SPECTRA RECONSTRUCTION 153

9. CONCLUSIONS 159

A. UNCERTAINTIES EVALUATION 161

A.1 MONTE CARLO UNCERTAINTIES EVALUATION 161

A.1.1 Pseudo-regular waves in a flume 161

A.1.2 Combined approach 163

REFERENCES 167

1 INTRODUCTION

Floating breakwaters (FB) present an alternative solution to conventional fixed breakwaters and can be effective in coastal areas with mild wave environment conditions (e.g. in bays, lakes or estuaries). The fact that FBs are only slightly conditioned by water depth and sea bed characteristics are other peculiarities of these structures. Therefore, they have been increasingly used to protect marinas or small craft harbours and, less frequently, the shoreline, aiming at erosion control.

The search for innovative approaches aiming at flood risk mitigation in coastal areas, and particularly deltas and estuaries of large rivers, has drawn attention to the potentialities of floating breakwaters, a versatile structure that shelters the coast and can perfectly cope with tide. On the other hand, high reflection can aggravate the waves in adjacent areas, posing possible problems there.

It should be stressed that this application of FBs is inherently different from the traditional one which aims at sheltering marinas. For example, in coastal areas there is a considerable benefit if a $2m$ high wave is reduced by say a 20%, since this may prevent flooding to occur, whereas such high waves cannot be tolerated in marinas.

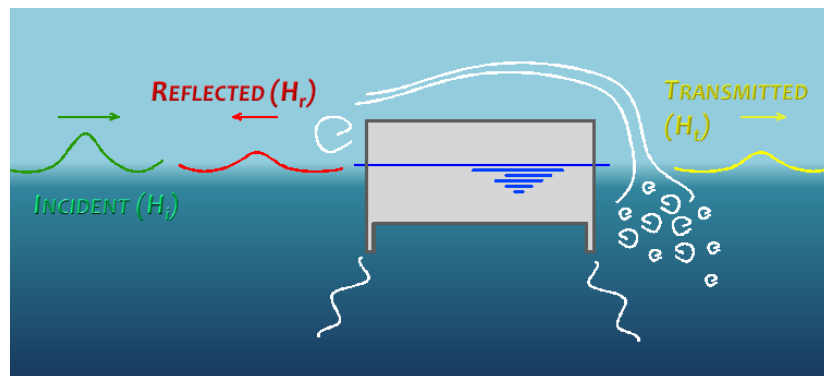


Fig. 1.1 – Concept sketch of a floating breakwater principle.

1.1 CONCEPT

The device partly reflects and partly dissipates the incident wave energy, so that the transmitted waves are reduced (Fig. 1.1). Energy is transmitted either directly, below or above the structure, or indirectly, as a consequence of the device movements. The latter mechanism is referred as wave radiation.

Direct energy transmission is affected by the main characteristics of the wave field: short or long-crested, and by the overtopping process. Energy transmission related to the device movements can be interpreted only by a strongly non-linear point of view of the interactions between the incident wave and the structure dynamics. In this picture a dominant role is played by the mooring forces and the reactions due to connections between modules.

The search for innovative approaches aiming at flood risk mitigation in coastal areas, and particularly deltas and estuaries of large rivers, has drawn attention to the potentialities of floating breakwaters (FBs), a versatile structure that shelters the coast and can perfectly cope with tide.

On the one hand, by reducing the wave that runs up the river or coastal dike, FBs can contribute significantly to mitigate the flooding hazard. On the other hand, high reflection can aggravate the waves in adjacent areas, posing possible problems there.

It should be stressed that this application of FBs is inherently different from the traditional one which aims at sheltering marinas. For example, in coastal areas there is a considerable benefit if the 1 or 2m incident wave is reduced by 20%, since this may prevent flooding to occur, whereas such high waves cannot be tolerated in marinas. The traditional FB function may be found for instance in Tsinker (1994) or Headland (1995).

PURPOSES AND APPLICATION If mega-float devices are excluded, FBs are only effective for marine protection with limited fetches, *i.e.* for relative small wave lengths. The possible application of FB as a mitigation measure against coastal flooding and erosion extends the possible use of these devices to cases with areas with longer fetches possibly subjected to severe wave conditions. Possible applications of FB for coastal protection are those that enhance the advantages of this kind of structures (see introduction), as for ex-

ample: 1) *lakes*, especially in presence of deep waters; 2) *lagoons*, especially if the mechanical characteristics of the bed are poor; 3) *river deltas*, especially if the position of the banks is evolving due to a dynamic sediment transport scenario.

WAVE TRANSMISSION AND REFLECTION COEFFICIENTS Commonly speaking the performance of a breakwater is described by its effects on the local wave field. The lower the height of the transmitted wave, the better the performance. In some cases, its reflection capacity has to be considered too, in order to define the agitation of the wave field on the structure wind side, *e.g.* for navigation purposes.

In common literature reflection and transmission coefficients are defined as reflected (or transmitted) wave height to incident wave height ratios. If these quantities are deduced on a timeseries statistical basis (*e.g.* zero down cross analysis) then the following definitions hold:¹

$$\rho_{rms} = \frac{H_{Rrms}}{H_{Irms}} \quad \tau_{rms} = \frac{H_{Trms}}{H_{Irms}} \quad (1.1)$$

One can define similar coefficients based on other statistical quantities such as $H_{1/3}$, $H_{1/10}$ and so on. By a spectral point of view, direct transformation of timeseries into frequency space leads to measures of energy spectral densities (S). The square root of *zeroth* moment of these distributions define, on linear wave theory basis, a wave height denoted as H_{m0} (which is proportional to $H_{1/3}$, in most narrow banded cases). Therefore:

$$\rho_{m0} = \frac{H_{Rm0}}{H_{Im0}} \quad \tau_{m0} = \frac{H_{Tm0}}{H_{Im0}} \quad (1.2)$$


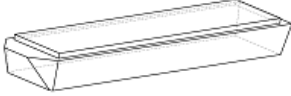

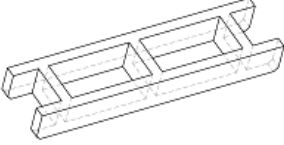
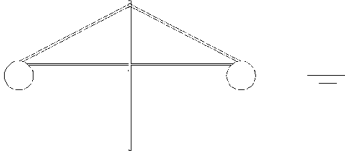
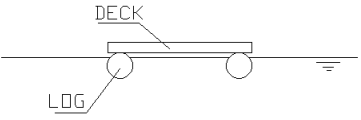
where

$$H_{jm0} = 4 \left(\int S_j(f) df \right)^{1/2} \quad (1.3)$$

¹ In the present work reflection and transmission coefficients are denoted by Greek letters to let frequent literature Latin letters (k, c) free for wavenumbers and celerities.

COMMON SHAPES AND MOORING SYSTEMS
 FB are commonly divided into four general categories: box, pontoon, mat and tethered float. Some floating breakwater of each category are shown below (Tabb.1.1 and 1.2).


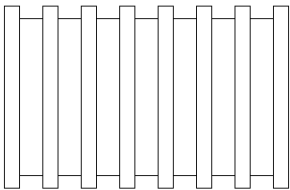
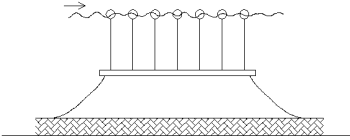
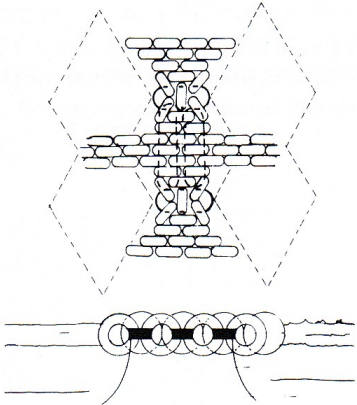
Tab. 1.1 – Various types of breakwaters (adapted from McCartney (1985))^a.

BOX		Sometimes named: Pontoon Solid rectangle shape Reinforced concrete units are the most common type. They may be empty (air filled) or filled with light weight material.
BARGE		Formed by array of dis-used vessels. Frequently employed by army.
PONTOON		Sometimes named Catamaran or Twin pontoon Catamaran shape.
ALASKA		Open compartment
A FRAME		
TWIN LOG		Deck is open wood frame

^a Continues to Tab.1.2

The "box" and "pontoon" categories have much larger model and prototype experience; and thus are the most frequently used. The typical size of box or

Tab. 1.2 – Continues from Tab.1.1: various types of breakwaters (adapted from McCartney (1985)).

TIRE MAT		Scrap tires strung on pole framework or bound together with chain or belting. Foam flotation is usually need.
LOG MAT		Log raft chained or cabled together.
TETHERED w/Spheres		Float placed in rows and connected to a horizontal support.
TETHERED w/Tires		Arrangement similar to spheres. Steel drums with ballasts can be used instead of tires

pontoon types FB are described in below 1.2. The *Mat* and *Tethered* types are much wider, of order $10 \approx 20 m$, but draft is quite smaller (less than a meter). Reinforced concrete modules are either empty inside or, more often, filled with a light material. In the former case the risk of sinking of the structure is not negligible. Connections are either flexible, allowing preferably only the roll along the breakwater axis, or pre- or post-tensioned, to make them act as a single unit. In the latter case the efficiency is higher, but the risk of damage is also larger. Interconnection between adjacent modules and mooring system are primary points of concern for this kind of structures.

Large breakwaters are sometimes built with used barges, ballasted to the de-

sired draft with sand or rock. Pontoon type are more effective when the overall width is larger than half the incident wavelength. In this case the expected attenuation is very good.

Within the mat category, the most used are made with tires. They are subjected to lower anchor loads, reflect less and dissipate relatively more than previous ones. Although less effective, they have a low cost, can be removed more easily and constructed with unskilled labour and minimal equipment, but the environmental impact is of course important.

Mat and Tethered float are seldom used due to a large environmental impact and small efficiency. The attenuation effect is based on dissipation of energy as the wave travel across the width of the device.

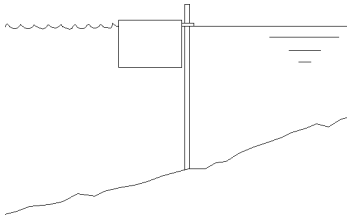
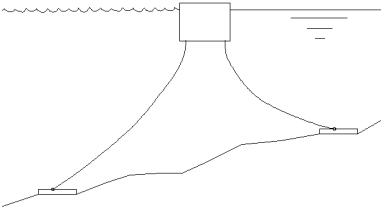
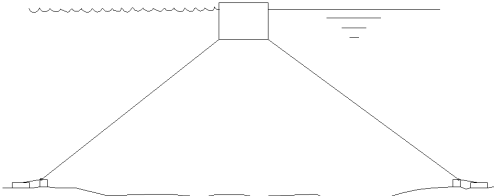
FBs efficiency is partly affected by the mooring systems. In general, FBs can be moored with cables (possibly elastic devices), with compliant chains, with short chains, tethered or constrained to piles. The main characteristics to be taken into account when deciding the mooring type, and evaluating systems functionality are enumerated below (Tab. 1.3).

QUALITATIVE COMPARISON WITH OTHER DEFENCE STRATEGIES When speaking of conventional types of breakwater we usually think at these gravity structures which foundation occupies at least the total area of the top elevated structure. To this set belong mound breakwaters, caissons, block walls, and their combinations. Submerged barriers are to be included when dealing with coastal protection issues. All this kind of devices are designed on the basis of an extended and firm literature. On the contrary, FBs related knowledge appears to be still spread, mostly among building companies technical reports. Hence very few studies concern a unified point of view in engineering terms.

A synthetic comparison with conventional breakwaters is therefore hard to be defined in an strictly economical frame. Some of the conditions that are in favour of the FB installations are due to their flexibility and low cost for return to the original environment.

Anyhow, total water depth structures does permit total reflection and dissipation of the incident sea. Hence their performance in classical terms (transmission coefficient) is anyway higher than an FB one.

Tab. 1.3 – Various types of FBs mooring systems.

Class	2DV example	Design Variables
PILES		number of piles per element; diameter of piles; height of pile/ water depth; material; connection characteristics.
CHAINS		number of chains; length of chains; position of fairleads [x,y,z]; position of anchors [x,y,z]; chains weight per unit length; connection characteristics; anchor type.
CABLES or TENSION LEGS		number of lines; length of lines; line material resistance; position of fairleads [x,y,z]; position of anchors [x,y,z]; joint characteristics; anchor type.

In order to quantify a reliable comparison on cost/effectiveness basis the following items must be taken into account at a pre-design state. 1) *Poor foundation*: FB may be the only solution where poor foundations will not support bottom connected breakwater. 2) *Deep water*: in water depths in excess of 6 m, bottom connected breakwater are often more expensive than FB. 3) *Water quality*: FB present a minimum interference with water circulation and fish migration. 4) *Ice problems*: FB can be removed and towed to protected areas if ice formation is a problem. They may be suitable for areas where summer anchorage or moorage is required. 5) *High tidal excursions*: The body performance do not change with water level changes (anyhow the mooring system stiffness variation must be considered) while in case of high tide, high over-topping

occurs at conventional breakwaters head, and in case of low tide a conventional structure may have a very high visual impact. 6) *Mean Water Level*: Long term variations of MWL can be faced with little adjustment on mooring system (chain lengths) while conventional breakwaters have to be adapted with high cost solutions. 7) *Visual impact*: FB have a low profile and present a minimum intrusion on the horizon, resulting suited to limit visual impact. 8) *Summer and under development marinas*: FB can usually be rearranged into new layout with minimum effort, to accommodate to future developments.

CRITICAL ISSUES With respect to actual and possible applications and on cost-effectiveness ratio the points to be taken into account can be enumerated as follows. 1) *Performance*: find solutions to enhance performance outside of nowadays working conditions (longer waves). 2) *Design*: unification of laboratory testing data and predictive formulas for designers. 3) *Structural*: correct evaluation/interpretation of wave loads under common and dramatic wave conditions. 4) *Mooring Materials*: a) protection of anchoring part from sand scraping, b) different FB behaviour between chains and elastic rigs.

1.2 PROTOTYPE INSTALLATIONS

Experience is only available with respect to the traditional use of FB, mainly after the second world war, as a consequence of their (partially) successful application in Normandy. The break water called "Bombardon" was used by the Allies in June 1944. It was a steel hollow cruciform "tube", 7.6 m high and wide, 61 m long. They were placed in two lines with a mutual distance of 244 m, in order to reduce the wave motion down to the wanted sea state (Fig. 1.2). The experimental and theoretical studies that were carried on are still forming the basis for FB development.

1.2.1 COMMERCIAL FBs

Huge number of installations and building companies can be reported. For the sake of simplicity we hereby cite some commercial dimensions. For example (Fig. 1.3), there are modules which are 15 ~ 20 m long, 2.5 ~ 5 m wide and

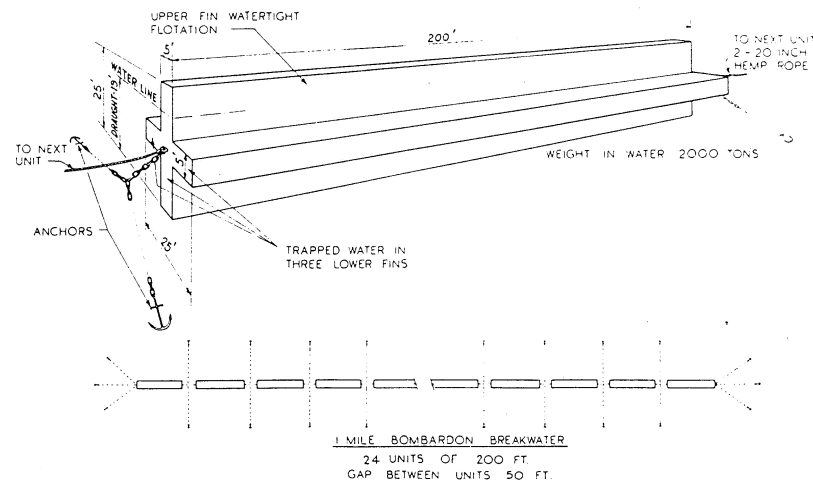


Fig. 1.2 – The "Bombardon" breakwater

1 ~ 2 *m* high. Their displacements are the order of 15 to 60 tons. These are useful for protecting areas presenting sea states characterized by wave lengths up to 20 *m*, or periods up to 3.5 *s* and maximum wave heights of 1.5 *m*.

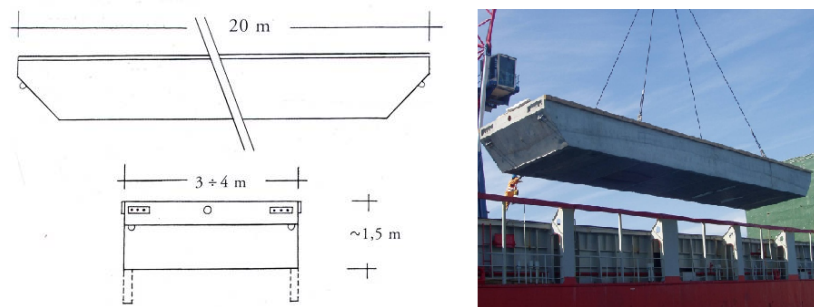


Fig. 1.3 – Example of commonly used floating modules

1.2.2 MEGAFLOATS

A wave attenuator design usually goes through a site specific process. In some cases megafloats have been installed in fairly open harbour areas. We report here some examples.

MONTECARLO, This FB, built up in Algeciras, E, and placed in Montecarlo
 CONDAMINE (Fig. 1.4), has been designed for a lifecycle of 100 years. It
 HARBOUR is 352 *m* long, 28 *m* wide at top and 44 *m* wide at bottom.
 Its freeboard measures 3 *m* on the leeside and 6.6 *m* on the seaside. The displacement is on the order of 160000 tons.

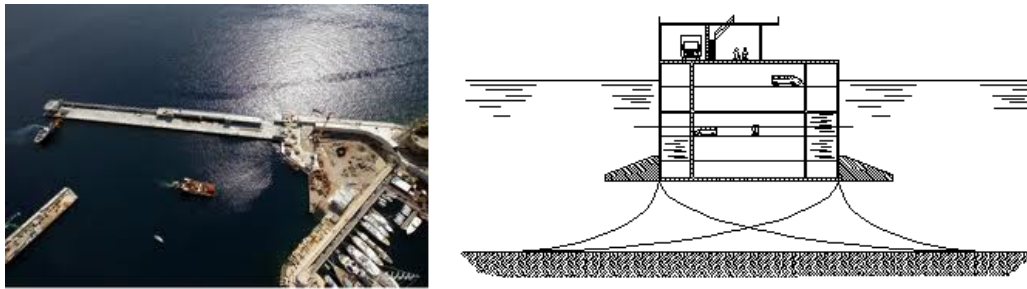


Fig. 1.4 – Semi floating dock in the Principality of Monaco

BINTUNY BAY, INDONESIA Two types of breakwaters are investigated, named the Eastern Traveller which is 73.15 *m* long, 18.89 *m* wide and 3.81 *m* high, and the Eastern Galaxy (91.44 x 27.43 x 5.48 *m*) pontoon breakwaters (Ajiwibowo and Yuanita, 2009).

1.3 WAVE ENERGY DISSIPATION

ENERGY BALANCE With classical definitions of transmission and reflection coefficients, such as in terms of statistic representative wave height (1.1) or characteristic spectral wave heights (1.2), one can define correspondent coefficients in energy terms. These are simply the squares of the formers, *i.e.* τ^2 and ρ^2 . A straightforward energy balance of the wave passing an FB can thus be written in non dimensional form:

$$\tau^2 + \rho^2 + \delta^2 = 1 \quad (1.4)$$

where δ^2 is an energy loss, or dissipation, coefficient.

If we separate the radiated waves generated by the FB induced motion, we must argue that from a physical point of view, transmitted wave is what remains after the processes of reflection and dissipation. Actually, the shape of the incoming wave is first deformed due to partial reflection and possible breaking induced by the FB. The energy that is not reflected passes below and in some cases above (overtopping) the structure. In both cases some energy is dissipated.

It must be added that reflection and transmission coefficients are usually di-

rectly derived from sampled time series analysis, and the techniques adopted do always carry an amount of error into the results. Related uncertainties do then spread when evaluating δ^2 through (1.4), reaching, in some cases the same datum order of magnitude (Pezzutto et al., 2012). A fundamental point for the description of energy losses in laboratory tests is then the implementation of a refined method for time series interpretation.

MEANING OF δ^2 It is common practice, in laboratory tests, to evaluate and report such additional parameter, as a rather qualitative descriptor of an FB behaviour. An investigation of the relationships occurring between the triad in (1.4) is not usually attempted. It could be useful to estimate these relationships, if any, with respect to a set of physical quantities, or better, a number of suitable non dimensional parameters. This for sake of a floating breakwaters practical knowledge implementation.

For example it may be interesting to check if higher energy loss do generally correspond to lower transmission coefficients, and if this apply to whole wave frequency field or to a certain bandwidth.

The possible answers on the coefficient triad dependences could be crucial for engineering purposes. For instance, the design of a floating protection may be focused on attempting high dissipative capacity to reduce wave transmission.

DISSIPATE AND HARVEST Recently growing debates into coastal engineering community are focusing on matching the demand of both coastal protection and renewable energies with the opportunity of using floating wave energy converters (Ruol et al., 2010b; Zanuttigh et al., 2010). Besides the relative advantages of a floating protection, utilization of a floating WEC may present the additional advantage of lowering overall costs through energy selling. This kind of integration, in which protection is the main target, would also pursue additional useful know-how in developing wave energy technologies. In general, installation of a WEC farm in relative shallow waters may reduce the transmitted energy in a way which could alter the coastal morphology. And this might be included in strategic environmental assessment for WEC farms (Azzellino et al., 2011).

Detailed evaluation of *device - wave field - coast interactions* has to be deputed to

coupled physical and numerical modelling. Morphological time scales have an order of magnitude which is at least 2 times higher than wave periods, hence fast numerical models (spectral models and depth averaged phase resolving schemes) are usually utilized to mimic these phenomena.

Recent attempt for implementing WEC interaction with phase averaged wave climates are due to Smith et al. (2012), who modify SWAN (Booij et al., 1999) source code including spectral changes at device location, according to user defined transfer functions. Beels et al. (2010) included in a mild-slope equation scheme a array of cells with assigned degree of absorption, by using the sponge layer technique.

Nørgaard and Andersen (2012) did also implement porous layers, but into a commercial Boussinesq model, to mimic WaveDragon device. Porosities were calibrated with physical models, since, as they state, "*detailed information on absorption and reflection is needed to accurately determine the wave transmission from a single or multiple devices in various sea conditions*".

Proceeding from that it turns out the importance of δ^2 accurate measurements for the calibration models which evaluate either WECs or FBs interactions with the environment.

1.3.1 DISSIPATIVE AGENTS

In the process of a wave passing a floating obstacle some energy is lost. In order to better visualize this concept, consider the Pierson-Moskowitz event facing a FB described in Fig. 1.5. No dimensionless coefficients are reported, but energy spectral densities retrieved by a frequency band by band application of (1.4).

The figure anticipates what is stated in the present job. As it can be seen, an amount of energy is dissipated, and this depends on wave frequency. Transmitted energies are more evident in the low frequency region, while reflected spectrum shape is deformed through the short waves region.

In the middle, a peak of energy loss is evident. Therefore, there should probably exist a characteristic wave period at which energy dissipation is maximum. The modal period of the above spectrum has been centred, for purpose, at the FB heave natural period. As the body resonates with the waves, the relative

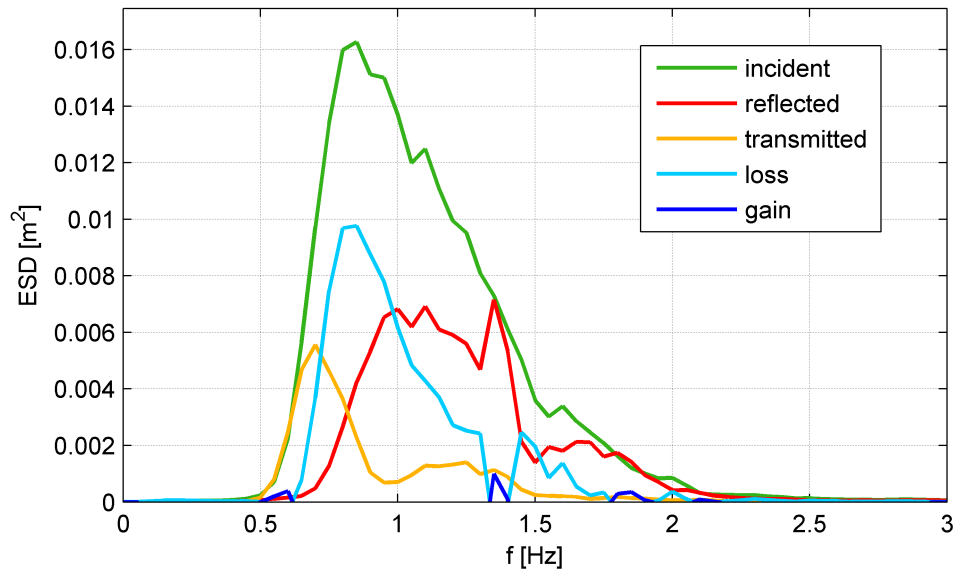


Fig. 1.5 – Energetic balance. Results of physical model irregular PM test described in Ch. ??

motions may be such strong that the boundary layer become turbulent and a lot of vortices separates, dissipating energy.

Moreover, at some frequencies an energy gain (instead of loss) can be experienced. Besides all errors (measurements and spreading) a gain is possible whenever energy transfers from low to high frequencies, due to involved nonlinearities.

The hydrodynamics analysis may be split into two regions: the unconfined region sufficiently below the air-water surface, and a close surface region, where vertical and horizontal velocities have the same order of magnitude.

UNCONFINED REGION Through large-scale tests, Koutandos et al. (2005) examined the behaviour of four FB configurations of different shapes under both regular and irregular wave conditions. They observed that a vertical plate, protruding downward from the front of the FB, significantly enhanced the efficiency of the structure, increasing dissipation and therefore reducing transmission. Koftis et al. (2006) showed that, by numerical simulation, protruding plates, qualitatively as much as each submerged structure edge, act as turbulent energy sources, which dissipate wave energy. The general conclusion of these two papers is that model scales that are too small to reach high-turbulent flow are likely to lead to slight underestimation of the

full-scale τ for high waves. In fact, dissipation increases faster than wave height and does not follow the Froude law.

? concludes that the effects of wave steepness should preferably be studied on large-scale models. This is certainly true for steady flow regimes. In wave motion things may differ significantly, especially for short waves, which rapid oscillatory flow direction changes do not let boundary layer to fully develop. Sumer and Fredsøe (1997) collected an extensive amount of data regarding the flow regime around cylindrical (circular) structures in oscillatory flows. They observed that, for fixed and relatively low Reynolds number (defined through amplitude of wave induced velocities) the characteristics of vortices around a cylinder do strongly depend on Keulegan-Carpenter number. The latter, for monochromatic waves, can be reduced to wave amplitude over cylinder section diameter ratio, no matter the wavelength. Vortex shedding events, causing sensible increase in energy dissipation, start to appear at $KC \approx 7$. As Re increases, while greater than approximately $10^{4.5}$, incipient turbulence and vortex shedding regimes are slightly anticipated to lower KCs .

For non circular shapes, flow asymmetries and relative instabilities must be taken into account.

NEAR SURFACE The most part of the wave energy is concentrated in this
FLOW region.

With respect to incoming waves that are relatively short, the FB behaves mostly as a rigid body. The dynamics are then comparable with that of waves facing a rigid wall, with the formation of a partial reflection field with evident nodes and anti-nodes. At these locations (anti-nodes) in waves are sufficiently high, white capping frequently occurs, with relative energy dissipation.

For relatively long waves, a free body does basically follow the flow, while a chain moored FB may react violently. In fact, the body reaching its maximum mooring allowed position is almost an impulse. Depending on wave height, there can be only little reaction, strong slamming or the body sinks and rapidly emerge, all this with release of impulsive waves and more or less air entrapment.

1.4 CONTRIBUTIONS OF PRESENT THESIS

Satisfactory descriptions of the dissipating processes enumerated above can be obtained only throughout very detailed numerical models (Reynolds averaged or DNS). For coastal engineering problems, at sea storm time scales, the application of these models is not feasible at all. Nevertheless, linearised potential solutions are basically conservative. The final purpose of this job is then to give a parametric point of view of a FB behaviour, in terms of wave transmission, reflection and dissipation coefficients. Results can be used as a basis for validating depth averaged wave models.

A number of parameters are identified, on the basis of literature and flume tests observation. A set of experiments has been designed and done according to those non dimensional quantities.

The description of dissipating processes appears to be crucial. However, with actual linear analysis methods, an error in determining it could be introduced when non-negligible wave steepness are considered. Two new algorithms based on modulated waves point of view are proposed.

Experimental results are interpreted in a second order quadratic fashion, separating the analysis of primary and related bound waves, with that of second harmonic free waves. For linear waves, detailed transfer functions which describe energy reflection and transmission have been derived. These are based on the proposed parameter set. For secondary free waves, the energy transfer from primary components is also analysed.

During this thesis development the following works have been published: Pezzutto et al. (2012); Martinelli et al. (2012); Ruol et al. (2010a, 2011, 2012a,b, 2013); Burcharth et al. (2012a,b)

1.5 THESIS ORGANIZATION

CHAPTER 2 Literature review of experimental investigations and related works on floating breakwaters is given together with a brief discussion on the definition of a FB efficiency.

CHAPTER 3 One of the targets of present job is the identification of fundamental parameters which better describe the transformation of the wave field which encounter a floating, compact shape, barrier. This chapter summarizes author referenced works on this subject. Three main parameters are identified: a scaled frequency, wave steepness and FB draft to water depth ratio.

CHAPTER 4 Provides a literature available algorithms for wave flume (2DV) reflection analysis. Each method is described in detail, together with discussion on the shortcomings of involved wave theories.

CHAPTER 5 Attempts an improvement on reflection analysis by empirical mode decomposition. A frequency shifting procedure for mode mixing mitigation is proposed.

CHAPTER 6 Derives the main contribution of this thesis: a new method for decomposing a wave field into incident and reflected linear superposing modulated waves.

CHAPTER 7 Draws the experimental set-up for the evaluation and verification of preceding assumptions made in Ch. 3. Laboratory devices, floating breakwaters models and test plans are described.

CHAPTER 8 Presents and discuss experimental results. Estimated reflection, transmission and dissipation coefficients are given with respect to previously identified non-dimensional parameters, together with approximated simple functions. An alternative depth dependent parameter is identified.

CHAPTER 9 Resumes the overall job and draws the conclusions.

2 EFFICIENCY OF FLOATING BREAKWATERS

This chapter provides a review of literature available experimental studies on floating breakwaters. The efficiency of a FB is frequently expressed in terms of the transmission coefficient τ , defined as the ratio between transmitted and incident wave height. The second part of the chapter discuss on the ambiguity of such a definition and presents an alternative effect oriented point of view. Most experimental reports are based on specific case studies, therefore provided results are very specific. The lack of a unified parametrization reduces the possibilities of comparisons.

2.1 LITERATURE REVIEW

In countless cases, experimental studies certified the efficiency of the different designs to specific installations. Only a small number of internal reports are available, though. In most cases they show the decrease of the incident regular wave with varying height and period for such designs. In a fewer number of cases, the behaviours under regular and irregular conditions are compared. The following list of available reports is therefore definitely incomplete.

In some cases the studies are not applied to specific installations but to prefabricated devices. One of first available technical report (Nece and Richey, 1972) provides experimental results on twin-hull pontoon and box pontoon FB.

A growing number of companies provide pre-fabricated modules for floating breakwaters (FBs), a traditional protection system with multiple benefits especially for the environment, suited for small marinas in mild sea conditions (wave periods up to 4.0s and wave heights smaller than 1.5m).

The most used type of pre-fabricated module is a chain-moored rectangular caisson with two vertical plates protruding downwards from the sides. As these shapes resemble a Greek π , they are referred to as π - type FBs. It is be-

lieved that these devices are more economical compared to other with different geometries, such as the simple rectangular shape usually named *box-type*.

MULTIPLE CONFIGURATIONS Ruol (1984) investigated on the importance of mooring cable elasticity for an Alaska Pontoon (open compartment). Better degree of protection from wave motion was observed with cable slope 1:1 with respect to 1:5.

Blumberg and Cox (1988), from wave flume experiments on various configurations (boxes, T shaped, and a catamaran), derived useful design curves in terms of both transmission coefficient and maximum horizontal wave loads.

Atzeni et al. (1998) filled a rectangular box with pressurized air at different pressures. Different mooring lines lengths were tested too. Two dissipating devices were mounted on seaside and leeside faces of the FB. They found that the lower the length of the cables, the better the performance in terms of transmitted wave.

Neelamani and Rajendran (2002b,a) focused their investigations on partially submerged T-type and \perp -type Fbs. The wave transmission, reflection and energy dissipation characteristics retrieved using physical models under regular and random waves. It was found that the coefficient of transmission generally reduces with increased wave steepness and increased relative water depth, d/L . Both breakwaters were found to be very efficient in dissipating the incident wave energy. A comparison of the hydrodynamic performance of \perp -type and T-type shows that T-type breakwater is better than \perp -type by about 20 – 30% under identical conditions.

Dong et al. (2008) performed an experimental study among three types of floating breakwater (a box, a double-box and board-net) aimed to protect fish and fish cages. The wave transmission coefficients of these three types of breakwaters under regular waves with or without currents were calculated. Results show that the board-net floating breakwater, which is a simple and inexpensive type of structure, can be adopted for aquaculture engineering in deep-water regions.

Koutandos et al. (2005) examined four different FBs configurations: a single fixed FB, the same FB with heave motion only allowed, a single fixed FB with attached front plate (impermeable and permeable) and a double fixed FB. The

attached plate in the front part of the FB significantly enhances the efficiency of the structure.

NUMERICAL INTERPRETATIONS Fugazza and Natale (1988) set up a linear coupled model (wave diffraction and body movement) for the description of a Box FB (Caisson breakwater) in regular wave fields. Laboratory tests agree with the theoretical solution. In some cases the hydrodynamic coefficient of heave-related added mass underestimate experimental values, when calculated under the assumption of potential flow.

Sannasiraj et al. (1998) adopted a two-dimensional numerical model to evaluate hydrodynamic coefficients and forces in an oblique wave field for multiple box shaped FBs (pontoons). It was found that the two-dimensional model is applicable to investigate the wave-structure interaction problems of the type herein considered.

Rahman et al. (2006) performed flume experiments in order to verify the presented linear numerical model for a rectangular section FB. Results are presented regarding the water surface elevations at different locations of both onshore and offshore side, the dynamic displacements of the floating body. Forces acting on mooring lines, estimation of the hydrodynamic coefficients of the structure (transmission, reflection and dissipation) were also given and compared with experimental results.

Gesraha (2006) provided both numerical and experimental study of a rectangular breakwater with two thin sideboards protruding vertically downward, a π -shaped floating. Results show that for short oblique waves higher transmission occurs when compared with rectangular breakwaters.

EXTREME LOADS Cox et al. (2007) reported a flume study aimed to examine a box type floating breakwater performance in both regular and irregular waves with particular emphasis on wave transmission and reflection, energy dissipation, motions and restraining forces. Occurrence of intense and short duration impact loads were noted.

Ruol and Martinelli (2007) tested different types of mooring for a Π -shaped FB: chains with different initial tensions and piles. Observations were focused on wave transmission, moorings loads and chain snapping. Simple numerical

simulations, based on irrotational flow, which are commonly used for design of moorings, were seen not to be suitable to describe the maximum loads. The added value of a more detailed investigation, in particular by means of physical testing, was established.

Martinelli et al. (2008) investigated the relevance of the layout on the performance of a π -shaped floating breakwater schemes under oblique waves. With increasing wave obliquity, wave transmission decreases, mooring forces due to snapping decrease and link forces slightly increase. The maxima of link forces are not much greater than the average loads and this is relevant for fatigue and reliability considerations.

ENERGY
DISSIPATION Williams (1988) carried out a flume study to investigate the hydrodynamic interaction between a train of regular incident waves and a partially immersed, substantially rectangular obstacle in an essentially two-dimensional domain. The interaction are considered for both fixed and floating obstacle modes. Experimental measurements have been taken of the obstacle reflection and transmission characteristics in both modes, together with the obstacle motion response in the floating mode, and comparison is made with the predictions of linear diffraction theory. The results of the investigation have enabled identification of the conditions under which the use of potential theory alone becomes invalid due to the significant presence of energy dissipation mechanisms in the interactive process.

Jung et al. (2004, 2005) investigated wave interactions with a fixed (2004) and free rolling (2005) rectangular structure in a wave flume, using particle image velocimetry (PIV). No overtopping occurred on the deck. The study focused on the detailed hydrodynamic field near the structure; two-dimensional spatial velocity maps on both sides of the structure were measured at eight different phases. Phase average was used to extract the mean flow and turbulence property from the repeated instantaneous PIV velocity measurements. The mean velocity field was demonstrated along with the generation and evolution of vortices and turbulent kinetic energy on both sides of the structure. For the free rolling structure, the results show that vortices were generated near the structure corners at locations opposing to that of the roll damping effect for waves with a period longer than the roll natural period of the structure.

He et al. (2012) investigated the complete hydrodynamic performance of floating breakwaters with pneumatic chambers, comparing them to equivalent ones without pneumatic chambers. Based on 2DV regular wave experiments, they gave results in terms of RAOs, transmission, reflection and dissipation coefficients. They concluded that the pneumatic chambers significantly enhanced the wave energy dissipation, especially for low frequency waves. As a consequence, the wave transmission is significantly reduced.

EMPIRICAL Uzaki et al. (2011) investigated experimentally performance
FORMULAE of wave absorption of a steel floating breakwater "FBT" which is composed of a box-type pontoon and truss structures. Truss structures are attached to the front and the rear of the pontoon and exaggerate the wave energy dissipation due to the wave breaking. Transmission coefficient, τ is also discussed and quantified with the aid of dimensional analysis. Values of τ are plotted against the ratio of the water depth h to the wavelength of incident waves L , while a universal empirical expression for τ is obtained.

Ruol et al. (2013) proposed a formula for τ , suited to chain moored π – type FBs, and introduced an important nondimensional parameter χ , basically equal to the ratio between the incident peak wave period and the FB natural period of oscillation.

Recently, several studies investigated on the sensitivity of the transmission coefficient relative Floating Breakwaters on non-dimensional parameters such as d/h (relative draft) and w/h (relative width). Koftis and Prinos (2011), by means of an extensive experimental dataset, analyse the performance of FBs in terms τ . They recognize that fixed and moored FBs have a very different behavior, and propose two simple formulas given as a function of h/L (L being the wavelength of incident waves), d/h and w/h .

Ruol et al. (2012a) performed 2D numerical simulations considering FB under regular waves, fully constrained (in order to roughly simulate tethered conditions), free to move vertically (simulating pile supports) and moored with loose springs (simulating the chain mooring). It was seen that the type of mooring system, not included in the formula, has a significant effect. FBs moored with loose chains are less effective than tethered ones. Considering wave periods smaller than the natural period of oscillation ($\chi_m < 1$) and rela-

tive drafts $d/h > 0.2$, FBs where roll and surge is impeded perform better than fixed ones. For periods close to the natural period of oscillation and drafts $d/h > 0.1$, FBs where roll and surge is impeded perform better than chain moored FBs. From these considerations, it must be concluded that the arbitrary application of the formula to FBs moored with other than loose chains leads in most cases to an over prediction of the transmission coefficient.

Abdolali et al. (2012) investigated FBs subject to regular waves constrained to move only vertically. They compared numerical simulations, experimental observations and the formula proposed by Ruol et al. (2013). The tested range included large values of χ (ranging from 1 to 7), and large values of relative draft (d/h between 0.20 to 0.45) and relative width (w/h between 0.66 to 1.66). Also these numerical investigations confirm that in these conditions the formula significantly overpredicts the numerical data.

2.2 OTHER POSSIBLE EFFICIENCY DEFINITIONS

The efficiency of a breakwater is commonly expressed in terms of a transmission coefficient. The latter is usually defined in statistical terms ((1.1) or similar) or through spectral averages (1.2). An analysis of Fig. 1.5 may be the starting point for a discussion on alternative formulations.

In most cases, flume irregular tests refer to standard synthesized JONSWAP or Pierson-Moskowitz spectra. Results (transmission coefficients) then refer to spectral fundamental parameters, which are the incident (target or measured) significant wave height and peak period. The shape of the transmitted spectrum, for single test cases, is hardly reported. So one could object that classical average definitions may be somewhat ambiguous.

LINEARITY Consider the case a 0.5 transmission coefficient for an irregular wave test is reported. A straight interpretation of that would be the multiplication for an even transfer function ($\tau^2 = 0.25$) of the incident spectrum to obtain the transmitted one, as depicted in Fig. 2.1. But, considering different shapes for the transfer function which conserve the integrals ratio (1.2), would lead to dramatic change in spectral shape (Fig. 2.2).

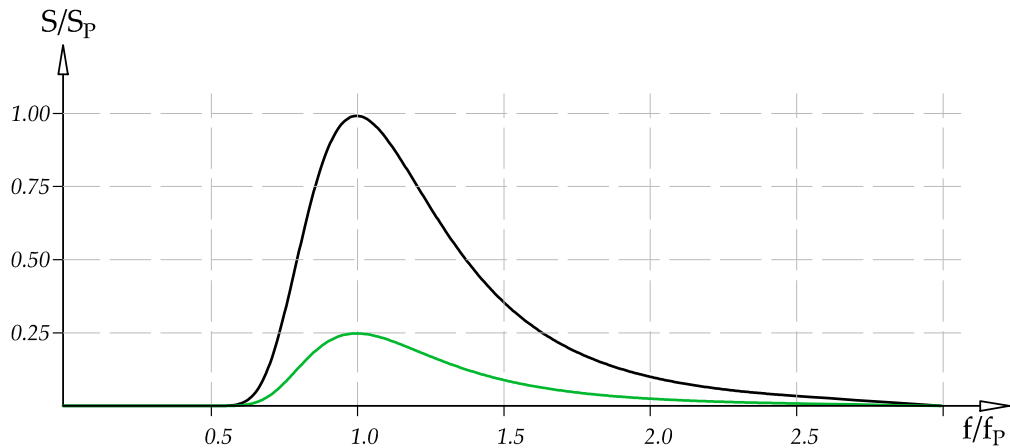


Fig. 2.1 – Even transmission ($\tau = 0.5$) of an incident spectrum (black). Green: transmitted spectrum.

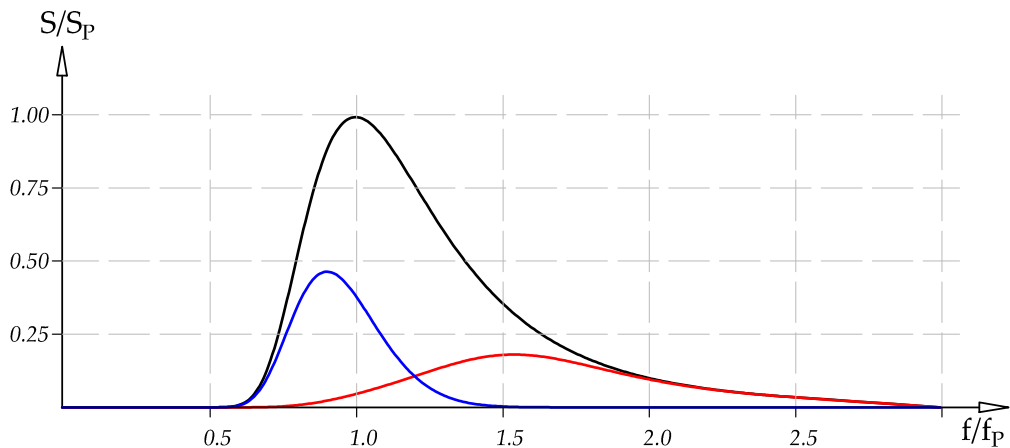


Fig. 2.2 – Linear transmission ($\tau = 0.5$) of an incident spectrum (black): low pass (blue) and high pass (red) filtered.

All these considerations are based on the hypothesis of a linear process (the existence of a transfer function). But, in many situations, it is not. Going back to Fig. 1.5 one can note that, besides estimation errors, a net energy gain could be admitted at some frequencies, as a consequence of energy transfer between wave components. Hence, wave height or energy attenuation coefficients may not be sufficient for description of wave effects.

EFFECTS

There's something more about spectral shapes. A breakwater is aimed to defend an environment from waves, and the effects on the environment are usually evaluated considering energy fluxes, not energies.

Action of long waves is more important than the one due to short waves, because the associated group celerity c_g is higher. With reference to Fig. 2.2, the reader would allow that the transformation which leads to red spectrum should be cast as more *efficient* than the one that transforms the incident waves into the blue distribution. But in terms of wave height (or energy) they are the same.

In terms of energy fluxes the following efficiency coefficient can be defined:

$$\tau_{EF} = \frac{(\int c_g S_t df)^{1/2}}{(\int c_g S_i df)^{1/2}} \quad (2.1)$$

For the real example of Fig. 1.5, $\tau_{m0} = 0.42$ and $\tau_{EF} = 0.47$. Consider that the latter could be a little higher, since, due to limitations of the reflection analysis algorithms, very long waves are not considered here.

These ambiguities can be solved performing simple regular wave tests. With respect to irregular tests, these take less operational time, since only a few waves are sufficient, hence the wave period grid can be more refined. The resulting transmission coefficient distribution can therefore be interpreted by fitting adequate transfer functions.

If relatively important non-linear events are to be captured, then bi-chromatic wave tests can be the option. These also allow to interpret energy transfer from the two primary waves to three super-harmonics and, which is more important, to one sub-harmonic. In both cases, few irregular runs should be performed for verification purposes.

2.3 NEEDS FOR A UNIFIED DESCRIPTION

In common literature FB efficiency is handled graphically in terms of τ versus non dimensional parameters, in such a way that each single structure is characterized by a single distribution. For example, this occurs using kw (or w/L) as the ordering parameter. With L we denote wave length, k the wave number, which is equal to $2\pi/L$, and w breakwater width.

Some authors give their results ordered with respect to some incoming wave characteristic period (which can be the spectral peak period T_p). Due to the

dimensionality of T , separated traces are again denoting single structures.

The physical meaning of most common variables is very clear, however they suffer some limitations when comparisons are attempted. For example, if w/L is chosen, usually the higher the ratio, the higher the efficiency of a box shaped FB. But then a thin wall would win against it.

There are of course a number of variables, frequently added by the authors, which enrich the presentation of results. But the comparison problem does remain. In some cases, the parametrization is very extended, and the number of variables to be considered is very high.

The identification of a small group of non dimensional variables, which should be physically meaningful, is then wished.

3 PARAMETERS IDENTIFICATION

This chapter provides the fundamental steps which have been done with author cooperation for the identification of three characteristic non-dimensional variables for the 2DV FB problem. The first one helps in describing the time scale (or frequency scale) of the process involved. The second one characterizes the dissipative events, while the third one is presented as an attempt to be verified in the present thesis. Some of the results have been already published.

3.1 TIME SCALE

While investigating floating structures properties, it is common practice to render the response amplitude operators (RAO) of such bodies. These are basically parametric relations describing the floating body motion amplitude to wave amplitude ratios, for all degrees of freedom. The peaks of RAOs diagrams correspond to resonant or nearly-resonant behaviours. If the sea state matches these conditions, then relevant scattered waves are expected, together with high forces.

In Fig. 1.5, an amount of energy is dissipated, and this depends on wave frequency. Transmitted energies are more evident in the low frequency region, while reflected spectrum shape is deformed through the short waves region. In the middle, a peak of energy loss is evident. Therefore, there should probably exist a characteristic wave period at which energy dissipation is maximum. And this has to be in connection with some dynamic FB characteristics.

3.1.1 FB NATURAL FREQUENCIES

RAOs of an FB physical model do need an extensive number of experimental runs to be correctly evaluated. If the model is sufficiently manageable, natural

frequencies can be rapidly estimated through free decay tests. A description is here recalled.

In order to measure an FB heave natural frequency, the FB is manually displaced downward from its equilibrium position. Then the FB is "instantaneously" released and let free to oscillate. During these operations, time-series of the lee and wake side positions are sampled by means of position transducers.

When interpreting the acquired signals, one might take account that "instantaneous" release of the body is never as much instantaneous as one wants. Therefore, a portion of signal corresponding to that time interval, namely $[t_0, t_1]$, during which the body freely moves, should be considered.

We consider a FB with mass M_s . Breakwater mass is later computed, by virtue of Archimedes principle, considering the immersed volume. Therefore M_s does include also mooring chains mass. However, being the latter on the order of $70g/m$, its incidence on the vibrating system is negligible. We also neglect other spring effects, due to the chains and to the measuring system (position transducers), being them on the order of 0.1% with respect to the magnitude of the body spring constant, that is $\gamma_w w$.

Under these assumptions, the FB should behave as a damped oscillator. Being z_0 the displacement at time t_0 , and v_0 the corresponding vertical speed, the body should move in vertical direction with the law $z(t)$ defined by the following vibrating system:

$$z_{,tt} + 2\epsilon z_{,t} + \omega_h^2 z = 0 \quad (3.1a)$$

$$z(0) = z_0 \quad (3.1b)$$

$$z_{,t}(0) = v_0 \quad (3.1c)$$

where ϵ is the damping coefficient (to be tuned), and ω_h the natural frequency related to heave motion.

During the tests the system appeared to be under-damped. However, small number of oscillations have been observed, namely in the order of $3 \sim 4$. Due to this behaviour, non-linearities in damping and mass coefficients are difficult

to be observed. Therefore we assumed these to be linear, getting:

$$z = z_0 e^{-\epsilon t} \left[\cos \omega t + \frac{1}{\omega} \left(\epsilon + \frac{v_0}{z_0} \right) \sin \omega t \right] \quad (3.2)$$

The reduced motion frequency may be recovered from:

$$\omega = \sqrt{\omega_h^2 - \epsilon^2} \quad (3.3)$$

The four parameters model has been then fitted to the sampled signals.

The procedure was first utilized by Martinelli et al. (2008), where the results relative to a π -type FB are given as function of T_P/T_h , with T_P being the wave period corresponding to the peak of the incident JONSWAP spectrum (for laterally confined structure, i.e., high length/width ratio).

Thanks to the choice of T_P/T_h (as an alternative to w/L), the transmission and reflection coefficients for different structures appeared to be described by approximately the same line. One possible reason for this interesting behaviour is that the response amplitude operator usually shows a peak in correspondence of a wave with a frequency equal to the natural frequency, and by using the suggested scaling variable, all the peaks occur at the same abscissa.

Of the six degrees of freedom of the FB, the heave oscillation has been selected because: *a)* only the response to the frontal waves is considered in wave tank tests, and other movements (sway, yaw, and pitch) are not present; *b)* heave always exists and is not considerably affected by the mooring type, whereas, for instance, surge-free oscillations are dominated by the horizontal mooring rigidity; *c)* heave contributes in a high degree to the formation of the transmitted wave field; and *d)* in a numerical code, the heave motion can be evaluated considering one degree of freedom only, because it is usually uncoupled from the other modes.

3.1.2 GEOMETRIC APPROXIMATION

The natural period of heave oscillation might not be easily available. The somewhat circuitous search for an alternative nondimensional variable produced a result that is a good approximation of T_P/T_h . T_h , or the corresponding

$\omega_h = 2\pi/T_h$, is found using the equation for the natural frequency of a simplified vertical undamped oscillation of a floating body, neglecting possible coupling terms of the heave motion with the rest of the motions of the structures:

$$\omega_h^2 = \frac{K}{M} \quad (3.4)$$

where K is the vertical spring stiffness and M the overall mass of the system. K is given by the buoyancy forces and the mooring stiffness in the vertical direction. Because moorings are hardly designed to restrain the vertical movements of the FB, the stiffness is totally dominated by the buoyancy forces F . Because a two-dimensional problem is discussed, all quantities are given per unit length, and the spring force F is given by

$$F = \gamma_w w z = K z \quad (3.5)$$

where w is FB width, z the vertical coordinate counted upward starting at *s.w.l.* and γ_w the water local weight. The overall system mass M is the sum of the structure mass M_s and the added mass M_a , which is essentially the mass of water that accelerates together with the body.

In Fig.3.1, M_a is simplified by the water mass trapped in between the two plates and the water mass trapped in half of a circle of the radius equal to half of the FB width w .

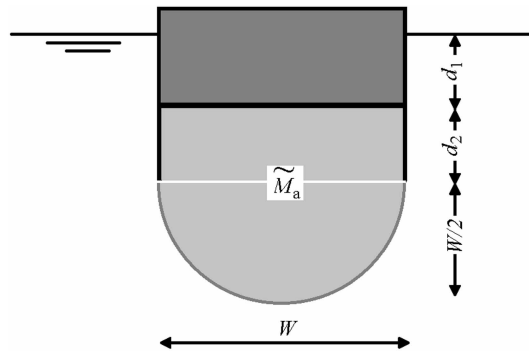


Fig. 3.1 – Graphical interpretation for added mass of the floating breakwater

According to Fig.3.1, the added mass in two-dimensions is assessed as

$$\tilde{M}_a = \rho_w \left(w d_2 + \pi w^2 / 8 \right) \quad (3.6)$$

Because the body mass is equal to the mass of the displaced water, the total estimated mass may be evaluated as

$$M_s + \tilde{M}_a = \rho_w w (d + 0.39w) \quad (3.7)$$

Replacing (3.5) and (3.7) into (3.4), an estimated expression for the heave natural frequency is obtained as follows:

$$\tilde{\omega}_h = \sqrt{\frac{g}{d + 0.39w}} \quad (3.8)$$

A regression analysis was performed based on experimental evaluation of the natural frequency, producing the following approximation:

$$\omega_h \approx \sqrt{\frac{g}{d + 0.35w}} \quad (3.9)$$

which reflects the database geometries and is not much different from (3.8). The assumption for the added mass (and the consequent calculation of the natural period of oscillation) is questionable, but it gives quite good approximation of real investigated cases, as proved by Fig.3.2.

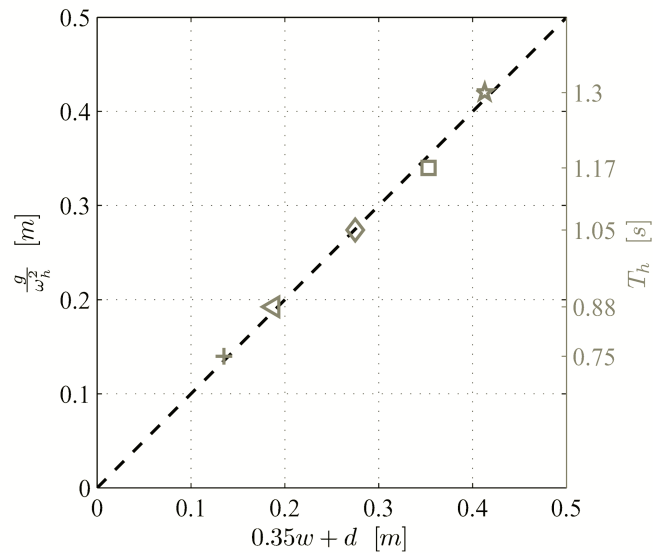


Fig. 3.2 – Linear regression of heave natural frequencies; + Sc0v07kg, ◁ Nc0c16kg, ◊ Dc0c32kg, ◻ Dc0c56kg, ☆ Dc0c76kg

The fitted results derive by several physical model tests carried out on 6 struc-

tures which are described in Tab. 3.1. Each investigation is characterised by a "model code" identifying the FB and test configuration. The first letter is not relevant in this context. The second letter describes the mooring system (c=chains, ..); a digit for the structure orientation (0 if perpendicular to the waves); a digit for the facility hosting the tests (c=flume,..); eventually a group of 4 characters with the target model mass and its unit measure ($\langle xx \rangle kg$).

Tab. 3.1 – Structures tested in the wave flume in Padova

FB code	mass [kg]	w [m]	h_s [m]	d [m]	h [m]
Sc0c16kg	16.2	0.25	0.150	0.100	0.515
Dc0c32kg	32.0	0.50	0.150	0.100	0.515
Dc0c56kg	56.3	0.50	0.283	0.178	0.515
Dc0c76kg	76.3	0.50	0.283	0.238	0.515
Mc0c76kg	76.3	0.50	0.343	0.238	0.515

All devices of Tab. 3.1 were moored with 4 chains, with submerged weight of approximately $70g/m$, anchored at a distance equal to twice the water depth ($h = 0.5 m$). The initial pretension is always very low, equal to the total chain weight. In shallow waters, chains may become fully extended in case of large waves. The sharp impact load that develops in case the chain is fully extended was studied in Martinelli et al. (2008).

Eq. (3.9) could also be justified numerically. The semicircular shaped added-mass (second term in (3.6)) is half of the addedmass relative to a plate moving in an unbounded fluid, that is, in absence of a free surface (Sarpkaya and Isaacson, 1981). In the presence of a free surface, the added mass is frequency dependent, $M_a(\omega)$, and may be determined solving the classical radiation problem (Newman, 1977; Chakrabarti, 1987). The natural oscillation is found iteratively computing $M_a(\omega)$ for $\omega = \omega_h$ (Mays, 1997; Senjanovič et al., 2008).

3.1.3 A PREDICTIVE FORMULA FOR Π -type FBs

? proposed a formula that is a modification of the Macagno's analytical rela-

tion. The latter is given by:

$$\tau_M = \left[1 + \left(\frac{kw \sinh kh}{2 \cosh (kh - kd)} \right)^2 \right]^{-\frac{1}{2}} \quad (3.10)$$

This relation is valid for a rectangular, fixed and infinitely long FBs (representing many aligned modules connected to each other) with draft d and width w , subject to regular waves. In (3.10), h is the water depth and k is the wave number relative to a regular wave. For irregular waves, where T_p is known, we evaluate the wavenumber assuming an equivalent period $T = T_p/1.1$.

Since Macagno's relation is based on linear wave theory in absence of displacements and dissipations, it is not expected to predict accurate results in presence of movements. Furthermore, it is not meant to be applied to floating II-type FBs.

The assumed scaling parameter $\chi \approx T_p/T_h$ is obtained directly from (3.9)

$$\chi = \frac{T_p}{2\pi} \sqrt{\frac{g}{d + 0.35w}} \quad (3.11)$$

Because χ is much easier to find than T_p/Th and has essentially the same value, ? propose that the experimental results of an FB efficiency (τ , ρ) are always plotted as a function of χ . The symbol χ_m is used if the mean wave period T is used rather than the peak wave period T_p .

The method proposed consists in evaluating τ by the multiplication of the Macagno's relation by a function of β :

$$\tau = \beta(\chi) \tau_M \quad (3.12)$$

Based on the experiments carried out in the wave flume of Padova University, β is given by the following expression:

$$\beta = \left[1 + \left(\frac{\chi - \chi_0}{\sigma} \right)^2 e^{-\left(\frac{\chi - \chi_0}{\sigma} \right)^2} \right]^{-1} \quad (3.13)$$

where $\chi_0 = 0.7919$ (with 95% confidence interval [0.7801,0.8037]) and $\sigma = 0.1922$, [0.1741,0.2103]. Eq. (3.13) is valid in the tested ranges: $\chi \in [0.5, 1.5]$,

and $d/h \in [0.2, 0.45]$.

For oblique waves, it is proposed that χ is evaluated with an equivalent (longer) wave period, obtained by the apparent wavelength ($L/\cos\theta$). Note that (3.13) is merely a fitting of the experimental results. The core of the proposed method is given by (3.12), that assumes χ as the most relevant variable of the process beside the prediction based on Macagno's relation.

The formula was fitted to cases with incident waves smaller than the free board height. Comparison with literature data also showed good agreement, at least for small incident wave heights. In case of large waves, the transmission is seen to be slightly under-predicted for small χ and over-predicted for large χ .

3.2 WAVE STEEPNESS

The same set of data, coming from extensive testing of structures enumerated in Tab.3.1, showed that even wave reflection and energy dissipation follow a generic law strongly depending on the preceding described parameter χ . However, the distribution of loss coefficients did not "collapse" into a single curve, as for τ (see Fig.3.3).

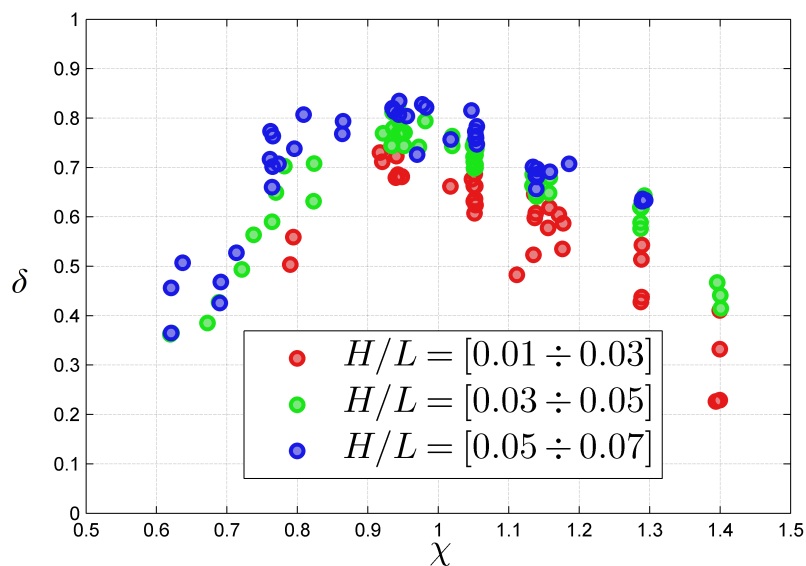


Fig. 3.3 – Dissipation coefficients for different Π -type floating breakwaters under irregular wave fields. Strong dependence on wave steepness is underlined by colours.

3.2.1 AN EXPERIMENT (PEZZUTTO ET AL., 2012)

In physical models, the dissipated energy is evaluated not at the breakwater itself, but in a wider control region (which contains the structure location) delimited by the sets of measurement instruments. In that control region, relative steep waves, if sufficiently reflected, tend to break. Proceeding from this observation, wave steepness, defined as the ratio of wave height (H) over local wave length (L), is considered as an additional parameter to be taken into account. Note that in Fig.3.3, H/L is defined as significant wave height over wave length corresponding to spectral peak period.

A set of experiments have been performed in a wave flume, on a Π -type, chain moored, FB. Wave heights and periods arrays have been determined on the basis of the FB geometry, in the way that the parameters involved would span their respective range of validity across the critical region of $\chi = 1$.

Only regular waves have been generated. This gave the opportunity to limit the uncertainties due to the separation of incident and reflected wave trains.

Test wave conditions have been designed in order to span a wide range of both wave steepness and χ parameter. The set can be divided into four series with fixed H/L . For each series eight wave periods were reproduced (Tab. 3.2).

Tab. 3.2 – Test target wave conditions in terms of wave heights for different periods (T) and wave steepness (H/L). Target values of χ are also reported.

H/L	0.01	0.03	0.05	0.07	
T					χ
0.8	0.01	0.03	0.05	0.07	0.67
0.9	0.01	0.04	0.06	0.09	0.76
1	0.02	0.05	0.08	0.11	0.84
1.1	0.02	0.06	0.09	0.13	0.92
1.2	0.02	0.07	0.11	0.15	1
1.3	0.03	0.08	0.13	0.18	1.09
1.4	0.03	0.09	0.14	0.2	1.17
1.5	0.03	0.1	0.16	0.23	1.26

EVIDENT
DISSIPATING
PHENOMENA

During the laboratory tests we recorded a list of information based on visual analysis of the wave field. These are mainly related to wave breaking and FB overtopping. The strength of breaking events is reported graphically in Fig. 3.4.

H/L	0.01	0.03	0.05	0.07	
T [s]					χ
0.8					0.67
0.9					0.76
1					0.84
1.1					0.92
1.2					1
1.3					1.09
1.4					1.17
1.5					1.26

Fig. 3.4 – Strength of breaking events. Visual judgement: cyan, none; pink, spilling-like breakers; red:plunging-like.

Fig. 3.5 describes, by the same point of view, the appearing magnitude of overtopping events.

H/L	0.01	0.03	0.05	0.07	
T [s]					χ
0.8					0.67
0.9					0.76
1					0.84
1.1					0.92
1.2					1
1.3					1.09
1.4					1.17
1.5					1.26

Fig. 3.5 – Strength of overtopping events. Visual judgement: cyan, none; pink, water on deck; red:water jet.

Another dissipative phenomenon we observed was the growth of noisy macrovortices at FB sides (flume walls) under waves steepness $H/L = 0.03$, and wave periods close to $1.1 \sim 1.2$ s.

We noticed some distortions of the 2DV expected wave field. In some cases a

channel cross mode was excited by the combined regular forcing of the paddle and FB motion. That occurred for wave periods close to $0.8 \sim 0.9$ s, *i.e.* wavelengths close to flume width.

Some asymmetries were enhanced during testing wave conditions with periods in the interval $0.9 \sim 1.1$ s. These became visible after approximately $40 \sim 60$ s from the beginning of the test. This has been taken into account when analyzing data records, cutting all the time-series at the point these instabilities show up.

RESULTS AND REMARKS Synthetic results are reproduced in Fig. 3.6, where dissipation coefficients relative to two extreme wave steepness test series are plotted against non dimensional time χ . It was concluded that incoming wave steepness is confirmed to be a fundamental parameter to be taken into account.

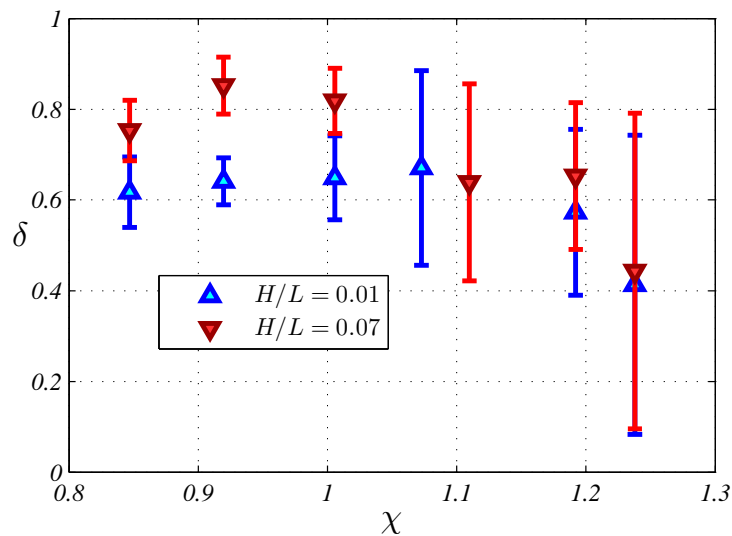


Fig. 3.6 – Dissipation coefficients for the two extreme wave steepness series and $\chi > 0.8$. Error bars are standard deviations for δ evaluated as App.A

The study anticipated one critical aspect discussed in present thesis. Since energy losses are usually evaluated as sons of standardized reflection and transmission analysis procedures, they may include some errors amplifications. These uncertainties have been evaluated via Monte-Carlo simulations (see App.A). For relative long waves, the estimated uncertainties have the same order of magnitude of the obtained results.

It was concluded that, in order to solve these conundrums, *i.e.* to have a correct description of H/L incidence on δ , more appropriate reflection analysis has to be considered.

3.3 RELATIVE WATER DEPTH

Consider a box floating breakwater, w wide, moored at a water depth h , one would argue that increasing the draught d of the FB, would augment the resistance opposed to water particles motion, determining lower wave energy transmission across the body.

This is a kind of intuitive proposition which does not consider a set of determining quantities. For example, an increase of draught, maintaining constant width w , corresponds to an increase of mass, which modifies the dynamic behaviour of the body (Fousert, 2006).

A π -type FB is nothing but a box-type FB with an economical increased draught, which cross section is modified attaching downward protruding plates. As shown in Sec.3.1, it does cause an increase of added mass which lowers the FB heave natural period.

With the term *relative depth* we consider here the draught over water depth ratio, *i.e.* d/h . The idea is to uncouple parametric behaviour of an FB with respect to all that is caused by an increase of mass. Since that has to deal with dynamic behaviours and can be described by precedent defined *characteristic time*.

4 REFLECTION ANALYSIS METHODS

This chapter provides a detailed review on available methods for the separation of a measured 2DV wave field into incident and reflected waves. All methods described hereby refer to the analysis of surface elevation measurements, provided by gauges placed in regions where the bathymetry is considered sufficiently even (absence of shoaling). The limitations of the algorithms and their background theories are also discussed.

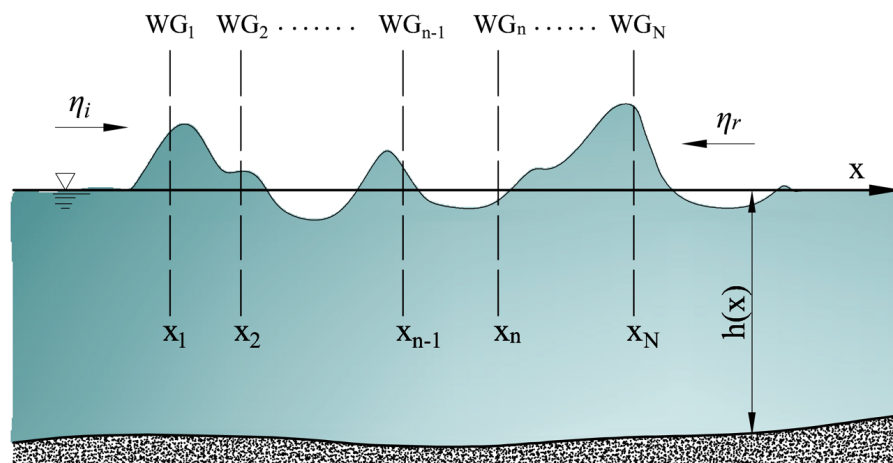


Fig. 4.1 – Wave gauges methods reference system

4.1 FREQUENCY DOMAIN

4.1.1 DETERMINISTIC METHODS

GODA AND SUZUKI Developed by Goda and Suzuki (1976), this is a method for the separation of incident and reflected 1D surface water waves, which has been widely used among the last decades.

Water elevation is sampled at two wave gauges, as shown below (Figure 4.1). The wave field is assumed to be a linear superposition of stationary monochro-

matic perturbations travelling in opposite directions:

$$\eta(x, t) = \sum_{j=1}^{\infty} a_j \cos(\omega_j t - k_j x + \phi_j) + b_j \cos(\omega_j t + k_j x + \phi_j) \quad (4.1)$$

Each component is identified with an Airy surface wave, travelling with the associated linear phase celerity. Hence, the wavenumbers should satisfy Stokes dispersion relation

$$(\omega_j)^2 = gk_j \tanh k_j h. \quad (4.2)$$

If we denote dt and $\Delta t = (M - 1) dt$ as the sampling time step and the total timeseries length (M samples), then (4.1) can be approximated by a discrete sum of Fourier modes. Being $\omega_0 = 2\pi/\Delta t$ the minimum resolved bandwidth, and $\pi/dt = (M/2 - 1)\omega_0$ the maximum observable circular frequency, then the application of FFT to the timeseries sampled at the n^{th} gauge returns the set of complex amplitudes of

$$\eta_n = \Re \left\{ \sum_{p=M/2-1}^{M/2} A_{pn} e^{ip\omega_0 t} \right\}, \quad (4.3)$$

where $i = \sqrt{-1}$ is the imaginary unit, and t is the discrete time. If the sample is sufficiently long, then the resolved frequencies are physically meaningful, and converge to a finite number of modes included in (4.1). Since a linear superposition hypothesis has been made so far, the following identity must hold:

$$A_{pn} = a_p e^{-ik_p x_n} + b_p e^{ik_p x_n}, \quad (4.4)$$

where $a_p, b_p \in \mathbb{C}^1$ and

$$a_p = |a_p| e^{i\phi_p} \quad (4.5a)$$

$$b_p = |b_p| e^{i\varphi_p}. \quad (4.5b)$$

Timeseries are recorded at two gauges, whose relative distance is $\Delta x = x_2 - x_1$. By means of straightforward algebra one can find the analytical expressions for incoming and reflected wave amplitudes, namely a_p and b_p . For the $p - \text{th}$

frequency band these are (Goda and Suzuki, 1976):

$$a_p = \frac{A_{p1}e^{ik_px_2} - A_{p2}e^{ik_px_1}}{2i \sin k_p \Delta x} \quad (4.6a)$$

$$b_p = \frac{A_{p2}e^{-ik_px_1} - A_{p1}e^{-ik_px_2}}{2i \sin k_p \Delta x}, \quad (4.6b)$$

while the observer phase shifts can be retrieved by:

$$\phi_p = \arg a_p \quad (4.7a)$$

$$\varphi_p = \arg b_p. \quad (4.7b)$$

The most evident practical limitation of this method is due to the singularities of (4.6), *i.e.* the wavenumbers satisfying $k = m\pi/\Delta x$, with $m \in \mathbb{N}_0$, can not be resolved. Hence the probes relative distance has to be designed, case by case, according to the expected wavelengths.

SANCHEZ AND CHEVALIER Recently Sanchez and Chevalier (2006) proposed a three equally spaced gauges method. In the following their equations are recovered, slightly modified in order to take into account non equally spaced gauges.

The method is based on the construction of the complex function:

$$F = \eta + i\chi, \quad (4.8)$$

where η is a linear wave packet (4.1) and

$$\chi = \sum_{j=1}^{\infty} \frac{\partial}{\partial k_j x} [a_j \cos(\omega_j t - k_j x + \phi_j) + b_j \cos(\omega_j t + k_j x + \varphi_j)]; \quad (4.9)$$

therefore

$$F = \sum_{j=1}^{\infty} [a_j e^{i(\omega_j t - k_j x + \phi_j)} + b_j e^{-i(\omega_j t + k_j x + \varphi_j)}]. \quad (4.10)$$

The right spectrum of F (positive frequencies) contains the whole set of incoming wave components, while the reflected wave components lie in the left spectrum of F (negative frequencies). The reflection coefficient can thus be obtained as the ratio of left over right first order spectral moments.

Passing at discrete variables, F is a timeseries evaluated at the reference gauge (WG_{n_1}), with η_n the sampled data and χ_n the 1st order difference computed with the discrete samples collected by the other two gauges (WG_{n_2} and WG_{n_3}). In the original method, WG_{n_1} is the central one (WG_2) and the three gauges are equally spaced. In general one can write:

$$\chi_{n_2} = \sum_{p=M/2-1}^{M/2} \frac{\cos k_p (x_{n_2} - x_{n_1}) A_{pn_3} - \cos k_p (x_{n_3} - x_{n_2}) A_{pn_1}}{\sin k_p (x_{n_3} - x_{n_1})} e^{ip\omega_0 t}, \quad (4.11)$$

and show that

$$\chi_{n_2}(t) = \sum_{p=M/2-1}^{M/2} \frac{\partial}{\partial k_p x} A_{pn} e^{ip\omega_0 t}. \quad (4.12)$$

This method suffers the same severe limitation of the one proposed by Goda and Suzuki (1976). In fact (4.11) is affected by the same singularities, and some wavenumbers would blow the relative component up.

4.1.2 LS METHODS

The opportunity of overcoming the singularities arisen in deterministic methods has been explored by a number of authors. To our knowledge, Mansard and Funke (1980) were the first ones who proposed a three gauges least squares method. This tool is basically intended for the minimization of errors due to the sampling apparatus noise and smoothing of actually measured nonlinearities. Later, Zelt and Skjelbreia (1992) expanded LS method to an arbitrary number of gauges, together with the introduction of a set of weighting parameters. The fundamental assumptions on the wave field are based on Airy point of view (4.1).

Some authors adapted the idea in order to recover more informations on the wave field. Among others, Grønbech et al. (1996) capture flume cross modes, Bakkenes (2002) use LS to separate long bound waves from the free ones in the near-shore region and Lin and Huang (2004) resolve at first approximation whole set of high and low frequency bound waves.

ZELT AND SKJELBREIA As already mentioned this method is based on Airy waves hypothesis. Incident and reflected wave Fourier coefficients, respectively A_{pn} and B_{pn} in (4.5), are searched for at a reference position (probe). Wave amplitudes are assumed to be constant in space, the measured event being thought stationary and periodic.

Anyhow, an error is admitted to be committed by the observer, allowing the measured timeseries to match (4.3). The p _{*t*}^{*h*} Fourier coefficients relative to the n – *th* gauge sample is assumed to be:

$$C_{pn} = A_{pn} + B_{pn} + \epsilon_{pn}. \quad (4.13)$$

The errors ϵ_{pn} included in (4.13) is intended to be a cumulative one, accounting for the following set of error sources: 1) gauges and hardware errors, such as: *a*) noise, *b*) non-linearities; 2) wave model mismatches: *a*) non-linear hydrodynamic effects, *b*) two dimensional wave motion (*e.g.* cross modes), *c*) viscous effects.

Probes calibration mistakes are here not intended as errors. Zelt and Skjelbreia (1992) search for the (a) minimum of the merit function:

$$E_p = \sum_{n=1}^N \mu_{pn} \epsilon_{pn}^2 \quad (4.14)$$

where μ_{pn} are a set of real positive valued weighting coefficients. This is not the function reported by Zelt and Skjelbreia (1992), but effectively the one that allow their final expressions and coincides with the one given by Mansard and Funke (1980).

Due to the quadratic feature of (4.14), its minimum is located in the \mathbb{C}^2 space where both derivatives with respect to a_p and b_p are zero. This traduces in a 2×2 linear system *i.e.* $\forall p \in \{-M/2 + 1, \dots, M/2\} \in \mathbb{Z}$:

$$\mathbf{Zu} = \mathbf{b} \quad (4.15)$$

where

$$\mathbf{Z} = \begin{bmatrix} \sum_{n=1}^N \mu_{pn} e^{-2ik_p x_n} & \sum_{n=1}^N \mu_{pn} \\ \sum_{n=1}^N \mu_{pn} & \sum_{n=1}^N \mu_{pn} e^{2ik_p x_n} \end{bmatrix}, \quad (4.16)$$

the vector of unknowns is

$$\mathbf{u} = [a_{pn} \quad b_{pn}]^T \quad (4.17)$$

and

$$\mathbf{b} = \left[\sum_{n=1}^N \mu_{pn} A_{pn} e^{-ik_p x_n} \quad \sum_{n=1}^N \mu_{pn} A_{pn} e^{ik_p x_n} \right]^T. \quad (4.18)$$

Matrix \mathbf{Z} (4.16) can be inverted only if its determinant:

$$\det \mathbf{Z} \propto \sum_{n=1}^N \sum_{q=1}^N \mu_{pn} \mu_{pq} \sin^2 k_p (x_n - x_q) \quad (4.19)$$

doesn't vanish, *i.e.*, for a given frequency $k_p (x_n - x_q) / \pi \in \mathbb{Z} \forall n, q$. This is again a practical limitation which limits the resolvable wavelengths whenever a gauges array is given. Anyhow, to avoid singularities, only a little care has to be taken when designing the experimental set-up. Furthermore, a large probe spacing would increment the errors due to deviation from linear celerity. The authors define the following heuristic "goodness" function:

$$\gamma_{pnq} = \frac{\sin^2 k_p (x_n - x_q)}{1 + [k_p (x_n - x_q) / \pi]^2}. \quad (4.20)$$

For a given circular frequency, a large value of (4.20) (better gauge spacing) means that $k_p (x_n - x_q) / \pi \notin \mathbb{Z}$ and relative probe spacing are not "too big". Starting from that, the weighting coefficients for the $n - th$ gauge are proposed to be

$$\mu_{pn} = \sum_{q=1}^N \gamma_{pnq}. \quad (4.21)$$

Analytic solutions are given by authors, however the numerical solution of (4.15) is not time consuming at all.

Finally, it is worth to notice that, in case of unitary weighting coefficients, this method includes some known particular cases such as Goda and Suzuki (1976)

($N = 2$) and Mansard and Funke (1980) ($N = 3$).

CROSS MODES IDENTIFICATION As previously mentioned, Grønbech et al. (1996) adapt the least squares method to account for flume cross modes. They basically admit that

$$A_{pn} = a_p e^{-ik_p x_n} + b_p e^{ik_p x_n} + c_p + \epsilon_{pn} \quad (4.22)$$

where c_p is the Fourier coefficient of the cross mode at p -th frequency band. This formulation suppose also that the gauges are placed in a line, parallel to the flume walls and orthogonal to the incident and reflected wave fronts. Skipping the already familiar LS procedure, the entries of (4.15) now read:

$$\mathbf{Z} = \begin{bmatrix} \sum_{n=1}^N \mu_{pn} e^{-2ik_p x_n} & \sum_{n=1}^N \mu_{pn} & \sum_{n=1}^N \mu_{pn} e^{-ik_p x_n} \\ \sum_{n=1}^N \mu_{pn} & \sum_{n=1}^N \mu_{pn} e^{2ik_p x_n} & \sum_{n=1}^N \mu_{pn} e^{ik_p x_n} \\ \sum_{n=1}^N \mu_{pn} e^{-ik_p x_n} & \sum_{n=1}^N \mu_{pn} e^{ik_p x_n} & \sum_{n=1}^N \mu_{pn} \end{bmatrix}, \quad (4.23)$$

$$\mathbf{u} = [a_p \quad b_p \quad c_p]^T \quad (4.24)$$

and

$$\mathbf{b} = \begin{bmatrix} \sum_{n=1}^N \mu_{pn} A_{pn} e^{-ik_p x_n} & \sum_{n=1}^N \mu_{pn} A_{pn} e^{ik_p x_n} & \sum_{n=1}^N \mu_{pn} A_{pn} \end{bmatrix}^T. \quad (4.25)$$

Analytic solutions can be computed with some algebra, however authors do not give them extensively. Anyhow, it is worth to notice that $\det \mathbf{Z}$ vanishes if

$$\sum_{n,q,r=1}^N \mu_{pn} \mu_{pq} \mu_{pr} \left[\cos(\Delta_{pnq} + \Delta_{pnr}) + 2 \cos \Delta_{pnq} - 2 \sin^2 \Delta_{pnq} \right] = 0 \quad (4.26)$$

where $\Delta_{pnq} = k_p (x_n - x_q)$. The latter condition must be avoided when designing a test set-up.

It must be pointed out that cross flume resonant modes are represented by standing waves. Hence, gauge placement at the centre of the channel would coincide with nodes of the series of odd cross modes, while these oscillations

would not be detected. It is then worth to place the gauges array line somehow away from the most probable nodes.

This method allow for the separation of flume channel cross modes without a great effort, thus reducing the sources of errors previously mentioned. It is therefore recommended to implement it when analysing data collected with more than 3 in line probes. If the number of instruments is $N = 3$ it reduces to a deterministic method, loosing its least squares minimization feature.

Increasing the number of gauges, would increase the length of the investigated domain, together with the uncertainties derived from the Airy wave celerity assumption. The following goodness function, which slightly modifies (4.20) is here proposed:

$$\gamma_{pnqr} = \frac{\cos(\Delta_{pnq} + \Delta_{pnr}) + 2 \cos \Delta_{pnq} - 2 \sin^2 \Delta_{pnq}}{1 + (\Delta_{pnq}/\pi)^2 + (\Delta_{pnr}/\pi)^2}. \quad (4.27)$$

BOUND LONG WAVES SEPARATION To second order Stokes approximation, waves impinging a beach force long free waves which travel back offshore together with the set of bound components. While the latter are phase locked to the fundamental components, the former travel with their own celerity. Their separation, throughout measurements analysis, is therefore wanted, heading to improvements in shore hydrodynamics knowledge.

These two sets (bound and free long waves) cannot be recognized by a time-frequency Fourier transform of surface displacement, just because they both belong to the same spectral bands. For that reason Bakkenes (2002) proposes an N gauges LS method which detects incident and reflected long bound wave components in shore regions.

The wave model (short wind waves) supposes a narrow band spectrum, so that long components can be clearly identified, therefore isolated by means of a low pass filter. In other words, the spectra of long and main components are disjoint. Hence, in the low frequency region, the Fourier coefficients are assumed to be composed by the sum of incoming and reflected bound components, plus reflected free components:

$$A_{pn} = \underline{a}_p e^{-ik_{2p}x_n/2} + \underline{b}_p e^{ik_{2p}x_n/2} + b_p e^{ik_p x_n} + \epsilon_{pn} \quad (4.28)$$

where the underline emphasizes bound components, and k_{2p} are the wavenumbers of the (1st order) main components. Note that no long free components are allowed. Care must be taken when recreating such a field in the lab, avoiding the generation of unwanted long waves (2nd order). The entries of (4.15) now read:

$$\mathbf{Z} = \begin{bmatrix} \sum_{n=1}^N \mu_{pn} e^{-ik_{2p}x_n} & \sum_{n=1}^N \mu_{pn} & \sum_{n=1}^N \mu_{pn} e^{-i(k_p - k_{2p}/2)x_n} \\ \sum_{n=1}^N \mu_{pn} & \sum_{n=1}^N \mu_{pn} e^{ik_{2p}x_n} & \sum_{n=1}^N \mu_{pn} e^{i(k_p + k_{2p}/2)x_n} \\ \sum_{n=1}^N \mu_{pn} e^{-i(k_p - k_{2p}/2)x_n} & \sum_{n=1}^N \mu_{pn} e^{i(k_p + k_{2p}/2)x_n} & \sum_{n=1}^N \mu_{pn} e^{2ik_p x_n} \end{bmatrix}, \quad (4.29)$$

$$\mathbf{u} = \begin{bmatrix} \underline{a}_p & \underline{b}_p & b_p \end{bmatrix}^T \quad (4.30)$$

and

$$\mathbf{b} = \begin{bmatrix} \sum_{n=1}^N \mu_{pn} A_{pn} e^{-ik_{2p}x_n/2} & \sum_{n=1}^N \mu_{pn} A_{pn} e^{ik_{2p}x_n/2} & \sum_{n=1}^N \mu_{pn} A_{pn} e^{ik_p x_n} \end{bmatrix}^T. \quad (4.31)$$

Usual considerations on $\det \mathbf{Z}$ singularities have to be done. Furthermore, since in shallow water regions triad interaction effects are enhanced, care must be taken on total probes array length. It should be verified that this dimension is sufficiently small compared to the main modulation beat length. This should be done in order to avoid interpreting the modulated amplitude of a travelling wave as a sum of incident plus reflected wave.

4.1.3 WEAKLY NON-LINEAR METHODS

Airy wave theory applied to signals projected onto discrete Fourier spaces may reveal its limitations for basically two interconnected reasons.

One is related to the FFT approach which underline a full stationary, even if periodic, point of view on the measured physics. In many cases events are highly transient, consider *e.g.* an N-wave or a solitary wave.

The second question is about the Airy phase celerity associated to a circular frequency. In case of non negligible wave steepness, Stokes bound wave com-

ponents cannot be neglected. Since they travel with the group celerity, they cannot be revealed by previous described method in a broad spectrum sea state.

Even if conventional Stokes and phase modulation 2nd order approaches may fail in shallow-intermediate waters, they are still a satisfactory point of view for most laboratory tests performed in intermediate-deep waters.

STOKES 2nd ORDER Some conundrums arise when trying to deterministically resolve a 2nd order sea state throughout a discrete Fourier decomposition. At a given frequency band the the main questions are related to the amount of energy of the local (in frequency terms) free wave and the other amounts relative to a set of bound waves. These can be deterministically determined by the free (1st order) components. The problem is how to detect the set of main components.

A frequent approach is the distinction of a principal spectral band, a sub-harmonic and a super-harmonic ranges. All the fundamental band couples are spanned, building tentative low and high frequency spectral bands (Lin and Huang, 2004). This would solve the problem in a narrow band sea state, but in a broad band the three regions are not disjointed. Furthermore, in a laboratory flume, free long and short waves must be admitted to exist at each frequency, even if not generated (*i.e.* suppressed) and even with most advanced absorption systems.

A practical solution may follow some iterations based on a satisfactory linear method together with a 2nd order Stokes-like formulation. Initially the measured data are assumed to be a superposition of Airy free waves, thus separated with *e.g.* Zelt and Skjelbreia procedure, to get the incident and reflected complex amplitudes, *i.e.* (a_p, b_p) for each frequency band centred at ω_p . The solution is used to construct the 2nd order components. For each couple (a_p, a_q), three super-harmonic ($G_{p,q}a_p a_q, p \leq q$) and one sub-harmonic ($G_{p,-q}a_p a_q^*$) are defined (Sharma and Dean, 1981) on local water depth h by transfer functions:

$$G_{p,q} = \tilde{\delta}_{p,q} \left[(\omega_p + \omega_q) \frac{H_{p,q}}{D_{p,q}} - L_{p,q} \right] \quad (4.32)$$

where

$$\tilde{\delta}_{p,q} = \begin{cases} \frac{1}{2} & p = q \\ 1 & \text{elsewhere} \end{cases} \quad (4.33)$$

and

$$H_{p,q} = (\omega_p + \omega_q) \left(\omega_p \omega_q - g^2 \frac{\mathbf{k}_p \cdot \mathbf{k}_q}{\omega_p \omega_q} \right) + \frac{1}{2} \left(\omega_p^3 + \omega_q^3 \right) - \frac{g^2}{2} \left(\frac{|\mathbf{k}_p|^2}{\omega_p} + \frac{|\mathbf{k}_q|^2}{\omega_q} \right) \quad (4.34a)$$

$$D_{p,q} = g K_{p,q} \tanh K_{p,q} h - (\omega_p + \omega_q)^2 \quad (4.34b)$$

$$L_{p,q} = \frac{1}{2} \left[g^2 \frac{\mathbf{k}_p \cdot \mathbf{k}_q}{\omega_p \omega_q} - \left(\omega_p^2 + \omega_q^2 \right) \right] \quad (4.34c)$$

with $\omega_{-p} = -\omega_p$, $\mathbf{k}_{-p} = -\mathbf{k}_p$ and $K_{p,q} = |\mathbf{k}_p + \mathbf{k}_q|$. The above notation is due to Schäffer and Steenberg (2003), and it has been chosen because of its compactness which eases implementation: sub and super-harmonics are collected into a single matrix which saves half memory. Note that (4.32) is not a pure number, but it has the dimension of a wavenumber ($[L^{-1}]$).

Once the 2^{nd} order components are built, they are subtracted from the original data, and the difference is passed again to the reflection analysis procedure. Algorithm stops when the norm of the components difference between two successive iteration reaches a desired tolerance. A detailed procedure is described in Prislín et al. (1997)

It must be mentioned that the kind of wave-wave interaction, hence the resulting modulation or second order description, does depend on the frequency interval of the interacting wave couple. This aspect must also be taken into account. The solution for that has been proposed by the next method.

DHWM The title acronym stands for "Directional Hybrid Wave Model" (Zhang et al., 1999), based on the 1D Hybrid Wave Model previously introduced by Zhang et al. (1996).

As revealed by Zhang et al. (1996), conventional Stokes perturbation approach (Longuet-Higgins and Stewart, 1960) and phase modulation approach (Phillips, 1981; Longuet-Higgins, 1987; Zhang and Melville, 1990) do not converge for

each interacting wave couple. The discriminant parameter is found to be the wavelength ratio of the shorter-wave to longer-wave component. HWM is, strictly speaking, a match between the two approaches. The distinction of principal spectral bands is done with reference to Fig. 4.2.

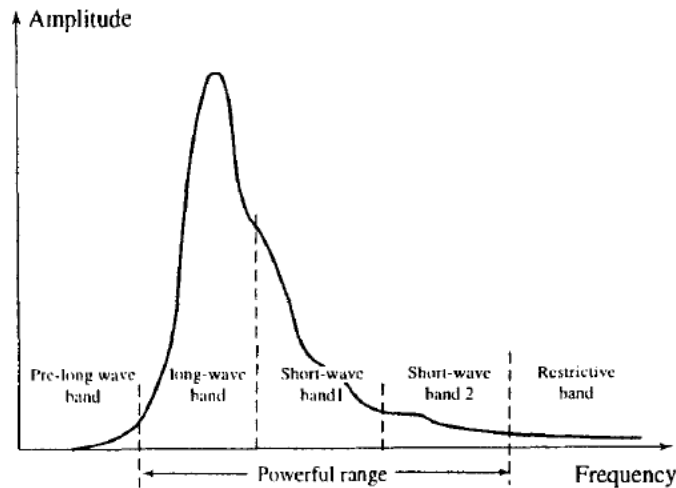


Fig. 4.2 – Frequency band division

Firstly the sampled signal is decomposed through FFT. Then, adopting the resulting spectrum as the image of a set of stationary free waves only (first order), each wave couple is analysed to get the interaction components. The non-linear components are firstly evaluated on the basis of long-wave band. If the shape of predicted long-wave spectrum (free+non-linear interactions) is close enough to the measured one, then the analysis move to the higher band. Else, predicted spectrum substitutes the primary one and computation is repeated until convergence. Similar, but not equally straightforward procedure is adopted for the shorter wave bands. For detailed description of band division adopted criteria and iteration steps please refer to Zhang et al. (1996).

DHWM is a further implementation of these concepts to formulate deterministic interpretation of a directional wave field in the frame of weakly non-linear wave state, up to second order in wave steepness. The above described algorithm loop is enriched at the beginning with a directional analysis, pursued throughout an extended maximum likelihood method, and another fitting procedure for identifying the initial phases.

4.2 TIME DOMAIN

4.2.1 DETERMINISTIC METHODS

FRIGAARD AND BRORSEN This method has been developed by Frigaard and Brorsen (1995) as a tool for real time reflection analysis to implement in a laboratory active absorption system (Frigaard and Christensen, 1995). The formulation is based on the same point of view of periodic stationary linear wave packet (4.1) propagating on uniform water depth described in Sec. 4.1. Wavenumbers are assumed to obey Stokes dispersion relation.

Wave elevation sampled at two gauges only are used, but the same principles can be extended easily to two distinct velocity probes, as showed later on by the author. Sampled signals are digitally filtered in time and then composed with simple arithmetic operations to directly get timeseries of incident and reflected waves.

It is worth to notice that the present method actually operates a mixed time-frequency domain, the time window corresponding to the filter length. In other words the wave field is assumed stationary inside each window. Since these windows are completely overlapping (except for the advancing time step), and the output are given at their centres, then it is included in this time domain section.

The design of the filters can be summarized as follows. One may want that the sum of the two filtered timeseries equals the incident wave field at a reference position, say WG_p , *i.e.* one wants to find the set of complex coefficients G which solves

$$\Re \left\{ \sum_{n=1}^2 G_n(\omega) \left[a(\omega) e^{-ik(\omega)x_n} + b(\omega) e^{ik(\omega)x_n} \right] e^{i\omega t} = a(\omega) e^{i(\omega t - k(\omega)x_p)} \right\} \quad (4.35)$$

By choosing $G_n = G_0 e^{i\phi_n}$, after some algebra, one can find three conditions which satisfy (4.35):

$$2G_0 \cos \frac{1}{2} (\Delta_{21} - \phi_2 + \phi_1) = 1 \quad (4.36a)$$

$$\Delta_{p2} + \Delta_{p1} + \phi_2 + \phi_1 + 4q\pi = 0 \quad \forall q \in \mathbb{Z} \quad (4.36b)$$

$$\Delta_{12} - \phi_2 + \phi_1 - \pi + 4r\pi = 0 \quad \forall r \in \mathbb{Z} \quad (4.36c)$$

where $\Delta_{np} = k(\omega) (x_n - x_p)$. The latter traduce in a reference gauge independent solution for the filter amplitude:

$$G_0(\omega) = -\frac{1}{2 \sin \Delta_{21}} \quad (4.37)$$

and two filter phases

$$\phi_1(\omega) = \Delta_{2n} + \frac{\pi}{2} \quad (4.38a)$$

$$\phi_2(\omega) = \Delta_{1n} - \frac{\pi}{2}, \quad (4.38b)$$

for the arbitrary choice of $q = 0$ and $r = 0$. Finally the frequency response function for the n^{th} gauge with reference to the p^{th} probe is:

$$G_1(\omega) = -\frac{ie^{i\Delta_{2p}}}{2 \sin \Delta_{21}} \quad (4.39a)$$

$$G_2(\omega) = \frac{ie^{i\Delta_{1p}}}{2 \sin \Delta_{21}}. \quad (4.39b)$$

It is worth to notice that these are the same coefficients which solve the two gauges problem in the frequency domain (Goda and Suzuki, 1976). Hence they suffer the same singularities of a deterministic linear method. The authors overcome this problem in the discrete frequency space by setting an upper threshold value for the gain, *i.e.* $|G| < 5$.

The main implementation steps involve the computation of the discrete convolution integral, *i.e.* the filtered timeseries

$$\bar{\eta}_n^{(m)} = \sum_{q=0}^{Q-1} g_n^{(q)} \eta_n^{(m-q)} \quad (4.40)$$

where $g_n^{(q)}$ is the impulse response of the digital filter at gauge n and q^{th} time step:

$$g_n^{(q)} = \sum_{r=0}^{Q-1} G_n(\omega_r) e^{ir\omega_q} \quad (4.41)$$

$\omega_r = r\omega_0$ is the r^{th} multiple of the frequency resolution $\omega_0 = 2\pi/T_{FIR}$ which corresponds to the filter length $T_{FIR} = Q\delta t$, and δt the sampling time step. The delay of the output with respect to input is $(Q/2 - 1)\delta t$.

Besides the singularities, another source of error is the mismatch between frequency resolution and physical frequencies. If they coincide there's no error, if not, the wave celerities are badly interpreted by the inversion of the dispersion relation, and a residue is wrongly deputed to the reflected wave. The practical solution adopted by the authors is the cosine tapering of the filter, which they show improves significantly the results.

DIRECT WAVENUMBERS RESOLUTION (DKR) One of the open issues in separating multi-directional wave fields is the accurate estimation of wave celerities. Wavenumbers are mostly computed proceeding from a more or less approximated dispersion relation which hold in their relative applicability ranges. The direct estimation of phase celerities from data samples...

Kitano et al. (2002) assumes that locally in time the wave field can be approximated by a sum of incident wave plus a reflected wave, which corresponding surface elevation signals are simple sinusoidal function of the phases. The sum of their quadratures can thus be determined by means of the Hilbert transform (HT) of the total signal, hence the following analytic signal holds¹:

$$\tilde{\eta} = \eta + i\hat{\eta} = ae^{i(\omega t - kx + \phi)} + be^{i(\sigma t + wx + \varphi)} \quad (4.42)$$

where

$$\hat{\eta}(t) = \int_{\mathbb{R}} \frac{\eta(s)}{t-s} ds \quad (4.43)$$

is the Hilbert transform of surface elevation (dashed integral stands for the Cauchy principal value integral). The whole set of unknown variables is assumed to be spatially stationary at current time t , but totally transient. Both

¹ In this case, amplitudes are real valued numbers and observer phases are grouped into the exponential argument to cope with common analytic signal notation.

frequencies and wavenumbers are different for the two linearly superimposed perturbations.

Assume (4.42) is known at three, equally spaced, reference points, *e.g.* $x_1 = x_2 - s$ and $x_3 = x_2 + s$. The couple of wavenumbers (k, w) can be obtained as combination of the three signals. Let define the two angles $\alpha = s(k + w) / 2$ and $\beta = s(k - w) / 2$, then

$$\tan \beta = -\Im \left\{ \frac{\tilde{\eta}_3 + \tilde{\eta}_1}{\tilde{\eta}_2} \right\} / \Re \left\{ \frac{\tilde{\eta}_3 - \tilde{\eta}_1}{\tilde{\eta}_2} \right\} \quad (4.44a)$$

$$\cos \alpha = \frac{1}{2} \left(\Re \left\{ \frac{\tilde{\eta}_3 + \tilde{\eta}_1}{\tilde{\eta}_2} \right\} \cos \beta - \Im \left\{ \frac{\tilde{\eta}_3 - \tilde{\eta}_1}{\tilde{\eta}_2} \right\} \sin \beta \right) \quad (4.44b)$$

Once the wavenumbers are known it is then straightforward to determine $\tilde{\eta}_{ip}$ and $\tilde{\eta}_{rp}$, respectively the incident and the reflected analytic signals at a reference position, *i.e.* x_p . The timeseries (η_{ip}, η_{rp}) are then recovered by taking the real part of these signals.

Notice that in this way no information on real amplitude and phases are required to get the wanted timeseries separation. If one requires these informations, then intrinsic frequencies may be computed by differentiating analytic signals phases with respect to time, *e.g.*

$$\omega(t) = \frac{\partial}{\partial t} \arctan(\arg \tilde{\eta}_{ip}) \quad (4.45)$$

and the amplitudes by taking their module:

$$a(t) = |\tilde{\eta}_{ip}|. \quad (4.46)$$

As ever, the practical implementation reveals some critical issues, the most of them related to the approximation of (4.43).

The infinite support of the integral in (4.43) is limited by the finite length of sampled timeseries. The authors show that the committed error depend on this length, and that it vanishes for sufficiently large time windows, being minimum at the centres of them and maximum at the sides. This hold in continuous time.

When passing at discrete numeric space, HT is frequently approximated by a

discrete convolution integral which, in most cases, is speed up with FFT sub-routines, taking advantage of Fourier Transform convolution theorem. Hence, HT is actually treated as a digital filter. Since for sinusoidal signals it does behave as a $\pi/2$ phase shifter, it is also frequently implemented as an option in FIR toolboxes. More detailed HT related discussions will be given in Ch.??.

The authors highlight some numerical issues. Firstly, they observe there's no proof concerning the boundedness of (4.44b) to unity, hence direct implementation may result in $\Im\{\alpha\} \neq 0$ (which actually is a proof that the local model is wrong). In addition to it, (4.44a) may face numerical oscillations, *e.g.* small α causes a nearly indeterminate 0/0 behaviour. Kitano et al. (2002) formulate a trick to overcome this problem. They observe that, invoking De L'Hospital theorem and exchanging variables

$$\begin{aligned} k - w &= \lim_{s \rightarrow 0} \frac{2\beta}{s} = - \lim_{s \rightarrow 0} \frac{\frac{\partial}{\partial s} \left(\Im \left\{ \frac{\tilde{\eta}_3 + \tilde{\eta}_1}{\tilde{\eta}_2} \right\} / s \right)}{\frac{\partial}{\partial s} \Re \left\{ \frac{\tilde{\eta}_3 - \tilde{\eta}_1}{\tilde{\eta}_2} \right\}} \\ &= - \frac{\frac{\partial}{\partial t} \Im \left\{ \frac{\tilde{\eta}_3 + \tilde{\eta}_1}{\tilde{\eta}_2} \right\}}{\frac{\partial}{\partial t} \Re \left\{ \frac{\tilde{\eta}_3 - \tilde{\eta}_1}{\tilde{\eta}_2} \right\}}. \end{aligned} \quad (4.47)$$

Therefore, in discrete time, if (4.44a) fails, it is replaced by

$$\tan \beta^{(m)} = - \frac{\Im \left\{ \frac{\tilde{\eta}_3 + \tilde{\eta}_1}{\tilde{\eta}_2} \right\}^{(m+1)} - \Im \left\{ \frac{\tilde{\eta}_3 + \tilde{\eta}_1}{\tilde{\eta}_2} \right\}^{(m-1)}}{\Re \left\{ \frac{\tilde{\eta}_3 - \tilde{\eta}_1}{\tilde{\eta}_2} \right\}^{(m+1)} - \Re \left\{ \frac{\tilde{\eta}_3 - \tilde{\eta}_1}{\tilde{\eta}_2} \right\}^{(m-1)}}. \quad (4.48)$$

Authors do not give any deterministic rule which help in detecting the above mentioned failures. Who writes notes that deviation from the solution does mainly depend on how β and α are computed. In fact arctan and arccos are defined in the half circle only, which causes uncontrolled π shifts in the solution. Wether this procedure leads to meaningful results or not should be verified. A simple way to do it is to check that the amplitude and phase spectra are disjoint (Bedrosian, 1963). Let's add an intuitive example which in some sense would quote last sentence. Consider the possibility of finding a time interval in which both the signal and its second derivative have the same sign. In such a case it is hard to think about a pure sinusoid since its second derivative is opposite in

sign. The simpler fitting function would be a sine shifted by a constant. If the incident wave or the reflected one present such a behaviour somewhere, then simply (4.42) does not hold.

It should be added that sampling time step and gauges spacing must be adapted case by case, since wavenumbers can be assumed stationary only in space and time ranges which ratio closely approximate the group celerity ω_k . In other words, the extracted data should nearly satisfy the following conservation equation

$$k_{,t} + \omega_k k_{,x} = 0 \quad (4.49)$$

which proceeds from the definition of wave phase of a locally linear perturbation.

4.2.2 WEAKLY NON-LINEAR METHODS

LASA The development of this method is due to Medina (2001). The first two letters in title acronym stands for "Local Approximation" which underline that a wave pattern is fitted to approximate locally (in time) N -gauges recorded water wave signals. The last two letters identify the algorithm used by the author to achieve the fitting, *i.e.* "Simulated Annealing". The local wave model is a linear superposition of incoming and reflected kind of bi-chromatic Stokes second order solutions, plus a constant shift. It can be rewritten as follows:

$$\begin{aligned} \eta = 2c + a_1 \cos \theta_1 + a_2 \cos \theta_2 + \underline{a}_1 \cos 2\theta_1 + \underline{a}_2 \cos 2\theta_2 \\ + b_1 \cos \vartheta_1 + b_2 \cos \vartheta_2 + \underline{b}_1 \cos 2\vartheta_1 + \underline{b}_2 \cos 2\vartheta_2 \end{aligned} \quad (4.50)$$

where the phases of incident and reflected components are

$$\theta_i = \omega_i t - k_i x + \phi_i \quad (4.51a)$$

$$\vartheta_i = \sigma_i t + w_i x + \varphi_i. \quad (4.51b)$$

Stokes linear dispersion relation governs the frequency-wavenumber couples (ω, k) and (σ, w) of, respectively, incident and reflected principal phases, while ϕ and φ denote the observer phase-shifts. This is the model described in the re-

ferred paper. The authors quote that other linear combinations of principal and bounded components have been investigated. It must be noticed that (4.50) is a limited Stokes model in the sense that it does not take into account the bound components generated by the interaction of distinct modes, *i.e.* $|\theta_1 \pm \theta_2|$ phased perturbations are not included.

The set of quantities that have to be estimated for completely resolving the wave field includes 17 dimensional variables, which are four frequencies ($\omega_1, \omega_2, \sigma_1, \sigma_2$), four observer phase-shifts ($\phi_1, \phi_2, \varphi_1, \varphi_2$), four free wave amplitudes (a_1, a_2, b_1, b_2), the mean level shift c and four bound wave amplitudes ($\underline{a}_1, \underline{a}_2, \underline{b}_1, \underline{b}_2$). The last quartet could be determined on conventional perturbation solution or phase modulation basis. Probably the author prefers to estimate it as a set of unknowns parameters, instead of adapting case by case the former or the latter deterministic theories (as done *e.g.* by Zhang et al. (1996)).

"Locality" is here intended in a relaxed sense: the model is considered stationary in time relatively to time-windows of duration T_w , but linear overlapping windows are used in order to minimize the error on parameters estimation. In other words, being $\eta(p)$ the resolved model (4.50) corresponding to the p^{th} window, the full signal is described by the following decomposition

$$\eta = \sum_{p=1}^P \gamma_p \eta(p) \quad (4.52)$$

where P is the total number of time windows and the triangular weights are

$$\gamma_p = \begin{cases} q - (p - 1) & q \in (p - 1; p] \in \mathbb{R} \\ p + 1 - q & q \in (p; p + 1) \in \mathbb{R} \\ 0 & \text{elsewhere} \end{cases} \quad (4.53)$$

The width T_w is evaluated on the basis of the whole timeseries spectral analysis, *i.e.* $T_w \approx \min\{T_{01}, T_v\}$, where $T_{01} = m_0/m_1$ is the spectrum mean orbital period, and T_v is the temporal peakedness parameter defined as the integral of signal variance spectrum divided by m_0^2 .

Assume that surface elevation timeseries are sampled at N wave gauges, then a system of $NPT_w/\delta t$ non-linear equations has to be solved with respect to $17P$ unknowns, being δ_t the sampling time step. The solvability condition requires

that the number of gauges is such that $N \geq 17\delta t/T_w$, *e.g.* two gauges would be sufficient for common laboratory conditions with $T_w \approx 2s$ and $\delta t = 0.05s$. However, these kind of trigonometric systems are full of attractive points which, in most cases, are fake solutions. Hence direct implementation of Newton-like algorithms may often lead to wrong solutions. The author the proposes the implementation of a technique which comes from artificial intelligence world. The optimization procedure comes under the name of Simulated Annealing and details of its implementation with respect to present case can be recovered in Medina (2001).

The method turns out to be very precise when applied to numerical data, and surprisingly stable with respect to noise. The goodness of the method has been given only in terms of overall MSE and no local singularities have been reported.

4.3 ERROR SOURCES AND LIMITATIONS

This section provides a general resume of the previous cited reflection analysis methods and their theoretical and practical limitations. Some of the methods are only discussed briefly, while others are also implemented and tested.

4.3.1 WAVE MODELS IN REFLECTION ANALYSIS

A great effort has been made in order to definitively solve reflection analysis with a small number of measurement points. All the proposed solutions given in literature, and revised in Ch. 4, can be resumed in three fundamental steps.

STEP 1 Firstly, an intelligible model for surface elevation is identified as a mapping $\eta : \mathbb{R}^d \rightarrow \mathbb{R}$ such that

$$\eta = \eta(t, \mathbf{x}, \omega, \mathbf{k}, a, \dots). \quad (4.54)$$

Usually (4.54) is enriched with some dependencies between variables, especially with a dispersion relation

$$\omega^2 = \Omega(\mathbf{k}, a, \dots). \quad (4.55)$$

STEP 2 The model is then approximate with the correspondent one based on discrete time and space variables ($\bar{\eta} \approx \eta$) to cope with a data sample discrete space. This procedure depends on the time resolution of the samples and the spatial distribution of the instruments. A set of equations is then built to match the discrete model with the samples:

$$F(\bar{\eta}, \mathbf{S}) = 0. \quad (4.56)$$

STEP 3 Finally comes the strictly speaking numerical part. The procedure adopted for solving (4.56) depend on its characteristics. Usually it is a linear system, or a set of linear systems, but in some cases it does involve transcendent functions. The formers can be directly inverted and, in some cases, solutions are already given in analytic form. The latter are very hard to be solved with common Newton methods and some more specific algorithms must be considered.

The choices in developing the preceding steps affects the following ones. In some cases, little approximations in the model lead to high advantages in the solution in terms of computational time, but the result can be physically meaningless. The efficiency of the optimal (if one exists) reflection analysis method should be a balance between its precision (in terms of results) and its numerical stability.

4.3.2 IS AN APPROXIMATED HYDRODYNAMIC MODEL REALLY NEEDED?

I want to discuss here about the choice of (4.54), and point out some notes which may be helpful in answering the title question.

In many cases authors consider analytic solutions of a linearised physics problem (such as Airy and Stokes ones):

$$\eta = \Re \left\{ \sum_{m=1}^M c_m e^{i\omega_m t} \right\} \quad (4.57a)$$

$$c_m = a_m e^{i(-k_m + \phi_m)} + b_m e^{i(k_m x + \phi_m)} \quad (4.57b)$$

$$\Omega = gk \tanh kh \quad (4.57c)$$

The application is made with respects to real problems which invalidate some hypotheses on which the analytic model is based on. For example (4.57) is a linear superposition of small amplitude waves, but in a so called irregular wave train a number of non negligible amplitude waves are usually observed. Furthermore one has to wonder if the observable components in a water wave timeseries are effectively stationary waves, *i.e.* if they really travel at their own phase speed. This comes together with the fact that the formalisms of (4.57) and a Fourier series are very similar, and the latter is adopted as an approximation of the former. But the match does make sense when the observer time window is not limited.

Some more detailed analytic solutions (Stokes 2^{nd} order or HWM) are used to get more detailed description of some so called non-linearities. A wavepacket of this kind

$$\eta = \Re \left\{ \sum_{m=1}^M (c_m + \underline{c}_m) e^{i\omega_m t} \right\} \quad (4.58a)$$

$$c_m = a_m e^{i(-k_m + \phi_m)} + b_m e^{i(k_m x + \phi_m)} \quad (4.58b)$$

$$\underline{c}_m = \sum_{p=1, p \neq m}^{P(m)} \underline{a}_p e^{i(-k_p + \phi_p)} + \underline{b}_p e^{i(k_p x + \phi_p)} \quad (4.58c)$$

$$\Omega = gk \tanh kh \quad (4.58d)$$

$$k_p \neq \Omega^{-1}(\omega_m) \quad (4.58e)$$

is considered to cope with non negligible wave steepness. Non-linearities are here intended in a weak sense, since the analytic solution comes from two successive linearised problems, and the result (4.58a) is still a linear superposition of monochromatic perturbations. What could be non-linear here is deputed to step two and three, *i.e.* the evaluation of the bound waves coefficients (4.58c), which can be determined on theoretical basis once (4.58b) are known. But the estimation could be linear also, this does depend on the kind of measuring instruments.

If the surface elevation is sampled with a sufficient spatial discretisation, then the same Fourier series likelihood can be adopted in space, and the wavenumbers, hence the celerities, directly estimated as spatial frequencies. Without

the need of a dispersion relation, and bypassing any second (or higher) order theory, at least verifying it. This traduces in a full Fourier-like point of view, stationary in space and time:

$$\eta = \Re \left\{ \sum_{m=1}^M \sum_{p=1}^P c_{mp} e^{i(k_{mp}x + \phi_{mp})} e^{i\omega_m t} \right\}, \quad (4.59)$$

where negative wavenumbers are of course allowed. As a consequence no hydrodynamic models are required to give an estimation of (4.59) since it is built up only starting with the hypothesis of linear superposing stationary monochromatic waves. The derivation from that of other physical quantities, such as pressure and radiation tensors, is not supported by any theory and may have no physical meaning. Anyhow, the definitions of reflection coefficients on spectral basis still hold.

The great game is the definition of a model which gets rid of the stationary point of view. In some sense, time window methods, do approach this need (Frigaard and Brorsen, 1995; Medina, 2001); even if some of them are not designed for it. Why can't we think that, for each direction of propagation, one and only one perturbation is passing at the observer place at a given time instant? Or at least that it passes in the observer region during a given time interval? If the motion is not stationary, then the local perturbation does not need to be described by an infinite sum of monochromatic waves, but only a few may be sufficient to estimate it. For example Medina (2001) uses a kind of Stokes second order solution, limited to super-harmonics only. There are also authors that treat the local wave as a linear superposition of two monochromatic waves travelling in two opposite directions (Kitano et al., 2002).

The goodness of each method is supported by the proposing authors, together with practical limitations for its applicability. In many cases the results does mainly depend much more on data manipulation and fitting procedures (Steps 2 and 3) than on the analytic model itself. As an example, one can easily compare the output of a LS-like approach on a linear wave packet, such as Zelt and Skjelbreia (1992), with a time window approach on a quite non-physical model such as Medina (2001). The results does not differ too much at first glance. Therefore, instead of trying to fit a very detailed model, approximating, and

loosing, the physics that are not involved, a more manageable adapting local tool would probably let the physics be interpreted in the post-processing, without forcing their observation.

4.3.3 AIRY MONOCHROMATIC WAVES

Assume that a linear Airy wave with amplitude a and frequency ω , traveling in positive x direction, is partially reflected from an obstacle at unknown distance by an amount ρ . The resulting surface elevation is then given by:

$$\eta = \Re \left\{ ce^{i\omega t} \right\} \quad (4.60a)$$

$$c = a \left[e^{i(-kx+\phi)} + \rho e^{i(kx+\phi)} \right] \quad (4.60b)$$

$$\Omega = gk \tanh kh \quad (4.60c)$$

FREQUENCY DOMAIN In order to assess the efficiency of a reflection analysis method for given frequency and ρ , let assume that (4.60) is measured by N in-line gauges, with a sampling frequency f_s for Δt s. Assume that a is a random variable with uniform probability in the interval $[0; 0.07\pi/k]$, and the same for ϕ and φ varying inside $[0; 2\pi)$. All these variables are independent, hence a Monte-Carlo approach can be used. Therefore, run the reflection method, with the random field as input, until the outputs of the method and their main statistics converge. Do this for all frequencies and reflection coefficient of interest.

For example, for a LS method, the convergence of the absolute error $\epsilon_\rho = E[\rho_{MC}] - \rho$ and its variance σ_ρ^2 has been considered (E is the expected value, and subscript MC denote the realizations vector). Iterations are stopped after the tolerance of 10^{-6} or the maximum number of 250 points is reached (minimum number of iterations is 10). Wave gauge spacing has been designed according to the best weighting coefficient (4.20) distribution for the range of frequencies $[0.01; 5]$ Hz, considering a minimum gauge spacing of 4 cm, according to common intermediate scale laboratory devices, and water depth is $h = 1m$. Fig. 4.3 shows the uncertainties revealed on reflection coefficient evaluation

for $N = 2$ (deterministic), $N = 3$ and 4 (least squares). The variance is mainly governed by the wave frequency: the worst points are concentrated around well defined band. As the number of gauges increase this band moves toward the lower frequencies and with a tail broadening in the same direction.

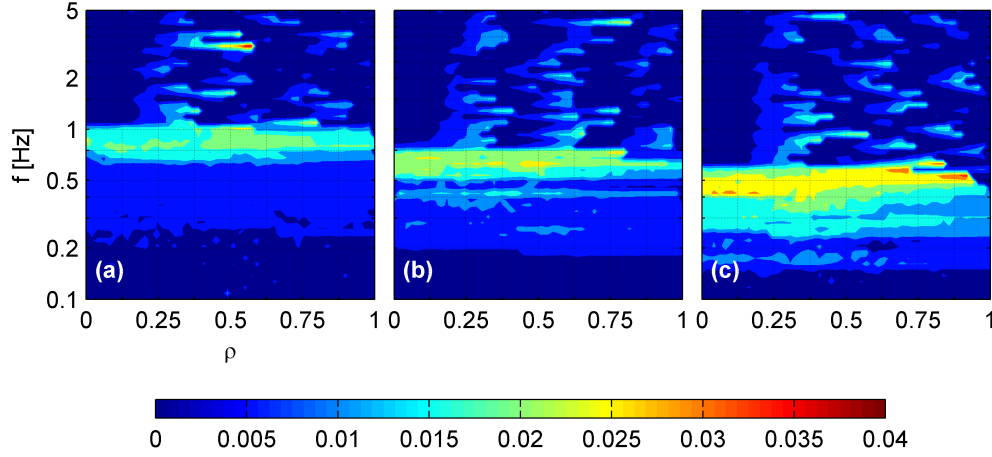


Fig. 4.3 – Variance on ρ evaluation in model (4.60) for LS methods: a) $N=2$ gauges (relative spacing is [0; 5] cm); b) $N=3$ ([0; 4; 9] cm); c) $N=4$ ([0; 5; 9; 13] cm). $f_s = 50\text{Hz}$ and $\Delta t = 100\text{s}$.

The same general behaviour is observed in Fig. 4.4 for the expected absolute errors. In this case ρ plays a fundamental role too: the bigger the reflection coefficient the lower the absolute error. The decay is linear in the low frequency region, and approximately super-linear in the upper region. The narrow band at approximately 4 Hz, in the $N=2$ case, corresponds to the region where (4.20) almost vanish.

Where the modulus of the absolute error plus the uncertainty have the same magnitude of ρ the methods are practically useless (shaded areas). Note that these high errors are due to the usual implemented low frequency cut-off, which enhances in case of either transient phenomena, or FFT frequency mismatches. For a given couple (ω, ρ) , the efficiency of a LS method does not depend upon the sampling frequency, nor the amplitude of the signal (Fig. 4.5), being the FFT frequency resolution an inverse function of the sample length Δt : the longer the data set, the smaller the frequency step, the better the evaluation.

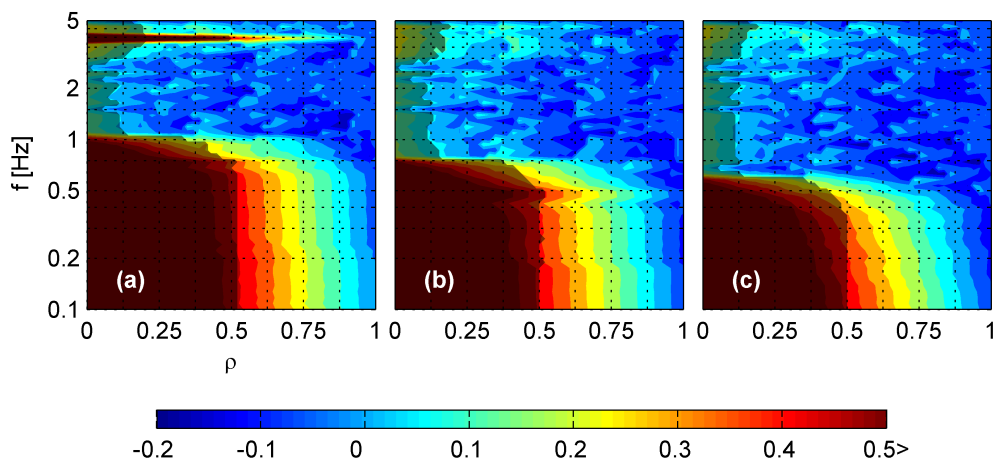


Fig. 4.4 – Absolute error ϵ_ρ in model (4.60) for LS methods. Symbols and parameters: same of 4.3, except for shaded area: $|\epsilon_\rho| + \sigma > \rho$.

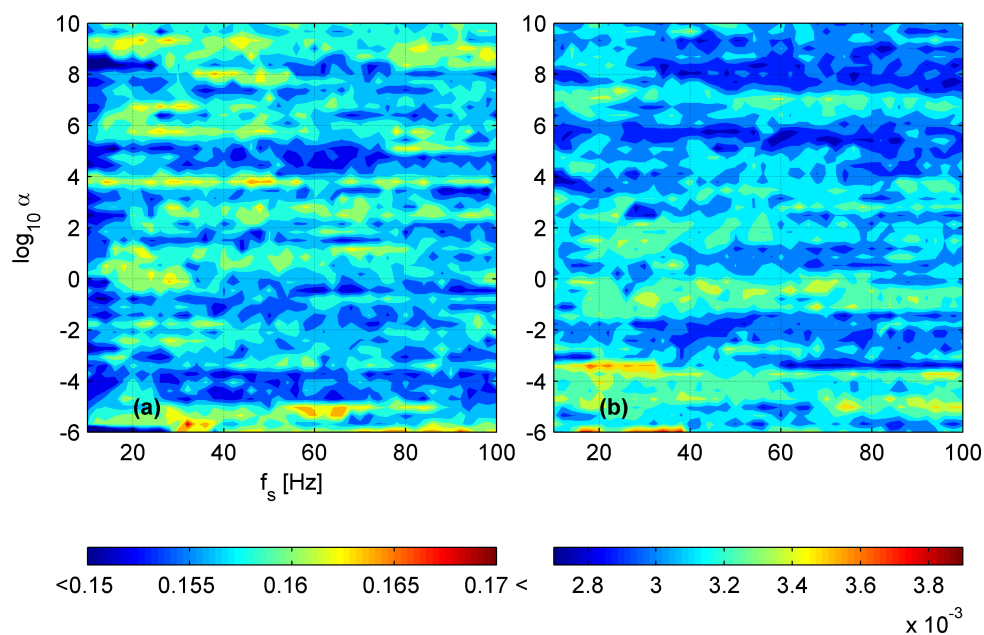


Fig. 4.5 – LS ($N=4$) sensitivity (MC) to sampling frequency and magnification amplitude for $\alpha\eta$ and η given by (4.60) with $\omega = 2\pi 1.033 \text{ rad/s}$, $\rho = 0.1$, $\Delta t = 20\text{s}$: a) ϵ_ρ ; b) σ^2

TIME DOMAIN For what concerns the time domain methods response to the simple model given by (4.60) the discussion must be split.

Apart from the half length filter delay of the optimal response, FB, the (FFT based) FIR approach introduced by Frigaard and Brorsen (1995) does behave

exactly in the same way as the classical frequency domain two gauges method. A slight improvement with respect to the latter is due to the singularities smoothing proposed by the authors. However, due to practical use, the finite length of the filter causes misjudgements in the frequency discretization. The response for a particular case of frequency mismatch is given in Fig. 4.6, together with the response of a generalized LS FIR filter, based on the least-squares coefficients of frequency domain methods.

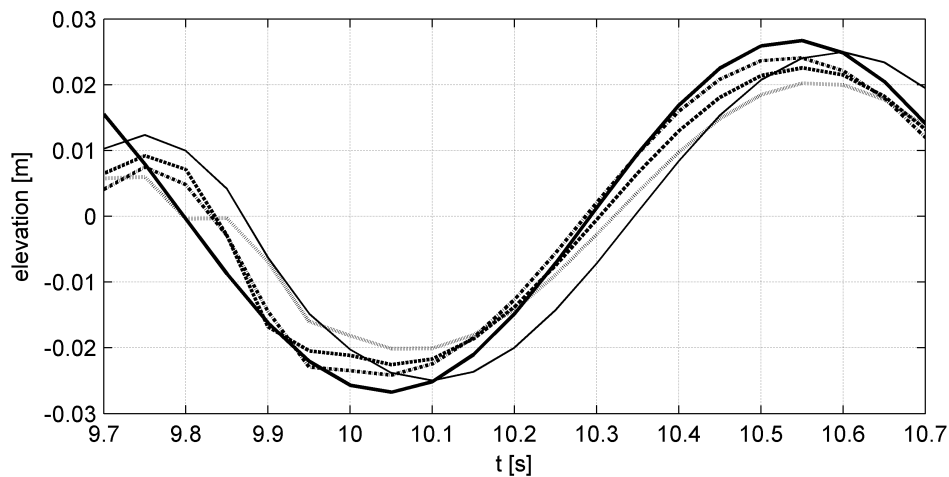


Fig. 4.6 – FIR filter outputs (incident wave) on (4.60) with $\omega = 2\pi 1.01 \text{ rad/s}$, $\rho = 0.5$, $\Delta t = 40\text{s}$, $\Delta t_{FIR} = 10\text{s}$: continuous line for true data; dashed, FB; dotted, GFB N=2; dash-dot, GFB N=3; thin continuous, GFB N=4.

The Hilbert transform based DKR of Kitano et al. (2002) does not suffer any frequency resolution problem of this kind. This is one of the main advantages. On the other hand it has to be stabilized in some way, since, as also reported by the authors, (4.44) are usually governed by strong singularities. As a consequence of that, the phases, and therefore the elevation timeseries, present a number of unwanted spikes. The inventors propose a change of variable in the equations, which in practice do linearly interpolate the data where these spikes occur. In the next chapter a useful tool will be introduced, which does help in the elimination of the spikes. Apart from that, the errors of this approach are only 2 orders of magnitude far from machine double precision (see Fig. 4.7). For what concerns the LASA approach nothing can be reported, since I did not get to a satisfactory, *i.e.* sufficiently robust and fast, implementation of Simulated Annealing algorithm. Medina (2001) reports an example based on (4.60)

showing negligible errors. If a proper implementation is achieved, in this case, there's no reason for the errors on the resolved parameters not being on the order of the SA imposed tolerance.

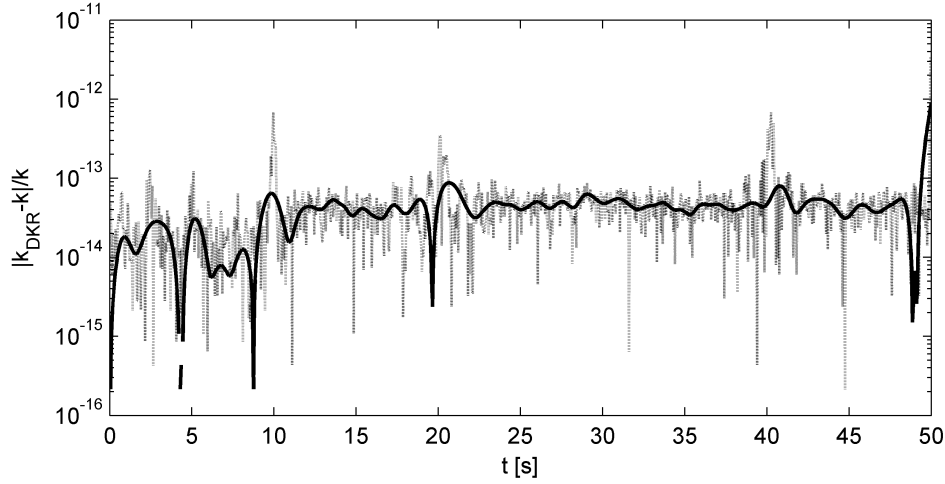


Fig. 4.7 – DKR wavenumber evaluation relative error on (4.60) with $\omega = 2\pi 1.01 \text{ rad/s}$, $\rho = 0.5$, $\Delta t = 40\text{s}$: dashed line, original method; continuous line, EEMD smoothed data set (see next chapter for EEMD).

4.3.4 INSTRUMENT NOISE

Assume that the overall acquisition system (gauges, wires, A/D interfaces, machine and software) do impose to the pure signal (4.60) an unknown noise v .

$$\eta = \Re\{ce^{i\omega t}\} + v \quad (4.61a)$$

$$c = a \left[e^{i(-k+\phi)} + \rho e^{i(kx+\phi)} \right] \quad (4.61b)$$

$$\Omega = gk \tanh kh \quad (4.61c)$$

In testing a process of this kind, the latter is usually intended in a Gaussian sense, with zero mean and an imposed variance. Its features, for a given acquisition system, can be deduced with a statistical analysis of still water samples. To get a better estimate one may want to verify the noise behaviour according to samples of known displacements. Since part of the acquisition system is unique for all signals a partial correlation between them should be expected.

An example is given in Fig. 4.8.

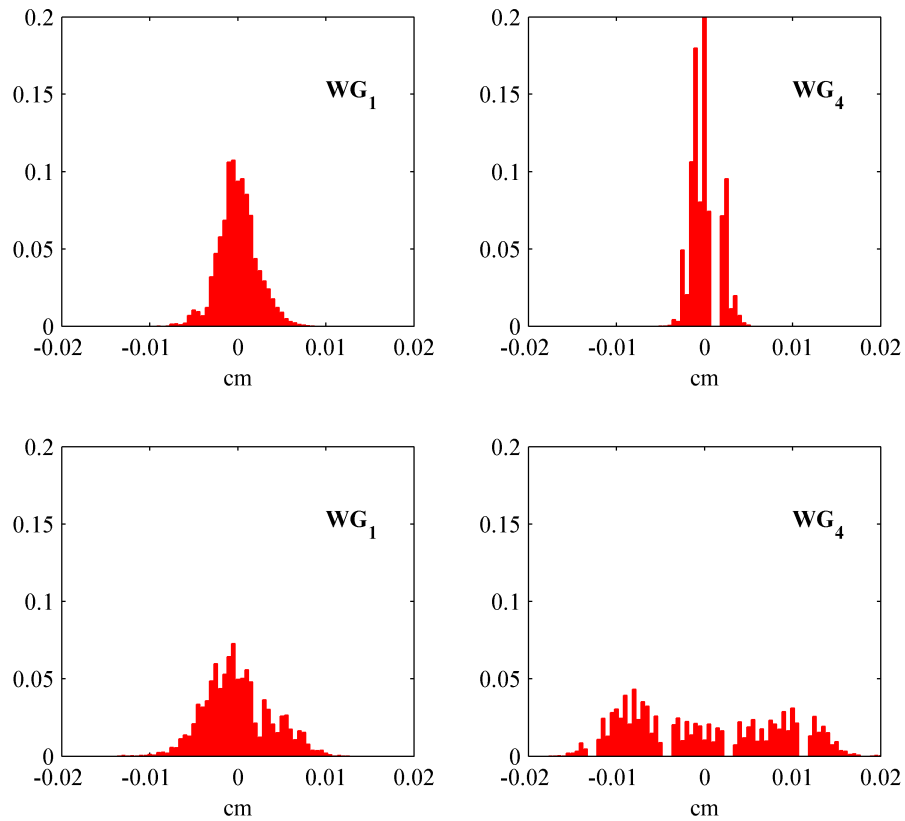


Fig. 4.8 – Normalized occurrence of sampled signal noise. In first line, wave generation system is off, and WG cross-correlation is 0.16; in second line, the system is on and cross-corr. is 0.39. The kind of noise is affected in a different way for each channel and distributions are not always Gaussian.

LS methods were designed to minimize the response due to these kind of unwanted inputs. By weighting the signals of different gauges, the noise-based error should decrease with the number of measurement points. Same considerations can be added for multi-gauge FIR based analyses. LASA noise response has been reported to be surprisingly good (Medina, 2001). Direct wavenumber resolution operations are based on three signals, which noise can strongly affect the results, hence a pre processing de-noising procedure should be wished.

4.3.5 WEAKLY NON-LINEAR WAVES (STOKES)

As far as waves present non negligible amplitudes (4.60) does not hold, and a better approximation for a regular wave would be a second order Stokes solution (4.62).

$$\eta = \Re \left\{ c e^{i\omega t} + \underline{c} e^{2i\omega t} \right\} \quad (4.62a)$$

$$c = a \left[e^{i(-k+\phi)} + \rho e^{i(kx+\phi)} \right] \quad (4.62b)$$

$$\underline{c} = ka^2 G \left[e^{2i(-k+\phi)} + \rho^2 e^{2i(kx+\phi)} \right] \quad (4.62c)$$

$$G = \cosh kh (\cosh 2kh + 2) \sinh^{-3} kh \quad (4.62d)$$

$$\Omega = gk \tanh kh \quad (4.62e)$$

The bounded components (\underline{c}) travel at the same celerity of the main components, therefore methods based on (4.60) (such as LS and FB) do not correctly evaluate it. Airy based solutions, in fact, do evaluate the wavenumber of the 2ω component as $\Omega^{-1}(2\omega)$ instead of $2\Omega^{-1}(\omega)$. Anyhow, as far as the concern is about regular waves, a deterministic evaluation of the parameters in (4.62) is easy to implement as an extension of linear based methods. However, in an irregular waves framework, a straightforward solution can not be achieved due to the coexistence of a free and several bound components at a given frequency. In this case, an iterative approach has to be designed (consider for example the DHWM).

4.3.6 NON STATIONARY WAVES

Assuming no interaction between components, an irregular wave field is usually approximated with a linear superposition of elementary modes. Let neglect here both standing waves, set ups, and other distortions, and focus on the periodic travelling part of a second-order Stokes-based formulation. Proceeding from that, one has to admit that a number of modes coexist at each frequency. These are described as a *free* wave (travelling with its own celerity) and a number of *bound* waves which travel at celerities governed by quadratic

interactions of free waves couples. Trigonometric manipulation of such a solution, considering a finite number of components and referring everything to free waves, leads to the following Fourier-like formulation.

$$\eta = \Re \left\{ \sum_{m=1}^M c_m(x) e^{i\omega_m t} \right\} \quad (4.63a)$$

$$c_m = \tilde{a}_m e^{i(-k_m x + \tilde{\phi}_m)} + \tilde{b}_m e^{i(k_m x + \tilde{\phi}_m)} \quad (4.63b)$$

in which the m^{th} wavenumber is the linear dispersion relation solution for the m^{th} frequency. Both amplitudes and phases result to be non-stationary. The ones related to the incident part are defined as

$$\tilde{a}_m^2 = \sum_{i=1}^{P(m)} \sum_{j=1}^{P(m)} a_i a_j \cos \Delta_{ij} \quad (4.64a)$$

$$\tan \tilde{\phi}_m = \frac{\sum_{i=1}^{P(m)} a_i \sin \Delta_{im}}{\sum_{i=1}^{P(m)} a_i \cos \Delta_{im}} \quad (4.64b)$$

where $\Delta_{ij} = [(k_j - k_i)x - \phi_j + \phi_i]$. Correspondent relations can be derived for the reflected modes. Now let define $a_{max} = \max\{a_i\}$, and $\alpha_i = a_i/a_{max}$, then the variation of envelope of incoming waves can be written as

$$\tilde{\alpha}_{m,x} = \frac{\sum_{i,j=1}^{P(m)} \alpha_i \alpha_j (k_i - k_j) \sin \Delta_{ij}}{2 \left(\sum_{i,j=1}^{P(m)} \alpha_i \alpha_j \cos \Delta_{ij} \right)^{1/2}} \quad (4.65)$$

which is a bounded quantity, in fact

$$0 \leq |\tilde{\alpha}_{m,x}| \leq \frac{\sum_{i,j=1}^{P(m)} \alpha_i \alpha_j |k_i - k_j|}{2 \left(\sum_{i,j=1}^{P(m)} (-1)^{1-\delta_{ij}} \alpha_i \alpha_j \right)^{1/2}} \quad (4.66)$$

where δ_{ij} is the Kronecker symbol.

The (4.66) states that in a finite amplitude framework, stationary Fourier-like components probably never exist. Hence linear wave superposition do involve celerities misjudgements especially in short and long waves. The beat-lengths of the envelopes are governed by the stronger products $\alpha_i \alpha_j$ which weight the lengths $2\pi/|k_i - k_j|$.

Most laboratory experiments are designed for testing the response of beaches and structures under strong events. In these cases the Airy small amplitude hypotheses do often fail, and the researcher has to deal with this kind of nonlinearities. In general, the higher the tested wave, the bigger the error committed when considering it as a superposition of linear waves.

Deterministic approaches has been proposed (only) up to second order expansion in a Fourier-like framework, so far. LS methods include the non-stationarity features inside the minimized overall errors, giving an average Airy based result for the gauges observation region. But, moving the gauges causes slightly different results.

LASA method assumes a local model which is something in between a deterministic second order and a linear wave. Therefore it may be helpful in detecting phases which do not travel at linear celerity. However, these are defined as bound waves of the single main components, and a deterministic dispersion relation is always included. As a consequence of that, other components which are not included in the local model can not be revealed, as can be deduced in Fig. 3 in Medina (2001).

DKR does not consider any non-stationary feature in the wave model. Hence each spatial variation of the envelope is detected as there were a superposition of two opposite travelling waves. As in the case of each linear based method.

4.3.7 TRANSIENT WAVES

Expressions in (4.64) are to be considered only an approximation which is valid to determine a relative small amplitude waves local water level. In principle each spatial variation of a quantity should be balanced somehow. In a mono-dimensional framework, this aspect is described by a conservation equation of the kind

$$\frac{\partial}{\partial t} (\cdot) + \frac{\partial}{\partial x} (c \cdot) = S \quad (4.67)$$

with c a characteristic celerity, and S a general source. For example, if the enclosed quantity is the description of a wave shape, *i.e.* its associated phase:

$$\theta = \int \omega dt - \int k dx + \phi \quad (4.68)$$

then it can be written

$$\frac{\partial k}{\partial t} + \frac{\partial \omega}{\partial k} \frac{\partial k}{\partial x} = 0 \quad (4.69)$$

which states that the wavelength travels in the phase space on the group celerity line.

Consider the quantity called *wave action* usually identified as $A = E/\sigma$ (where E is local energy and σ the local intrinsic frequency). If a single mode exists, this quantity also follows a conservation law:

$$\frac{\partial A}{\partial t} + \frac{\partial}{\partial x} (c_g A) = 0 \quad (4.70)$$

in which $c_g = \partial\omega/\partial k$ is group celerity. Conservation of fluxes is not guaranteed in a multi-modes system Hayes (1970). Anyhow, since local energy has to deal with the envelope, an amplitude spatial variation should be balanced with an amplitude modulation. As far as a measured signal is decomposed into a set of Fourier modes, in frequency domain the transient features of the wave motion are misinterpreted. For example the ramp up-ramp down of the beginning-end of a laboratory test, which are usually pursued varying the stroke amplitude while keeping constant frequency, are projected into Fourier space as long wave components. And stationary based methods do reveal an amount of partial reflection in these regions. A usual solution to that is the exclusion from the analysed data set of these known transient states; but there may be others which are not known. Windowed approaches does in principle help, as far as window (filter) lengths are sufficiently small compared to the modulations, and spatial gauges relative positions are of the same order. DKR does resolve transient wavenumbers and envelopes, but their consequent spatial variation is excluded.

Transient wave features can be observed in an alternative space only, *e.g.* through decomposition into a mixed time-frequency space, and following quantities paths (amplitude, phases, ...) in their characteristic spaces. This discussion, and what should come from it, does definitively crash with the *incident-reflected* paradigm and all actual reflection analysis methods.

4.3.8 OTHER ERROR SOURCES

Wave flume experiments may be corrupted by the growing of disturbances which deviate the motion from the pure idealistic 2DV features. It is a common practice to avoid generation close to facility resonant frequencies, especially in case of regular waves tests. For these wave fields, due to the regular forcing of the paddle, near-resonant phenomena enhance in magnitude. These phenomena are hardly observed in most irregular wave fields (Grønbech et al., 1996).

5 MODULATED WAVES

As seen in previous chapter, the correct decomposition of a wave field into free and bound waves is a hard task. The need in distinguishing between these components is related to the correct evaluation of their celerities, which final scope is the evaluation of corresponding travelling quantities. This chapter discuss on the possibility of pursuing such analyses proceeding from empirical mode decomposition (EMD). This recently introduced technique suffers some limitations when applied to wave flume waves. An improvement for smoothing the mode mixing phenomenon is proposed.

5.1 AM-FM DECOMPOSITION

If the phenomena to be interpreted are highly transient, then the standard frequency domain decomposition leads to identify waves in a space and time where no waves exists. Consider as an example the Fourier set of components of a Dirac delta function, which spectrum does affect the whole frequency space in a uniform way.

This feature has moved a lot of researchers to define more suitable tools for the analysis of a digital signal. The key for the development of these new points of view is the observation of the DS in a mixed time and frequency domain, or better the observation of the frequency content of limited parts of the signals. These limited parts, or "windows", must have well defined properties in order to accomplish certain dualities similar to Fourier and Inverse Fourier Transforms. One of the pioneers is *Gabor* time window applied to FT, from which basis the integral *Wavelets* transforms were derived. The latter are considered to be *the tool* for the analysis of transient signals. And this is due to the fact that their mathematical bases are well formed.

The *finite* length of the wavelet, or window, is actually the limit which defines

the locality of the analysis. In other words, this approach does not fully satisfy the need for extracting signals instantaneous features, and sudden changes in intrinsic properties may not be revealed. For that reason, some attempts on the use of *Hilbert* transform were done by a number of researchers.

5.1.1 HILBERT TRANSFORM

The Hilbert Transform \hat{f} of the function f is defined as (King, 2009a)

$$\hat{f}(t) = \frac{1}{\pi} \rlap{-}\int_{\mathbb{R}} \frac{f(s)}{t-s} ds \quad (5.1)$$

where the dashed integral means that the Cauchy principal value must be taken. For some functions, their HT is very manageable. For example, \sin 's is just itself with a $\pi/2$ phase shifted argument (*i.e.* its *quadrature*). Proceeding from that, if $f = a \cos \theta(t)$, with $a_{,t} = 0$, then

$$\mathcal{A}(f) = f + i\hat{f} = ae^{i\theta(t)}. \quad (5.2)$$

The latter is called the *analytic signal* representation of f (King, 2009b). The amplitude is readily given by $|\mathcal{A}(f)|$ and the phase can be retrieved as $\arg f + i\hat{f}$. The derivative of the phase angle with respect to time is usually defined as instantaneous frequency of f :

$$\omega(t) = \theta_{,t}. \quad (5.3)$$

If the representation is given in space also, then the instantaneous wavenumber vector can be retrieved

$$\mathbf{k}(t) = -\nabla\theta. \quad (5.4)$$

5.1.2 TWO IMPORTANT THEOREMS

If $\omega_{,t} \neq 0$ then the signal is said to be frequency modulated (FM). In case of amplitude modulation (AM) the representation (5.2) may be ambiguous as states the following

Bedrosian's Theorem. (Bedrosian, 1963) Let $f(t)$ and $g(t)$ denote two L_2 complex function of real variable t , which Fourier transforms are $F(u)$ and $G(u)$. If one of the following two propositions is true:

a) the supports of the two Fourier transforms are disjoint in the way that

$$\begin{aligned} \text{supp}\{F(u)\} &= \{u \in \mathbf{R} \mid |u| < a\} \\ \text{supp}\{G(u)\} &= \{u \in \mathbf{R} \mid |u| > a\}, \end{aligned}$$

b) f and g are both analytic, i.e. their real and complex parts are Hilbert couples, then

$$\widehat{fg} = f\hat{g}.$$

Hence we can be sure that $\Re\{a(t)e^{i\theta(t)}\} = a(t)\cos\theta(t)$ only if it satisfies the first Bedrosian hypothesis (being both amplitude and phase real valued function of time). The local properties of an AM-FM modulated wave can thus be studied in a Hilbert fashion only if the AM spectrum is disjointed from the FM one. However this is only a sufficient condition, and there's no way of checking it *a priori*. An error evaluation on the features of HT is given by the following

Nuttall's Proposition. (Nuttall, 1966) Let $f(t) = a(t)\cos[\omega_0 t + \phi(t)]$ be an AM-FM signal with imposed modulations $a(t)$ and $\phi(t)$, $\mathcal{Q}f(t) = a(t)\sin[\omega_0 t + \phi(t)]$ its quadrature and \hat{f} its HT; and let $S(\omega) = \int_{\mathbf{R}} a(t)\exp i[\phi(t) - \omega t]dt$ be the spectrum of the modulations. Then, the energy difference between Hilbert transform and quadrature is given by twice the energy in S below $-\omega_0$, i.e.

$$\begin{aligned} E &= \int_{\mathbf{R}} [\hat{f}(t) - \mathcal{Q}f(t)]^2 dt \\ &= 2 \int_{-\infty}^{-\omega_0} |S(\omega)| d\omega \end{aligned}$$

The evaluation of (5.1.2) needs the knowledge of the modulation couple, when not the exact quadrature, making it useless for many practical applications. It must be added that it is an average measure of the committed error, and therefore gives no local informations of its distribution along the data sets.

5.1.3 FINITE HT

Truncated HT is the name which identifies the same integral (5.1) but evaluated on a interval $[a, b] \subseteq \mathbb{R}$, and not on the whole \mathbb{R} . When the integration extremes are symmetric with respect to origin, then the integral is named *Finite* HT:

$$\hat{f}_a(t) = \frac{1}{\pi} \int_{-a}^a \frac{f(s)}{t-s} ds \quad a \in \mathbb{R}^+ \quad (5.6)$$

In practical engineering applications one has to treat with finite and discrete signals. It is worth to evaluate, at first, the error committed in the finite continuous case. For example, consider the FHT of the function $f(t) = \sin t$ (King, 2009a):

$$\begin{aligned} \hat{f}_a(t) &= \frac{1}{\pi} \int_{-a}^a \frac{\sin s}{t-s} ds = \int_{-1}^1 \frac{\sin as}{t-s} ds = \\ &= \frac{\sin t}{\pi} [\text{Ci}(a+t) - \text{Ci}(a-t)] \\ &\quad - \frac{\cos t}{\pi} [\text{Si}(a+t) + \text{Si}(a-t)] \end{aligned} \quad (5.7)$$

where

$$\text{Ci}(z) = \text{fl} + \log z + \int_0^z \frac{\cos y - 1}{y} dy \quad (5.8a)$$

$$\text{Si}(z) = \int_0^z \frac{\sin y}{y} dy \quad (5.8b)$$

and fl is the Euler's constant. Hence

$$E[\hat{f}_a(0)] = \left| \hat{f}(0) - \hat{f}_a(0) \right|^2 = \left(1 - \frac{2}{\pi} \int_0^a \frac{\sin y}{y} dy \right)^2 \quad (5.9)$$

from which

$$\lim_{a \rightarrow \infty} E[\hat{f}_a(0)] = 0. \quad (5.10)$$

It is then expected that for a finite signal, the wider the time interval the lower the error on evaluating its quadrature (see Fig. 5.1).

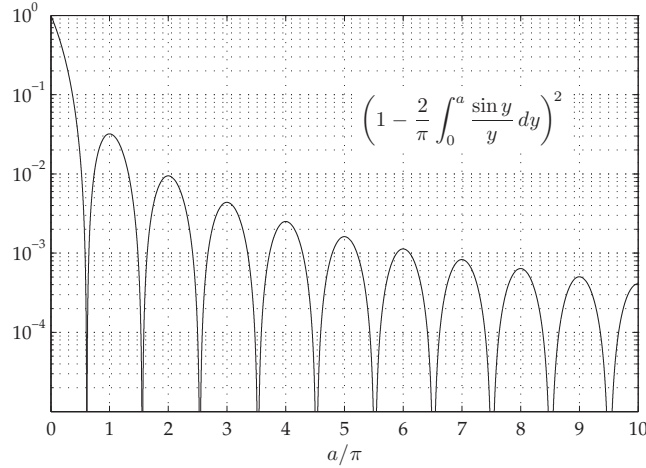


Fig. 5.1 – Distance of FHT (\hat{f}_a) from HT (\hat{f}) defined at the centre of the interval for $f(t) = \sin t$

5.1.4 DISCRETE HT - IMPLEMENTATION

In digital signal processing there exist different techniques for evaluating the quadrature of a signal. The most common implementations of Discrete HT are developed on the similarity of (5.1) with a $1/\pi t$ convolution integral. The latter can be computed in discrete frequency domain via an FFT approach, which takes advantage of FT and convolution relation:

$$\mathcal{F} [\hat{f}(t)] (\omega) = \mathcal{F} \left[\frac{1}{\pi t} * f(t) \right] (\omega) = \mathcal{F} \left(\frac{1}{\pi t} \right) \mathcal{F} [f(t)] (\omega) \quad (5.11)$$

This direct approach has several limitations because the whole signal is needed. In fact the application to non-overlapping data sub-sets introduces errors due to the discretization, eventually leading to negative frequencies inside the set. Moreover, the practical application in real-time is also prevented.

In order to overcome this sort of limitations, a FIR filter can be designed. In this case the Hilbert transfer function which has to be implemented is simply

$$\mathcal{H} (\omega) = -i \operatorname{sgn} \omega = \mathcal{F} \left(\frac{1}{\pi t} \right) \quad (5.12)$$

It can be shown that the discrete sequence $h^{(m)}$ which satisfy the need

$$\mathcal{H} (\omega) = \sum_{m=-\infty}^{\infty} h^{(m)} e^{-i\omega m} \quad (5.13)$$

is the following ideal impulse response

$$h^{(m)} = \begin{cases} \frac{2}{\pi m} \sin^2\left(\frac{\pi m}{2}\right) & m \in \mathbb{Z}, m \neq 0 \\ 0 & m = 0. \end{cases} \quad (5.14)$$

There are some tips to be considered when designing a FIR filter. An odd impulse response length (type IV) Hilbert filter (Parks-McClellan algorithm) should rather be better than an even length one, for the response of the latter is half a data step shifted. The former still present some problems close to zero frequency and half sampling frequency neighbourhood. Anyhow, for our practical applications this is not a trouble since the most of energy is concentrated inside a narrow region. Reilly et al. (1994) propose a *complex filter* approach which helps in solving most FIR limitations.

5.1.5 HT AND WATER WAVES

The analytic signal representation (5.2) is very manageable and we would like to see if it can be used in reflection analysis.

To our knowledge, one of first attempts of observing water wave features in a Hilbert fashion were pursued by Melville (1983). HT is linear in its arguments, that is $\widehat{af + bg} = a\hat{f} + b\hat{g}$, with a and b constant. It follows that for $f = \sum_i a_i \cos \theta_i(t)$, with $a_{i,t} = 0$

$$f + i\hat{f} = \sum_i a_i e^{i\theta_i(t)}. \quad (5.15)$$

Hence a wavepacket must be first decomposed in order to get its analytic representation. A simple way of overcoming Bedrosian theorem is then band pass filtering, in order to treat separated narrow banded signals, which amplitudes frequencies are lower than the carrier ones.

For a single mode travelling in one direction, and sampled at a number N of gauges, its features can be determined by simple first differences of the analytic signals $\{ \eta_n = a_n e^{i\theta_n}; n = 1, 2, \dots, N \}$.

At m^{th} time step one gets

$$\omega_n^{(m)} = \left(\theta_n^{(m+1)} - \theta_n^{(m)} \right) / \left(t_n^{(m+1)} - t_n^{(m)} \right) \quad (5.16a)$$

$$k_{n+\frac{1}{2}}^{(m)} = \left(\theta_n^{(m)} - \theta_{n+1}^{(m)} \right) / \left(x_{n+1}^{(m)} - x_n^{(m)} \right) \quad (5.16b)$$

$$a_{n+\frac{1}{2}}^{(m)} = \left(a_n^{(m)} + a_{n+1}^{(m)} \right) / \left(x_{n+1}^{(m)} - x_n^{(m)} \right) \quad (5.16c)$$

Let again stress on the fact that the results of the latter discrete evaluations must be verified through determination of correspondent group celerity, and should approximately suite a discrete version of (4.49), for which $N > 2$ gauges are needed.

5.2 EMPIRICAL MODE DECOMPOSITION

If $c_{,t} = 0$ then $\hat{c} = 0$, which leads to the fact that the HT of a function is independent from its shifts. And thus the analytic signal representation may be little confusing. Furthermore, inside the intervals where the sign of the signal equals its second derivative's one, the analytic signal has decreasing phase and therefore presents negative frequencies. This intuitively means that more than one mode is present at that time.

A new promising point of view for the decomposition of wave modes has been recently proposed by Norden Huang (Huang et al., 1998, 1999; Huang and Shen, 2005). A real signal which could overcome the above questions is defined as an *intrinsic mode function* (IMF) with the following properties: *a*) in the whole timeseries, the number of extrema and the number of zero crossings must either equal or differ at most by one; *b*) at any point, the mean value of the envelope of the local maxima and the one of the local minima is zero. By author experience, an IMF is an AM-FM signal which can be treated with significant results.

The extraction of IMFs is done with a sifting numeric process on a digital signal, which goes under the name of *empirical mode decomposition* (EMD), throughout spline identification of local envelopes (Alg. 5.1).

The single mode extraction is done with Fun. 5.2. A key point of the function is the scheme used to define the local extrema (lines 3 and 4) at the side ends

Algorithm 5.1: EMD

Data: x non monotone**Result:** the set of IMF $z[i]$ and a residue r , such that $\sum_i z[i] + r = x$

```

1 set  $x_0 = x, i = 1$ ;
2 repeat
3    $y = \text{sift}(x_0)$ ;
4   store the  $i^{\text{th}}$  IMF as  $z[i] = y, i = i + 1$ ;
5   set  $x_0 = x_0 - y$ ;
6 until  $x_0$  is monotone;
7  $r = x_0$ 

```

of the signal. The decomposed IMFs results very sensitive to this particular choice, which is arbitrary and always introduce some (in principle unknown) errors. The original procedure has been refined through the years in order to solve spline ending effects contamination (Deng et al., 2001; Zhidong and Yang, 2007; Wu and Qu, 2008; Qingjie et al., 2010).

The exiting condition at line 2 must also be properly defined, since it severely affects the successive IMFs. Again, no unambiguous definition has been given, but some conditions are proposed, which efficiency varies case by case. A proper choice is left to the user. Fun. 5.2 is called iteratively by Alg. 5.1 until its residue is monotone.

Note that the monotone residue r is actually stored as the last IMF. The mono-

Function 5.2: sift(x)

Data: x non monotone**Result:** the IMF y , the residue r

```

1 set  $y = x$ ;
2 while  $y$  is not IMF do
3   find local maxima( $y$ ) and connect with spline  $y_M$ ;
4   find local minima( $y$ ) and connect with spline  $y_m$ ;
5   compute the envelopes mean  $\bar{y} = (y_M + y_m)/2$ ;
6   "detrend" the signal  $y = y - \bar{y}$ ;
7 end
8  $r = x - y$ 

```

tonicity exiting condition at line 6 must be designed carefully to prevent infinite loops. Statistical post processing are recommended for stating the significance of each IMF. Some authors propose an in-algorithm condition for accepting or discarding (putting it into the residue) an IMF (Ayenu-Prah and

Attoh-Okine, 2010).

It has been shown by Dätig and Schlurmann (2004) that two close modes may be not effectively separated by EMD. Attempt for solving conundrums related to *mode mixing*, *i.e.* the non perfect separation of intuitively superimposed modes, were pursued by inserting *temporary* oscillations (Wang, 2005), by differentiation (Wu et al., 2010), by noise assisted ensemble approach (EEMD) (Wu and Huang, 2009; Torres et al., 2011), with morphological filter and blind source separation (Tang et al., 2012) and through wavelet shrinkage (Zhidong et al., 2011). Even if there's no proof of IMFs orthogonality, all the cited refinements show an improvement on this direction.

Hilbert transform of IMFs decomposed signals has been named Hilbert-Huang Transform (HHT). Until now no mathematical basis have been formulated, therefore EMD-like decompositions remains an empirical tool. On the other hand it is a totally data adaptive scheme and, in many cases, HHT renders physically trustworthy outputs.

By applying an iterative spline sifting procedure, similar to EMD, the single IMF can be normalized into a simple FM signal with unit amplitude. This permits to fit first Bedrosian hypothesis. The application of HT to these signals goes under the acronym of NHT (normalized Hilbert transform). In order to get rid of Nuttall proposition, a direct quadrature (DQ) method has been proposed. The latter makes use of the the preceding normalization procedure (Huang et al., 2009).

5.2.1 EMD-LIKES AND WATER WAVES

Besides the identification of EMD limits in separating two stationary modes with close frequency, Dätig and Schlurmann (2004) were the first to pursue a detailed investigation of EMD efficiency in treating wave gauges sampled signals.

The experiments reported in the cited paper relate to numerical simulations of Stokes 2^{nd} order wave fields, equipped with a 3^{rd} order dispersion relation. They simulate bi-chromatic groups at distinct positions, in a flume, propagating in one direction, and neglecting the existence of spurious modes. Correspondent wave flume timeseries are EMD processed with a slope method to

prevent spline-end contamination, and finally compared with the two IMFs extracted from the numerical prediction.

The separated signals resemble effectively the predicted ones as far as the ratio of the two fundamental frequencies remains low, apparently in contradiction with the first part of the job. For higher ratios, the *riding* wave "steals" some low frequency energy from the *carrier*. Apart from wave-wave interactions, which are deputed to be the main reason of the mismatches (between the model and the physics for first and then between decomposed modes), it should be noted that the fundamental frequencies ratios are all integers, and therefore that most harmonics do coincide. Probably, repeating the experiments with different initial phases would have led to somehow different results.

A method for enhancing the decomposition of bi-chromatic wave groups with fundamental frequency ratios close to unity has been proposed by Wang (2005). He inserts some known modulation by multiplying the analytic signal of the data set by $e^{-i\omega_0 t}$. If the frequency ω_0 is properly selected then the frequency ratio grow up to an acceptable value. EMD is then applied to both real and imaginary parts. Each resolved IMF couple is then reassembled and demodulated to get the real IMF. Note that, due to the frequency shifts the IMF features of the outputs are not ensured.

5.3 REFLECTION OF AN AM-FM WAVE

The procedure developed by Kitano et al. (2002) (see 4.2.1) has showed a great power in determining the local wavenumbers in a *quasi*-regular wave field. However some limitations begin to occur in the presence of secondary maxima and minima, since the analytic signal built with HT might be a fake. This probably proceeds from the fact that the basic model describes the superposition of two single modes, travelling in opposite directions, while a number of modes should in principle be assumed. On the other hand, there's no concern if one wants to assume that at single instant, in a single place, a single perturbation of the mean water level exists. But, if this perturbation is assumed to be an AM-FM wave, due to Bedrosian theorem, it is hard to show that its HT is its true analytic couple. And, to our knowledge, there's no way of building

it unambiguously. We must conclude that the DKR procedure does not perform well if timeseries are not single modes which can be cast into a Bedrosian frame. In this fashion, the decomposition of the record data through an EMD process into IMFs seems to be a consistent procedure to be coupled with.

As previously mentioned, the standard EMD process suffers some limitations when applied to water waves due to the local disappearing of low energetic components (such as reflected unwanted free waves in a flume), and mode mixing usually occurs at each level.

This problem is of main concern here. As reflection analysis is our main target, the decomposed modes at each wave gauge should be comparable, *i.e.* the bases has to be the same gauge by gauge. As far as the EMD invokes adaptive decomposition, data set at distinct gauges are expected to decompose according to distinct (adaptive) bases. In Fig. 5.2 an example of EMD decomposition for a test case taken from Pezzutto et al. (2012) is reported. This is a clear case of mode mixing. At about $t = 20s$ secondary maxima start appearing in the troughs due to the arrival of high frequency free waves (first row). This leads the sifting procedure to include them into IMF_1 (second row), and the fundamental wave is deputed to IMF_2 . Fig. 5.3 reports the same outputs related to the samples of WG3. Here no mode mixing occurs, since the phases of second order free waves make them undetectable by EMD. It is clear that IMF_1 of the two figures are far to be comparable. Hence it is impracticable to process them together for further analyses.

A number of procedures for solving these phenomena have been tried, but no one of them gave us successful results when analysing our flume timeseries. Among others, the error assisted EEMD it is able to un-mix the modes only if huge artificial noise is inserted. But the higher the noise, the higher the number of realizations that have to be computed to have a convergent estimation. In many cases the mean outputs were not pure IMFs. On the contrary, small noise brought to almost pure IMFs but mode-mixed.

The procedure proposed by Wang (2005) seems to be very effective, however, according to the author, case sensitive. Therefore an algorithm has been designed to make it as automatic as possible.

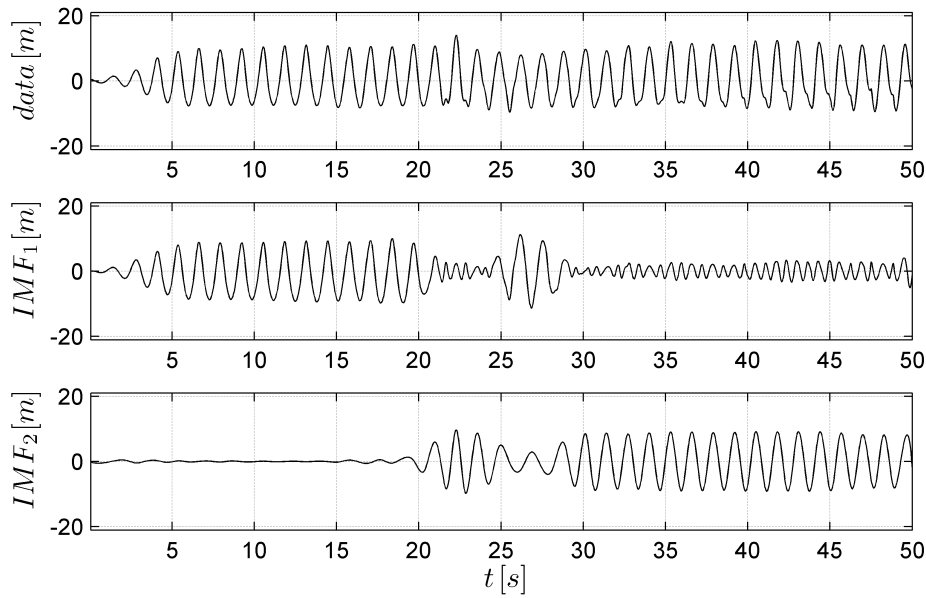


Fig. 5.2 – EMD decomposition of data sampled at WG_1 (first row).

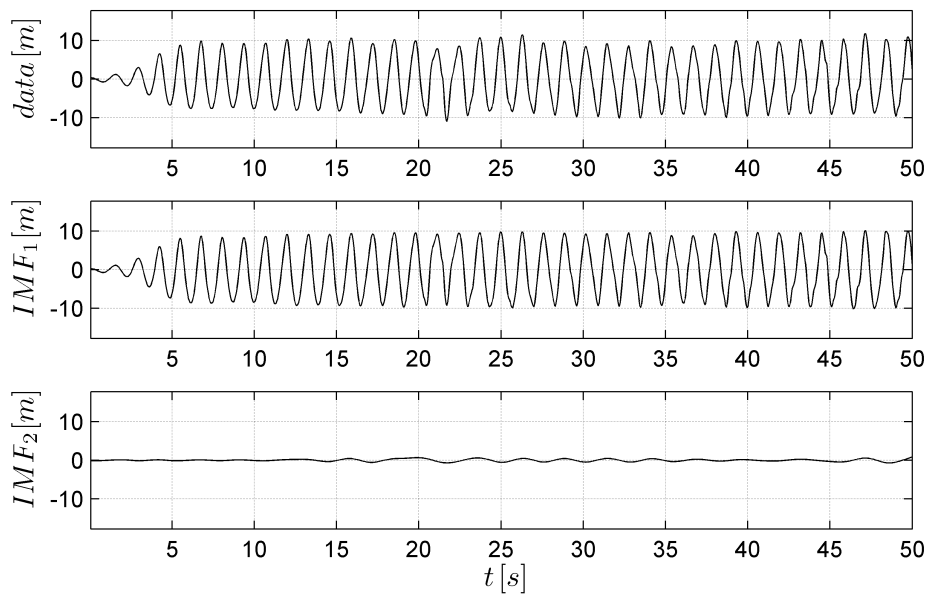


Fig. 5.3 – EMD decomposition of data sampled at WG_3 (first row) for the same test of Fig. 5.2.

5.4 MODE MIXING ELIMINATION IN EMD (ω EMD)

The algorithm outlined below proceeds from the idea of Wang (2005). In the cited document the original signal transformed into its correspondent analytic form via HT. The composition is correct as far as the data set is represents a

sum of modes with AM disjointed by the FM. After the selection of a proper frequency ω_0 , the signal is frequency shifted with respect to it. The sifting procedure, Fun. 5.2, is then applied to the real and the imaginary parts separately, which are then recomposed into the analytic form and frequency re-shifted. The correspondent IMFs are the real parts of these outputs. Some conundrums still exist on how to select the best ω_0 . A solution for that is hereby proposed. In the former procedure the frequency shift is done only once at the beginning of the sifting scheme (and once at the end to recover the real data). Suppose that the best ω_0 has been selected, and the first IMF has been extracted with success. It is reasonable to think that, at this point, the (frequency shifted) residues may have a modified frequency content which does not permit the extraction of other well un-mixed IMFs. And this does depend on the choice of ω_0 . Hence we should re-shift the residues in order to achieve our purposes, and keep history of the successive frequency shifts. This is equivalent to shift and un-shift at beginning and at the end of each IMF extraction. Which does make sense if we have a receipt for a proper choice of ω_0 . In pseudo language terms, this traduces to the substitution, inside Alg. 5.1, of the Fun. 5.2 calls with calls of the Fun. 5.3. A *proto*-algorithm would be Alg. 5.4.

Function 5.3: $\text{Asift}(y_0, \omega_0)$

Data: $y_0 = \mathbf{A}x_0$ where x_0 is the real signal to be sifted; ω_0

Result: y sifted

- 1 $y = y_0 e^{-i\omega_0 t};$
 - 2 $[y_R, r_R] = \text{sift}(\Re y);$
 - 3 $[y_I, r_I] = \text{sift}(\Im y);$
 - 4 $y = (y_R + iy_I) e^{i\omega_0 t};$
-

5.4.1 PROBLEM DEFINITION

The idea is to search into a range of possible ω_0 and minimize some *goodness* indicators in order to cope with the condition in line 4 of Alg. 5.4. Suppose we have chosen an ω_0 and extracted the first real and imaginary shifted IMFs, respectively y_R and y_I . First of all we want them to be an analytic couple. This

Algorithm 5.4: *proto- ω EMD***Data:** x non monotone**Result:** the set of IMF $z[i]$ and a residue r , such that $\sum_i z[i] + r = x$

```

1 set  $x_0 = x, i = 1$ ;
2 repeat
3   | set  $y_0 = \mathcal{A}x_0$ ;
4   | while not satisfied do
5   |   |  $y = \mathbf{Asift}(y_0, \omega_0)$ 
6   |   end
7   | store the  $i^{\text{th}}$  IMF as  $z[i] = \Re y, i = i + 1$ ;
8   | set  $x_0 = x_0 - y$ ;
9 until  $x_0$  is monotone;
10  $r = x_0$ 

```

can be controlled by requiring that

$$\chi_A = \|y_I - \hat{y}_R\| \quad (5.17)$$

is small.

Then we would like to satisfy Bedrosian theorem, *i.e.* we would like that the extracted IMF has disjointed amplitude and phase spectra. The IMF is recovered by means of

$$y = \Re \left\{ (y_R + iy_I) e^{i\omega_0 t} \right\} \quad (5.18)$$

and its amplitude a and phase θ throughout a standard DQ procedure. Instead of taking the spectra of the overall series, we measure their boundedness by extracting their respective DQ features. The ratio of the mean frequency of the envelope over the mean IF has to be low

$$\chi_d = \frac{\bar{\omega}_a}{\bar{\theta}_t} \quad (5.19)$$

this is a measure of the separation of respective spectral peaks (in a Fourier sense). Moreover we would like that the changes in the envelope to be smooth enough, *i.e.*

$$\chi_a = \frac{\sigma^2(\tilde{a})}{\bar{a}} \quad (5.20)$$

where \tilde{a} is the *de-trended* envelope. Finally the frequency should be also subject to a similar condition:

$$\chi_\omega = \frac{\tilde{a}_\omega}{\tilde{\omega}}. \quad (5.21)$$

The last two conditions provide successful results when applied to a kind of *quasi-regular* wave motion. Similar parameters may be introduced to take into account a so called *irregular* wave field, where simple average and de-trending may lead to kind of confusing interpretation. A possible way may come through decomposing the envelopes through EMD procedures, in order to get their general trends.

It was also noted that, the less iterations in Alg. 5.2, the higher the confidence that could be given to the extracted IMF. Hence, denoting with N_R the iterations for extracting the real IMF, and N_I the correspondent for the imaginary part, the following parameter should be low enough.

$$\chi_N = \sqrt{N_R N_I} \quad (5.22)$$

Our game is the the minimization of the following *goodness* indicator

$$\chi = \prod_j \chi_j^{\alpha_j} \quad (5.23)$$

where a choice for the exponents α_j is left for normalizing their respective behaviours. The goal must be reached with a proper choice of the shifting frequency ω_0 .

5.4.2 POSSIBLE CHOICES FOR ω_0

The single sifting procedure physiologically selects the IMF presenting the higher local frequency. For a *quasi-regular* wave field, we do almost know the frequency content, and that it is relatively stable in the record. Hence we can emphasize, shift up to the EMD recognizable region, the energies we want to extract as an IMF.

Given an ω_0 , everything that lies in the range $(0; \omega_0)$ will be mirrored with respect to $\omega_0/2$, and the energy content of higher frequencies will be shifted down, mixing together with the other energies. If there's no energy above ω_0 ,

i.e. $\omega_0 > \omega_{max}$, then no mixing will occur, and what will prevail will be the very low frequency IMFs. Some examples are given below in Fig.5.4 in a spectral fashion. In the limit case where $\omega_0 \geq \omega_{max}$ the whole content is mirrored. By choosing very high ω_0 it may come the case that the highest frequencies could not be revealed due to the limited time resolution. It is worth to notice that with this kind of procedure the lower frequency components are extracted first, differently from the standard EMD algorithm.

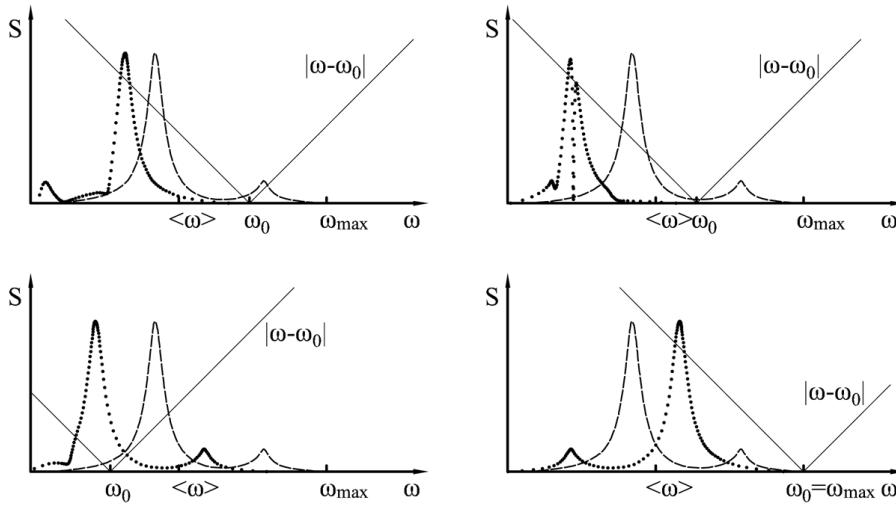


Fig. 5.4 – Frequency shifts of the analytic signal. Some examples by a spectral point of view. Dashed line: frequency image of the original signal; dotted line: frequency shifted signal.

The problem now shift on how to identify the frequency content of the original series. In principle we don't want to have it from an FFT analysis. In this case ω_{max} would be automatically determined by the Nyquist frequency. Even if this could be solved by setting a threshold, FFT is a restriction since it does not consider modulated amplitudes. We can initially suppose that no mode-mixing occurs and compute the Hilbert marginal spectrum with a standard, and very fast, EMD-DQ procedure. And then make a decision on its output. The best option we found is to build the timeseries of the local frequencies correspondent to the locally most energetic IMF. The mean value of this series is set as a reference value ω_{ref} . We then search for the best multiplier μ which gives

$$\omega_0 = \mu \omega_{ref} \quad \mu \in [0; 3] \in \mathbb{R} \quad (5.24)$$

The upper and lower bound have been determined by experience. For regular waves, $\mu = 2.5$ is sufficient for mirroring the whole spectrum and extracting the fundamental wave. Values close to zero resulted necessary for extracting third and higher components.

The overall approach permits the extraction of the most energetic components as first IMFs. In case of irregular waves this effect may be not possible, although it has been shown its effectiveness in a bi-chromatic field. It is reasonable to think that a similar procedure can be done only by the use of a time dependent frequency shift.

5.4.3 PATTERN-SEARCH OF ω_0

We propose an automatic optimization procedure for the search of ω_0 . The MATLAB *patternsearch* has been implemented in the code, with the objective function defined as (5.23). Results obtained for the same test case of 5.2 are outlined in Fig. 5.5. The effectiveness of ω EMD is clear.

Once the optimal decomposition of WG_1 is completed, and history of the ω_0 *best set* is kept, there are two options: proceeding with ω EMD for the other sets, or decompose them according to Kitano et al. (2002) and the stored ω_0 *best set*. Results are shown respectively in Fig. 5.6 and Fig. 5.7. By choosing the first way, a better decomposition is assured but it is not said that the IMFs can be compared together with the other set ones. On the contrary, one can think that the second option allow some dependency of the basis, while being also much faster. The bad new is that the outputs might be not pure IMFs (see second row in Fig. 5.7).

A mixed way between the two does probably allow better results. Passing to ω EMD the ω_0 history we force *patternsearch* to look inside a narrow interval for the best choice, fastening the calculation (not much). This results in pure IMFs and *hopefully* much more similar basis (see Fig. 5.8). Final implementation follows as Alg. 5.5. The function **patternsearch** does iteratively call Fun. 5.3 in order to compute the objective parameter.

Algorithm 5.5: ω EMD**Data:** x non monotone, ω_0 **Result:** the set of IMF $z[i]$ and a residue r , such that $\sum_i z[i] + r = x$

```

1 set  $x_0 = x, i = 1$ ;
2 repeat
3   if  $\omega_0$  is empty then
4      $IMF_0 = EMD(x_0)$ ;
5     evaluate  $\omega_0$  as weighted average of  $IMF_0$  set;
6     set  $\omega_{0L} = 0, \omega_{0R} = 3\omega_0$ ;
7     set  $y_0 = \mathcal{A}x_0$ ;
8     else
9       set a small  $\delta$ ;
10      set  $\omega_{0L} = \omega_0 - \delta > 0, \omega_{0R} = \omega_0 + \delta$ ;
11    end
12  end
13  minimize  $\chi$  of (5.23) pathsearching best  $\omega_0 \in [\omega_{0L}, \omega_{0R}]$ ;
14  store  $\omega_0$ ;
15  store the  $i^{th}$  IMF as  $z[i] = \Re y, i = i + 1$ ;
16  set  $x_0 = x_0 - y$ ;
17 until  $x_0$  is monotone;
18  $r = x_0$ 

```

5.4.4 OTHER FUNDAMENTAL CHOICES

The basic EMD procedure requires some choices which are usually case dependent. Two exit conditions have to be defined for both the global algorithm and the sifting function. Moreover it must be implemented a method for minimizing end effects, *i.e.* a method for a good choice of the external *hidden* extrema, necessary for the sifting splines construction.

About the last issue we have adopted some tricks. Due to the presence of secondary maxima, the standard *last two* extrema extrapolation may result in unreal very high external extrema. Hence we make use of a *last three* extrema linear regression. Wave flume timeseries are possibly recorded with ramp-up and ramp-down, preceded (and followed) by (almost) steady zeros at the beginning and at end of the record. This prevents the identification of unreal ending extrema, minimizing the growth of end effects for successive siftings. Since the ramps might not be included for some reason, we smooth the data set endings with artificial ramps. These have the duration of approximately $2 \div 3$ main periods.

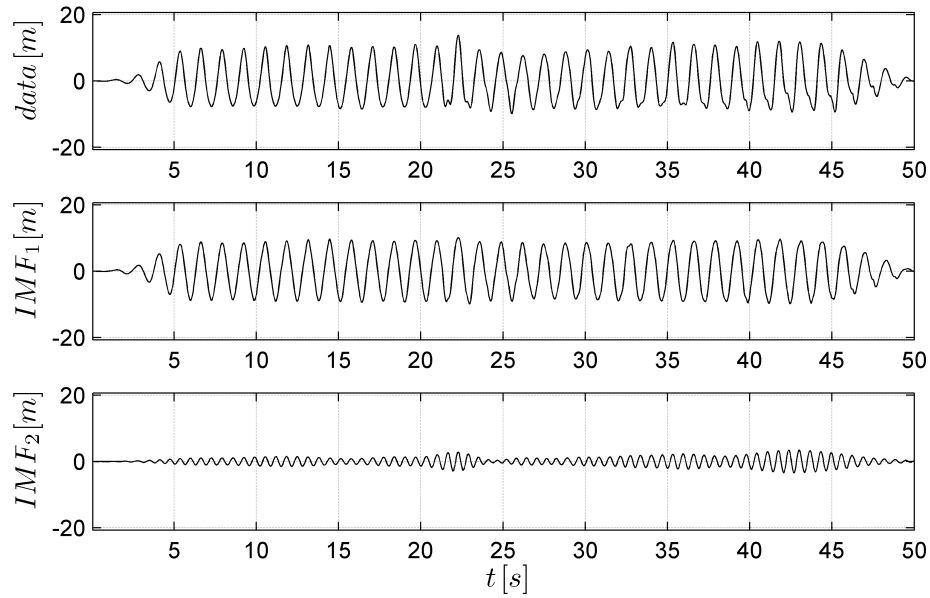


Fig. 5.5 – ω EMD decomposition of data sampled at WG_1 (first row).

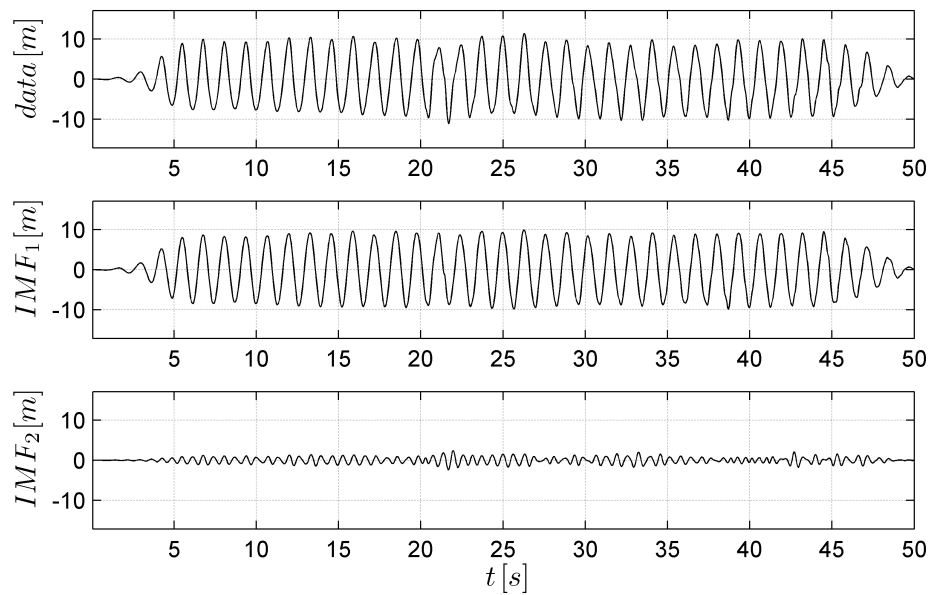


Fig. 5.6 – ω EMD decomposition of data sampled at WG_3 (first row).

The ω EMD exit condition is designed according to what follows. It is meant that the decomposition continues until the residue is monotone. The mean value of all TS is close to zero (mean water level); furthermore, the most energetic IMFs are usually extracted at first with ω EMD; hence there's no need in searching for too many IMFs. An *or* condition is implemented, that is to say

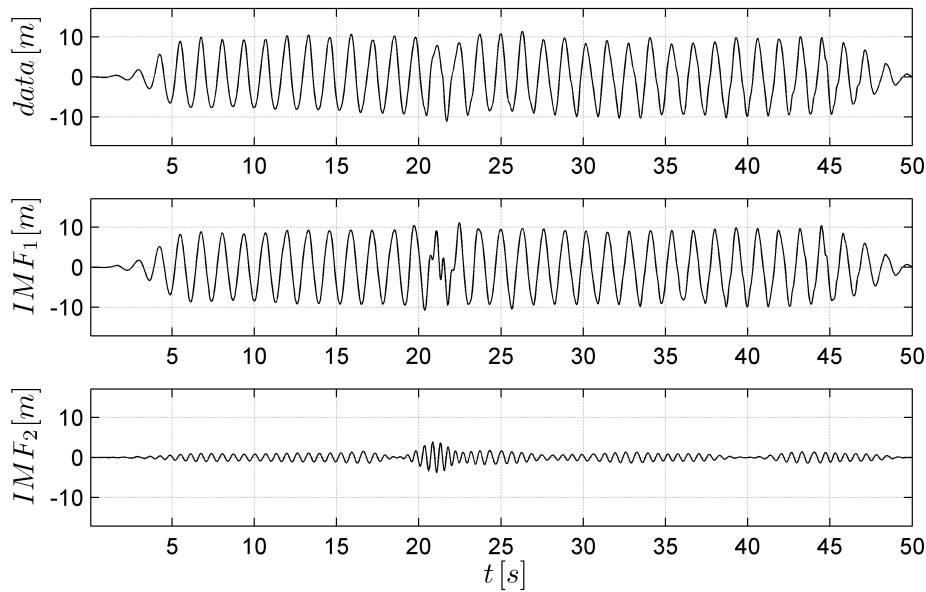


Fig. 5.7 – Kitano et al. (2002) EMD decomposition of data sampled at WG_3 (first row) with reference to ω_0 retrieved from ω EMD of WG_1 .

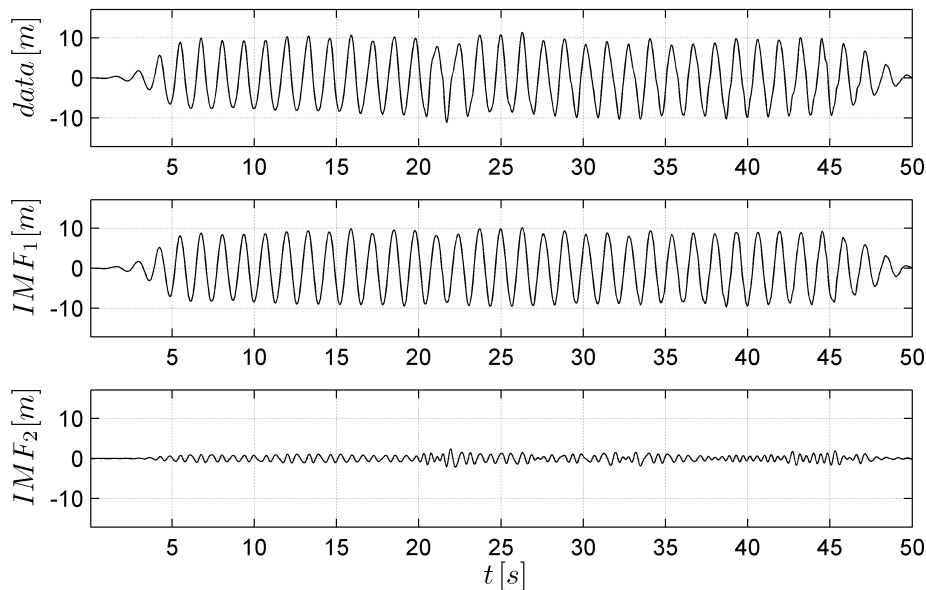


Fig. 5.8 – ω EMD decomposition of data sampled at WG_3 (first row) with reference to ω_0 retrieved from stored best ω EMD.

that procedure stops whenever the residue is sufficiently low or a sufficient number of IMFs has been extracted.

Last few words about the exit condition of the sifting function. At each sift iteration the average distance of the current residue with the previous iteration

one is checked. If this value is less than a prescribed toleration (10^{-3}) then the iterations stop. Here the output is analysed: if it matches IMF requirements, the function exits successfully, otherwise the tolerance is decreased by an order of magnitude and the sifting continues. By doing that no infinite loops has been observed until now. However, since the number of iterations is usually on the order of 10 or lower, a maximum number of 100 sifting (probably much lower) is enough.

5.4.5 PERFORMANCE ON NUMERICAL WAVE DATA

We repeated the sims of Dätig and Schlurmann (2004) for a bi-chromatic wave packet, but only locally in the low frequency domain, in order to show improvement with respect to standard EMD. For each couple (f_r, f_s) an MC sim was run accounting for uniform probability phase shifts (riding Vs carrier, and carrier Vs time window) and remainder of window duration Vs carrier cycles. Window duration varies between 29 and 30π s.

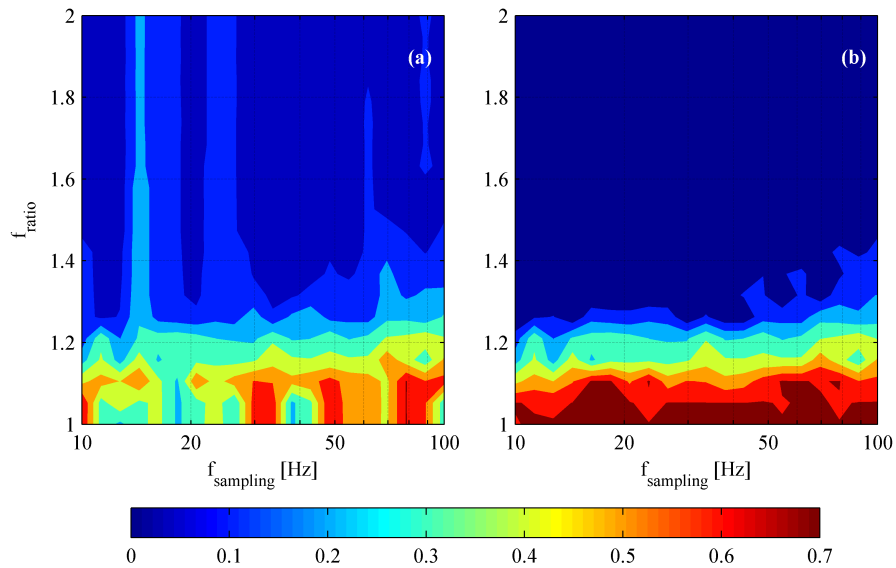


Fig. 5.9 – ω EMD performance on bichromatic series: *rms* between waves and correspondent IMFs: a) carrier; b) riding (*NSims_om_{EMD}.m*).

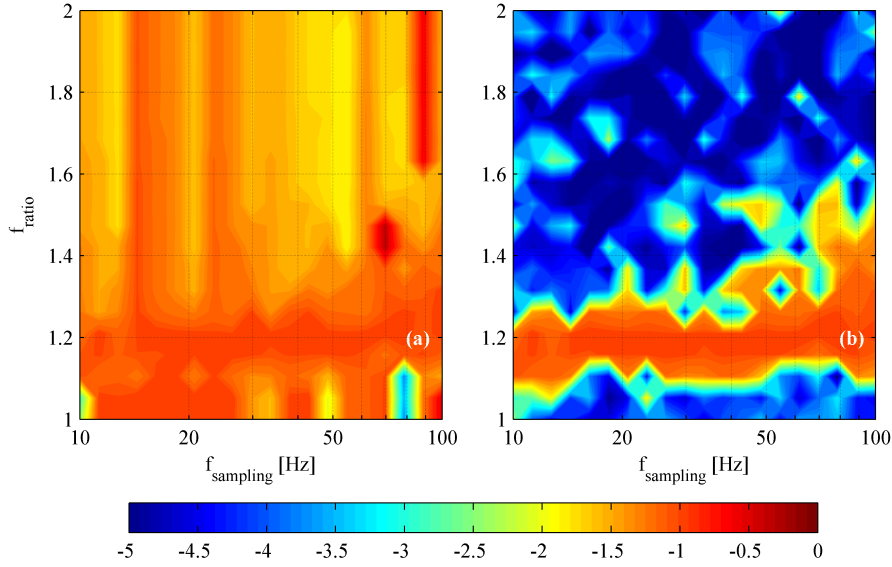


Fig. 5.10 – ω EMD performance on bichromatic series: log-uncertainty on *rms* between waves and correspondent IMFs: a) carrier; b) riding (*NSims_om_EMD.m*).

5.5 REFLECTION ANALYSIS OF ω EMD DECOMPOSED WAVES

We discuss here the performance of the coupled ω EMD-DKR, as a tool for separating modulated incident and reflected waves. The concept of *separation* underlines an important hypothesis: *i.e.* waves that travel in opposite directions due linearly superimpose. If one wants to get rid of that, then an interaction model should be taken into account. We hereby consider that at each order an IMF is the sum of two modes travelling in two opposite directions.

In previous paragraphs we have identified the possibility of a direct wavenumber resolution 4.2.1 as a powerful tool for the reflection analysis of laboratory waves. Each reflection analysis procedure needs a number of comparable single modes, relative to different locations. A method for getting this kind of data from measured timeseries has been proposed as a ω EMD.

However, also with this small improvement, the resolved basis are still measurement point dependent. This causes the algorithm to be very unstable and provide no success. More research has to be done in this direction.

Since, up to now, no mathematical proofs have been introduced for EMD, probably a good intermediate step for wave packets analyses would be based on suitable wavelet, or other Fourier derived projections.

6 ON ANOTHER TIME DOMAIN APPROACH

In the previous chapter we have identified in EMD like procedures a possible tool for the separation of a wave train in a finite number of modulated modes that can be treated with DKR. In order to apply DKR we need in principle the superposition of no more than two modes: one coming in and one going back. These can present very different frequencies. Both phases and amplitudes can be modulated. But the respective AM and FM modulations must have disjointed spectra (to cope with Bedrosian hypotheses) otherwise the HT built analytic signals may be incorrect.

Moreover, amplitudes should be constant in space, or, at least, should not vary too much in the observation region ($a_{,x} \approx 0$). Same assumption are made for the phases space derivatives, *i.e.* the local wavenumbers ($k_{,x} \approx 0$). That is to say that a certain local (in space) stationarity is assumed. Therefore, why not to restrict to a local time stationary point of view?

A single Fourier mode is not modulated, and therefore its analytic couple is readily determined. Instead of decomposing the whole series through EMD, there may be an option of DKR processing the local Fourier modes.

6.1 WAVE MODEL

Consider a linear superposition of incident and reflected cylindrical waves, for which the wavenumbers k_m and w_m real positive valued, but not necessary linked to corresponding frequencies $m\omega_0$ through any dispersion relationship. Assume that this model is valid on a local support, *i.e.*

$$\eta = \sum_{m=1}^{\infty} \left(a_m e^{-ik_m x} + b_m e^{iw_m x} \right) e^{im\omega_0 t} + c.c. \quad (x, t) \in \Gamma \in \mathbb{R}^2. \quad (6.1)$$

Consider a set of three equally spaced gauges:

$$\mathbf{x} = \begin{bmatrix} -s & 0 & s \end{bmatrix} \quad s \in \mathbb{R} \quad (6.2)$$

with s sufficiently small, then the samples of (6.1) taken at these points can be approximated by

$$\eta_n = \sum_{m=1}^M \left(a_m e^{i(2-n)(\alpha_m + \beta_m)} + b_m e^{i(n-2)(\alpha_m - \beta_m)} \right) e^{im\omega_0 t} + c.c. \quad (6.3)$$

for a sufficiently short time duration. Once the samples are projected into discrete Fourier space, then each complex amplitude can be treated by DKR (instead of the local approximate analytic signal) to estimate the associated phase angles

$$\alpha_m = s (k_m + w_m) / 2 \quad (6.4a)$$

$$\beta_m = s (k_m - w_m) / 2. \quad (6.4b)$$

Fourier coefficients a_m and b_m can thus be retrieved, and timeseries of incident and reflected waves reconstructed by inverse FFT.

6.2 DKR TIPS AND TRICKS

The correct phases resolution is deputed to the correct evaluation of two angles, which are defined as sum and difference of the wavenumbers of incident and reflected elementary waves, namely α and β . In the original equations these are evaluated through the inversion of a cosine and a tangent, which are defined in the half circle.

This leads to frequent misinterpretation of the quadrant in which the angles are to be found, and the most part of the spikes in the definitive solution. A solution is given here in a generalized form, valid for both analytic or Fourier points of view.

6.2.1 CORRECT ANGLES REPRODUCTION

Let η_{mn} be the m^{th} local mode at the n^{th} gauge and $\mathcal{A}\{\eta_{mn}\}$ its analytic representation or the m^{th} Fourier coefficient at a local window. Let define the following quantities

$$\mathcal{A}_q = \mathcal{A}\{\eta_{m3} + (-1)^q \eta_{m1}\} (\mathcal{A}\{\eta_{m2}\})^* \quad (6.5)$$

and

$$B_{pq} = i^p \left[\mathcal{A}_q + (-1)^p \mathcal{A}_q^* \right]. \quad (6.6)$$

The angle β_m the quadrant of β_m is readily given by

$$\beta_m = \arg (B_{01} + iB_{10}) \quad (6.7)$$

since the solution has a 2π periodicity. For angle α_m consider the quantity:

$$C_m = \frac{1}{4} (B_{00} - iB_{11}) e^{i\beta_m}, \quad (6.8)$$

then

$$\Re\{C_m\} = |\mathcal{A}\{\eta_{m2}\}| \cos \alpha_m \quad (6.9)$$

which inverse defines an angle in the half circle. To get the true quadrant of α_m one may note that

$$\Im\{C_m\} = (b_m^2 - a_m^2) \sin \alpha_m \quad (6.10)$$

where a and b are, respectively, the amplitudes of incident and reflected waves. If the relation between the two envelopes is known, then the *sgn* of $\sin \alpha_m$ can be deduced. Since the signs of $b_m^2 - a_m^2$ are not known in principle, the solution presents an alternative. Hence an initial guess has to be made. In a local Fourier framework, a good guess would be the imposition of spatial linear phases with Airy wavenumbers.

In the original Hilbert transform approach it is more difficult to achieve disambiguation of the phases. In this case a useful initial choice seems to be the linear wavenumber of the principal frequency content. The latter, if determined with a Fourier approach, appear to be consistent only with narrow banded sig-

nals. Transient and modulated ones must be treated locally, again with an FFT (which precision depends on the window width), with a DQ approach (only if the signal is sufficiently smooth in the IMF sense), or maybe better a wavelet decomposition.

6.2.2 WAVES RECONSTRUCTION

Once the spatial phases mismatches (wavenumbers) are known, Kitano et al. (2002) propose a direct reconstruction of the incoming and reflected waves at the central gauge. In case the wavelength is on the order of the gauge spacing, the same two gauges method singularities may blow the local solution up. When this occurs, a local interpolation can substitute the wrong datum. Some other uncontrollable errors may arise both in case of particularly disturbed data. For this, a weighted LS approach can help in stabilizing the outputs at each point. For this purpose the local solution is retrieved through inversion of a matrix like (4.16), which in this case reads:

$$\mathbf{Z} = \begin{bmatrix} \sum_{n=1}^N \mu_{mn} e^{-2ik_m x_n} & \sum_{n=1}^N \mu_{mn} e^{i(w_m - k_m)x_n} \\ \sum_{n=1}^N \mu_{mn} e^{i(w_m - k_m)x_n} & \sum_{n=1}^N \mu_{mn} e^{2iw_m x_n} \end{bmatrix}, \quad (6.11)$$

being k_m and w_m the wavenumbers of m^{th} incident and reflected components. The latter can be rewritten in terms of α_m and β_m :

$$\mathbf{Z} = \begin{bmatrix} 2 \cos(2\alpha_m + 2\beta_m) + 1 & 2 \cos(2\beta_m) + 1 \\ 2 \cos(2\beta_m) + 1 & 2 \cos(2\alpha_m - 2\beta_m) + 1 \end{bmatrix} \quad (6.12)$$

where μ_{mn} are set to one, since no weights are involved in precedent calculations ((6.5) and what follows). The right hand side vector is

$$\mathbf{b} = \left[\sum_{n=1}^N A_{mn} e^{i(2-n)(\alpha+\beta)} \quad \sum_{n=1}^N A_{mn} e^{i(2-n)(\alpha-\beta)} \right]^T. \quad (6.13)$$

Analytic solution can be extracted with little algebraic effort.

$$\begin{bmatrix} a_m & b_m \end{bmatrix}^T = \frac{D_m^*}{|D_m|^2} \mathbf{S}_m \begin{bmatrix} A_{m1} & A_{m2} & A_{m3} \end{bmatrix}^T \quad (6.14)$$

Where

$$\mathbf{S}_m = \begin{bmatrix} \chi \zeta^3 (\zeta^2 + \chi^2 + 1) & \zeta^2 (\zeta^2 - \chi^4) & -\chi \zeta (\chi^2 \zeta^2 + \zeta^2 + \chi^2) \\ -\chi \zeta (\chi^2 \zeta^2 - \zeta^2 + 1) & \zeta^2 (\chi^4 \zeta^2 - 1) & \chi \zeta^3 (\chi^2 \zeta^2 + \chi^2 + 1) \end{bmatrix} \quad (6.15)$$

and

$$D_m = (\zeta^2 - 1) (\zeta^4 \chi^2 + \zeta^2 \chi^4 + 2\zeta^2 \chi^2 + \zeta^2 + \chi^2) \quad (6.16)$$

with the following positions: $\zeta = e^{i\alpha_m}$ and $\chi = e^{i\beta_m}$. It seems that there's no way to reduce to $\sin \alpha_m$ free forms. Hence the somehow iterative procedure, described in previous section, must be kept, for correct reproduction of both amplitudes and phases.

SINGULARITIES The solution (6.14) blows up whenever the modulus of (6.16) vanishes. A little trigonometric manipulation leads to following form (omitting for convenience the m subscript):

$$\begin{aligned} |D_m| &= 2 \left| (e^{2i\alpha} - 1) (\cos 2\alpha + \cos 2\beta + 1) e^{2i(\alpha+\beta)} \right| \\ &\leq 2 \left| (e^{2i\alpha} - 1) \right| |(\cos 2\alpha + \cos 2\beta + 1)| \\ &= 4 |\sin \alpha| |(\cos 2\alpha + \cos 2\beta + 1)| \end{aligned} \quad (6.17)$$

which has the usual solution

$$\alpha = q\pi \quad \forall q \in \mathbb{N} \quad (6.18)$$

i.e. $(k + w)s = 2q\pi$, and vanishes also on the curves where

$$\cos 2\alpha + \cos 2\beta = -1. \quad (6.19)$$

These are represented in Fig. 6.1. For simple linear waves, $\beta = 0$, hence only (6.18) holds. In case of deviation from linear celerity, or m^{th} component is a superposition of a number of modes, the β assumes a whatsoever value on the

circle, and the condition (6.19) must be checked too.

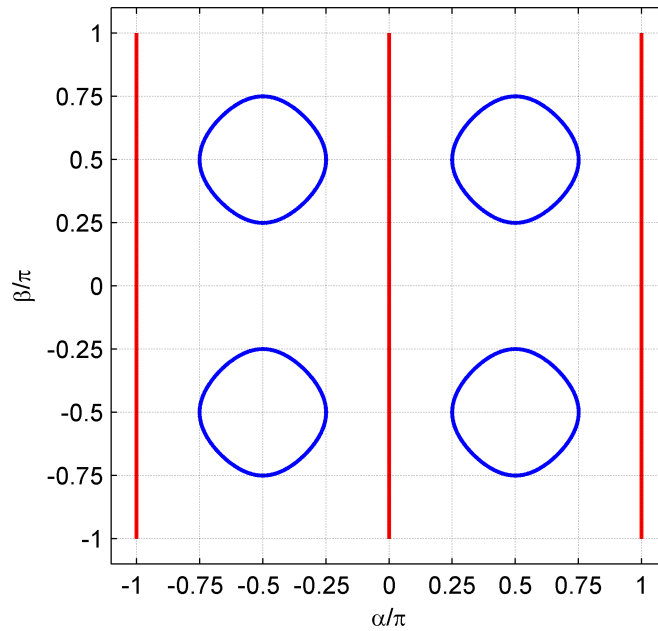


Fig. 6.1 – Singularities of the solution (6.14). Red: (6.18), Blue (6.19)

6.3 LOCAL TREATMENT

6.3.1 ALGORITHM

If the wave motion is assumed stationary, then the adaptive wavenumbers reconstruction can be described by the following Alg. 6.1.

6.3.2 GAUGE SPACING

It can be shown that the smaller the relative spacing of the gauges triplet, the higher the first frequency at which $\det \mathbf{Z}$ (6.12) vanishes. On the other hand, if gauges are too close, the cross spectra are too correlated, hence it may be not possible to measure significant phase changes, especially for long perturbations. Increasing sampling frequency does help in detecting time variations on the order of the spatial ones. However, if their magnitude is comparable with overall noise disturbances one, the significant informations may not be correctly retrieved.

Algorithm 6.1: Fourier DKR

Data: η ($M \times 3$ data set), s (gauge spacing), h water depth, f_s sampling frequency

Result: η_i (incident), η_r (reflected)

- 1 $A = FFT(\eta)$ keeping only 1 side;
- 2 **for** $m = 1$ to $M_w/2 + 1$ **do** *i.e.* for each frequency
- 3 linear waves $k(m) = \Omega^{-1}(h, frequency_m)$;
- 4 $p = \text{sgn}\{\sin k_m s\}$;
- 5 compute β_m (6.7) and C_m (6.8);
- 6 $\cos \alpha_m = \Re C_m$;
- 7 $\sin \alpha_m = \text{sgn}\{\Im C_m\} \sqrt{1 - \cos^2 \alpha_m}$;
- 8 $\alpha_m = p \arg\{\cos \alpha_m + i \sin \alpha_m\}$;
- 9 **repeat**
- 10 compute \mathbf{S} (6.15) and D (6.16);
- 11 $[a_m, b_m] = D^* \mathbf{S} A_m^T |D|^{-2}$ from (6.14);
- 12 $p = \text{sgn}(|b_m|^2 - |a_m|^2)$;
- 13 **until** amplitudes converge;
- 14 **end**
- 15 $\eta_i = iFFT([a a^*(M_w/2 : 2)])$;
- 16 $\eta_r = iFFT([b b^*(M_w/2 : 2)])$;

In practice, relative gauges spacing is limited by the gauges dimensions, and singularities may occur very soon. With a loss of locality, but with a sufficient increase of stability, a fourth gauge should be added. If correctly placed, annoying singularities does disappear. The fundamental triplet is then used to resolve phases mismatches, while the fourth enters the LS amplitude estimation only.

6.3.3 WINDOW LENGTH

Let's take this very simple model

$$\eta = a \cos(2\pi ft - kx + \phi_i) + \rho a \cos(2\pi ft + kx + \phi_r) \quad (6.20)$$

and evaluate the error on the incident wave computed by Alg. 6.1 as

$$Err = \frac{\|\eta_{i,2}^{FDKR} - \eta_{i,2}\|}{\|\eta_{i,2}\|} \quad (6.21)$$

where subscript 2 stands for second wave gauge.

Now set zero initial time, zero second gauge position, and let vary the initial phases of incident and reflected components, respectively ϕ_i and ϕ_r in the whole circle. This corresponds to analyse the response with respect to the window attack for all possible situations with respect to the observer at central gauge.

If window length (M_w points) covers an even number of integer periods, then the FFT error would be minimum. A window of this kind can be selected through a zero crossing analysis, or after determining a characteristic period of a sufficient long record. For sake of locality, let M_w be the distance between three subsequent zero down crosses (2 periods). In most cases this can not be taken exactly, due to the mismatch between sampling frequency f_s and wave frequency. Therefore let analyse the error dependence on window length to period ratio, *i.e.* $M_w f / f_s$. Results are shown in Fig. 6.2 for $f = 0.9 \text{ Hz}$ and $f_s = 100 \text{ Hz}$.

If time window length is not correctly chosen, then, for small changes (2 time steps) with respect to optimal length, the error would be raise up an order of magnitude, due to FFT leakage, independently from the phases. Error is low at the corners and positive diagonals of the panels of Fig. 6.2, *i.e.* the two waves are in phase at central gauge. If they have opposite observation phases, then the error is maximum.

Fig. 6.3 repeats optimum window width analysis for various reflection coefficients. Black contour lines represent the observer phase of window attack ϕ_w / π defined by posing $c \cos(2\pi f t - kx + \phi_w) = \eta$ of (6.20) at gauge 2. For example, a value of 1 (2) means that, at window start, the observer sees a trough (crest); and a zero down(up)-cross is denoted by 0.5 (1.5). Even if only integer ϕ_w / π lines pass through error local minima, there seem to be no option for choosing best attack position.

6.3.4 IMPLEMENTATION TIPS

ROUND-OFF ERRORS The precision of FFT depends upon the CPU and on the kind of implementation. Usually the round-off errors are on the order of machine precision. For the present utilization of Fourier coefficients, even these

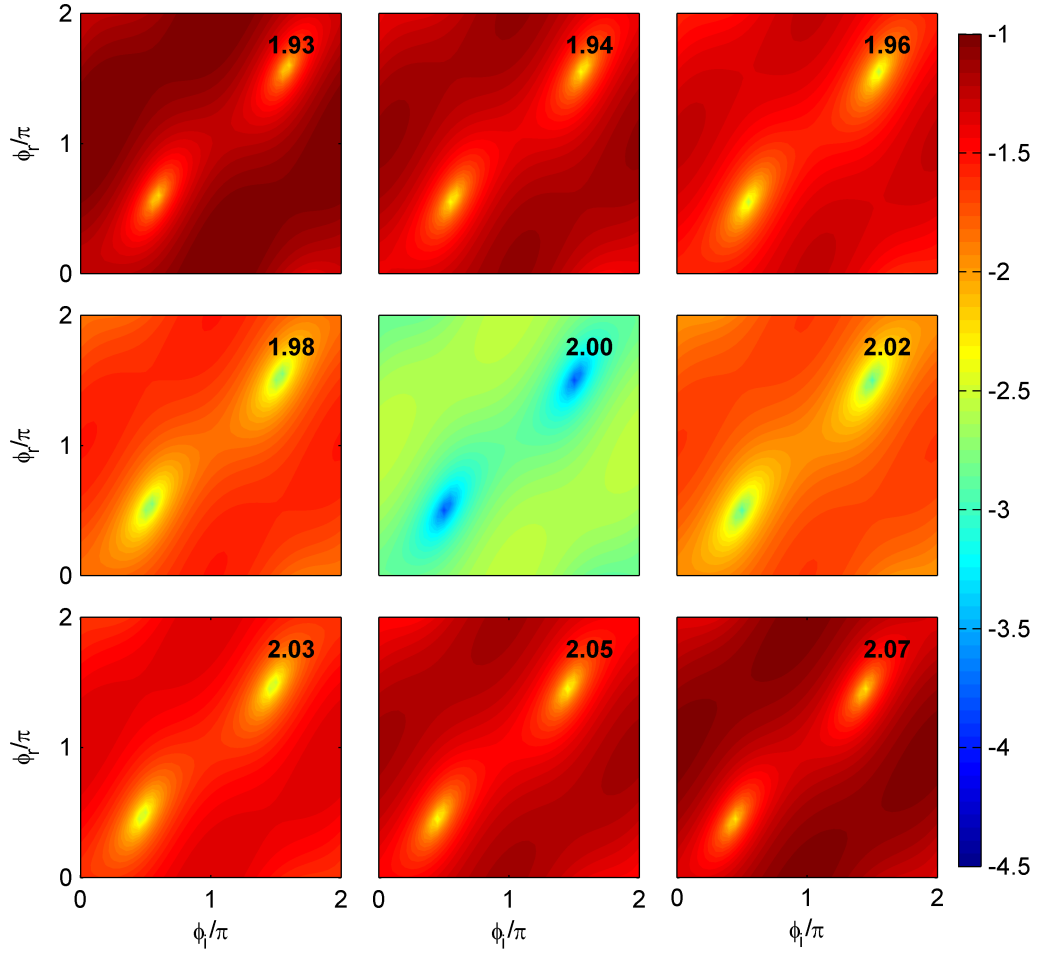


Fig. 6.2 – Log_{10} of FDKR error at various window length over period ratio (bold face). Water depth is 0.6 m , $a = 6.5\text{ cm}$, $\rho = 0.9$, $f = 0.9\text{ Hz}$ and gauge spacing is $s = 0.04\text{ m}$.

small errors appear to be a critical point. The uncertainty spreading involved in (6.5) and (6.6) may lead to wrong solutions.

Consider as an example, two linear waves (incident and reflected) with the same frequency. In this case the solution for β_m must be zero, being the difference of two equal wavenumbers (6.4). Then real part of (6.7) argument must be finite, and the imaginary part must be zero. Due to errors spreading, the latter absolute value will result $2 \sim 3$ orders of magnitude greater than FFT round-off error. In case the former (real part) is small too, then β_m results sufficiently far from zero to affect sensitively the final solution.

For expected solutions far from $\pi/2$ multiples, accumulated errors are small compared to the components of (6.7), hence their ratio results very close to the

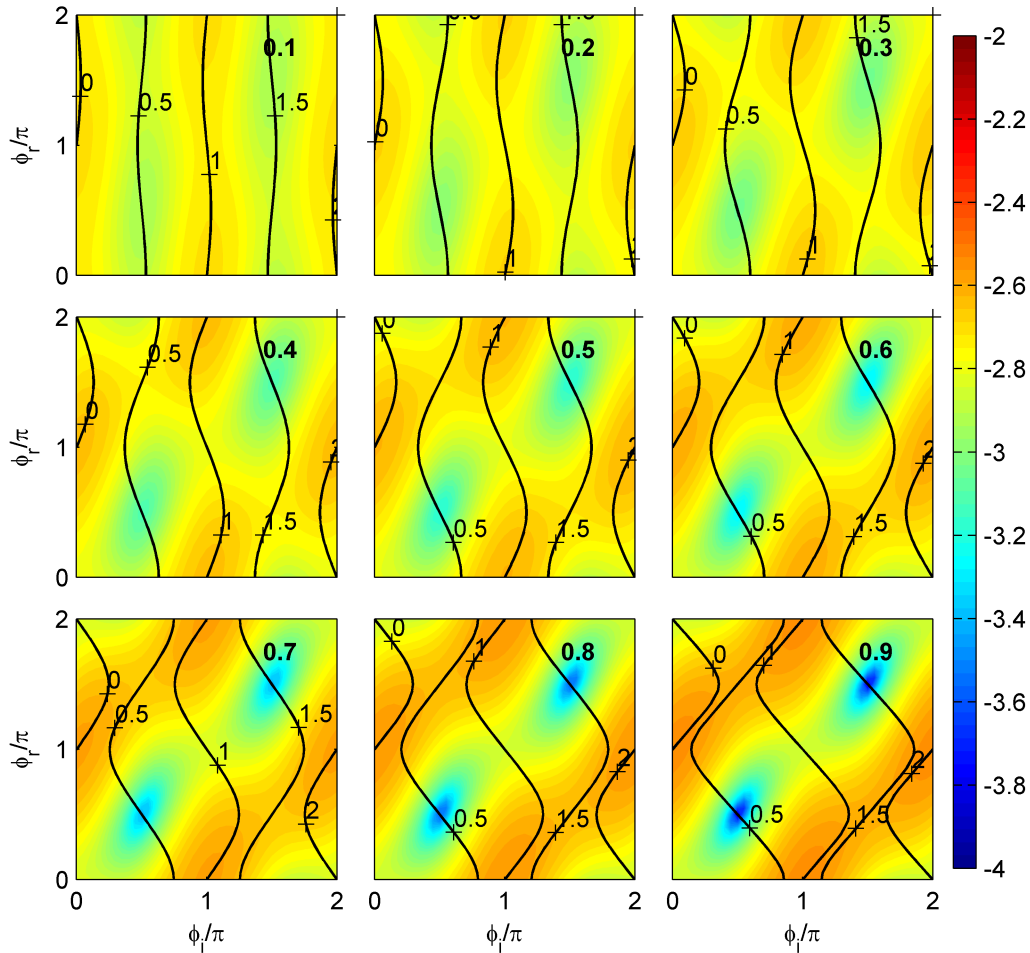


Fig. 6.3 – Log_{10} of FDKR error (color) for various reflection coefficients (bold face). Black contours: ϕ_w/π . Water depth is 0.6 m , $a = 6.5\text{ cm}$, $f = 0.9\text{ Hz}$ and gauge spacing is $s = 0.04\text{ m}$.

desired one.

As a rule of thumb for circumvent these problem, one can set a threshold of about $10^3\epsilon_M$ (where ϵ_M is machine precision) for both complex and real part of Fourier coefficients and (6.5).

SINGULARITIES Close to the classical singular lines (6.18) the solution may explode, hence one should exclude interested components to be processed. Note that gauges must have been spaced to prevent these singularities to occur at significant frequencies (according to linear wave theory).

For what concerns the curves (6.19), the angles lying in their neighbourhood,

while not exactly on them, can be transformed to the linear solutions, *i.e.*

$$\alpha_m = s \mathbf{\Omega}^{-1}(m\omega_0) \quad (6.22a)$$

$$\beta_m = 0 \quad (6.22b)$$

which is still regarded as a good approximation.

Whenever these solutions are not sufficient, one may put a quality condition for very unreliable components. For example $|a_m| + |b_m|$ should not be too big, with respect to the m^{th} Fourier coefficient of the original sample.

UNITARY REFLECTION COEFFICIENTS It may happen that, the absolute values of incident and reflected amplitudes are very close. The algorithm is then unable to determine the right quadrant for α_m . The solution should be forced to the linear one.

WRONG COSINES Despite the error smoothing, the local approximation model may be wrong, at least for some components. In some cases this is revealed by the appearance of absolute values bigger than unity for $\cos \alpha_m$ (6.9). It seems that there's nothing to do with it.

6.4 GLOBAL TREATMENT

6.4.1 ALGORITHM

In general, we will process wave gauge signal belonging to small time windows (compared to the whole record), as described by Alg. 6.2, which helps in satisfying our needs. The choice of the windows length (line 2) appears to be an important point to discuss. The opportunity of overlapping them and changing their shape, thus modifying accordingly the merging (averaging) procedure at line 10, may also affect the final results. These aspects are discussed below.

Algorithm 6.2: Windowed Fourier DKR

Data: η ($M \times 3$ data set), s (gauge spacing), h water depth, f_s sampling frequency

Result: η_i (incident), η_r (reflected)

```

1 set  $iw = 1$ ;
2 choose a time  $window$ ;
3  $M_w = length(window)$ ;
4 repeat
5    $\eta_0 = \eta(window)$ ;
6    $[\eta_{0i}(iw)\eta_{0r}(iw)] = FDKR(\eta_0, s, h, f_s)$  Alg. 6.1;
7   shift  $window$ ;
8    $iw = iw + 1$ ;
9 until  $window(end) \geq M$ ;
10  $\eta_i = merge(\eta_{0i})$ ;
11  $\eta_r = merge(\eta_{0r})$ 

```

6.4.2 WINDOW SHAPE

The big part of the error is due to FFT leakage, causing side-ends distortions. Cosine tapering, such as with Tukey windows, is frequently invoked in spectral analysis to preserve certain symmetry and limit side-ends effects. The three panels in Fig. 6.4 show the error due to application of three simple shapes: a rectangular, a triangular (Bartlett) and a Hann window.

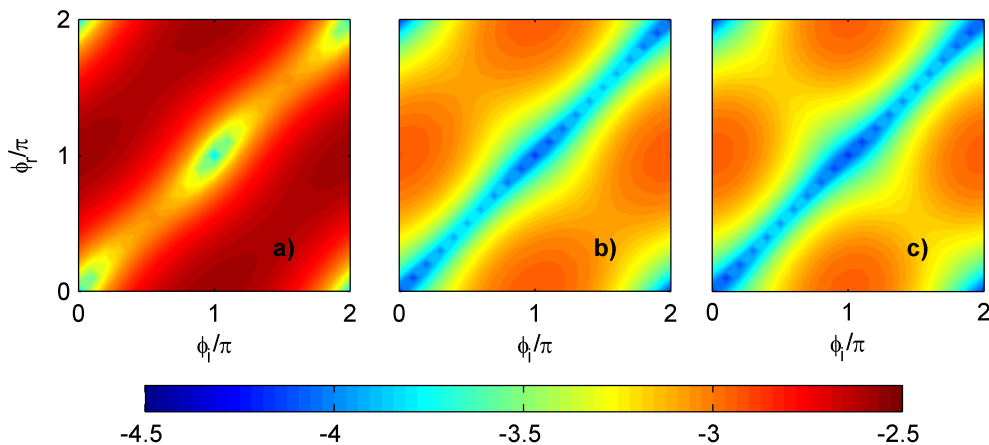


Fig. 6.4 – \log_{10} of FDKR error for various window type: a) rectangular, b) Bartlett, c) Hann. Other data: same as Fig. 6.2.

Since the errors are concentrated at the ends, a zero ended window is preferable. As side-ends are smoothed out, the resolution becomes better, and local

minima appear also on the first diagonal of the diagram. This aspect is emphasized in case of raised cosine type windows. In principle the shape should be designed according to the expected error distribution. However, this can be done for regular waves only. As modulations and non-harmonic components start to enter the domain, the error distribution may vary a lot from case to case.

The choice at line 2 of Alg. 6.2 is then determined as a Hann window, of length M_w , correspondent to an even number of periods M_T . In particular M_w will be the minimum even number of points between M_T down zero-crosses plus the zero-closer one.

The window shape is then used in the merging procedure only (Alg. 6.2, line 10), not in pre-processing. Hann heights are intended as coefficients to be used for weighted average of the results at each time step.

The first weighted point will appear with a delay depending on the overlapping width. For example, if windows are overlapped approximately of $M_w/2$ (depending on the choice of each support) then the cited point will be ready after reading $1.5M_w$ points, plus the computational time. The latter is very small: non optimized, non compiled (Matlab interpreted), Alg. 6.1 elaborates $M_w = 200$ points in approximately 0.002 s on a single *i5* processor, e.g. $1/5$ time steps when sampling at $f_s = 100\text{ Hz}$.

6.4.3 WINDOW OVERLAP

There may be severe changes in the prevalent frequency, especially in transient zones. Hence, taking zero crosses as the only feature for decision on windows lengths may induce sensible errors. At present, the strategy can be described as follows.

First of all, a local characteristic period (T_{car}) is determined on the basis of zero-down cross analysis. To define it for the whole data set, a cubic spline interpolation is used.

Local window length is decided on the basis of a pre defined number of down-crosses (M_{zdc}). This should satisfy the need of minimizing the FFT error for the most energetic components. The overlapping intervals are also decided on ZDC basis: the window advance is on the order of one zero down cross.

Each window signal is processed by *FDKR* and the results are then weighted with Hann coefficients. Since the length is designed to accomplish a local period demand, and since the minimum errors are expected at the window centre, the closer the local period $T_{car}^{(m)}$ (at a given instant) to the characteristic window local period $T_{car}^{(w)}$, the lower should be the committed error. For that, an additional set of weights is applied:

$$\gamma_m = e^{-|T_{car}^{(m)} - T_{car}^{(w)}|^2} \quad (6.23)$$

Since the signal is divided into a number of partial overlapping windows of different length, the weights (both Hann and (6.23)) are normalized according to window length.

Results at a given time are then averaged according to the so determined weighting coefficients.

6.5 PERFORMANCE

6.5.1 FDKR

LINEAR WAVES (NUMERICAL) Figures 6.5 and 6.6 compares the performance of the adaptive FDKR versus a LS method, where wavenumbers are the linear solutions. Results are given for a single Hann window, covering 2 periods.

It is seen that if FFT is unable to resolve correctly the frequencies, FDKR adapts wavenumbers decreasing the error by an order of magnitude, with respect to classical LS (Fig. 6.5). If the frequencies are matched, the errors of both methods are not far from machine precision, and are mainly due to round-off (Fig. 6.6).

WEAKLY NON-LINEAR WAVES (NUMERICAL) When dealing with second order Stokes solutions FDKR resolves finds an approximation for the phases of the bounded component, while the Airy based LS does not.

If the FFT resolution is sharp (Fig. 6.7) FDKR errors are the same of the corre-

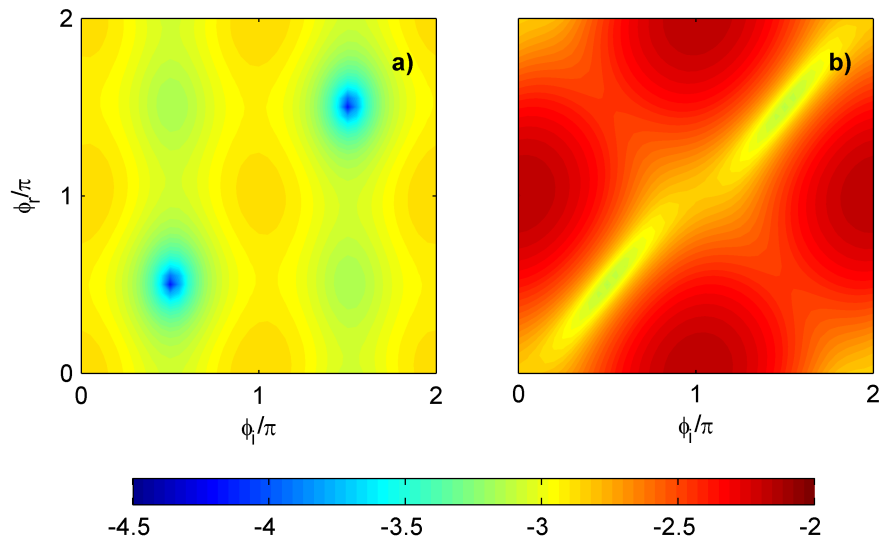


Fig. 6.5 – Log_{10} of error for a) FDKR, b) LS. Results are Hann windowed. Other data: same as Fig. 6.2.

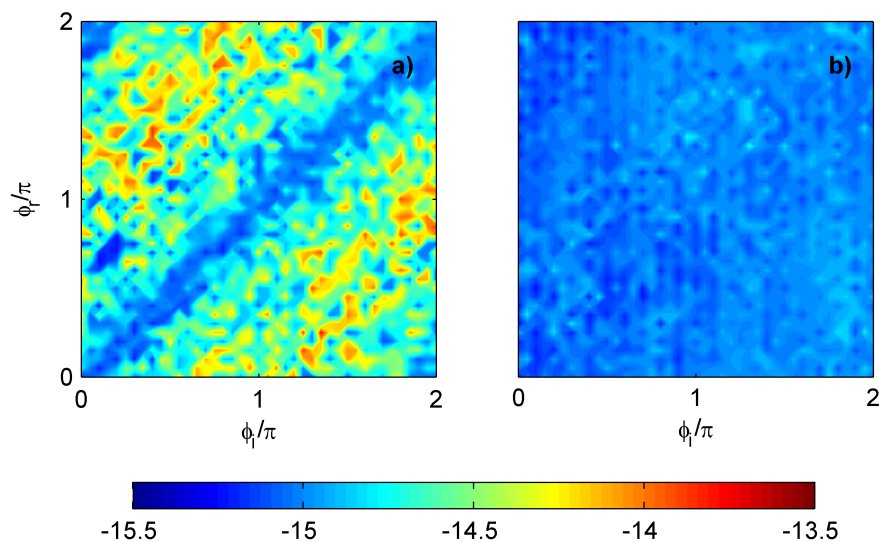


Fig. 6.6 – Same as Fig. 6.5, except for $f = 1$ Hz.

spondent linear case (Fig. 6.6).

If FFT resolution does not match the wave frequencies (Fig. 6.8) then FDKR adapts the phases at each frequency, and solved the problem with an error which is again, in the most part of the graph, similar to the linear case one (Fig. 6.5). In both cases the precision of the LS method is the same, since it is governed by the mismatch of the second harmonic phases.

The sharp high error lines in Fig. 6.8 (left panel) are due to second harmonics. When the incident and reflected components have a phase difference (which

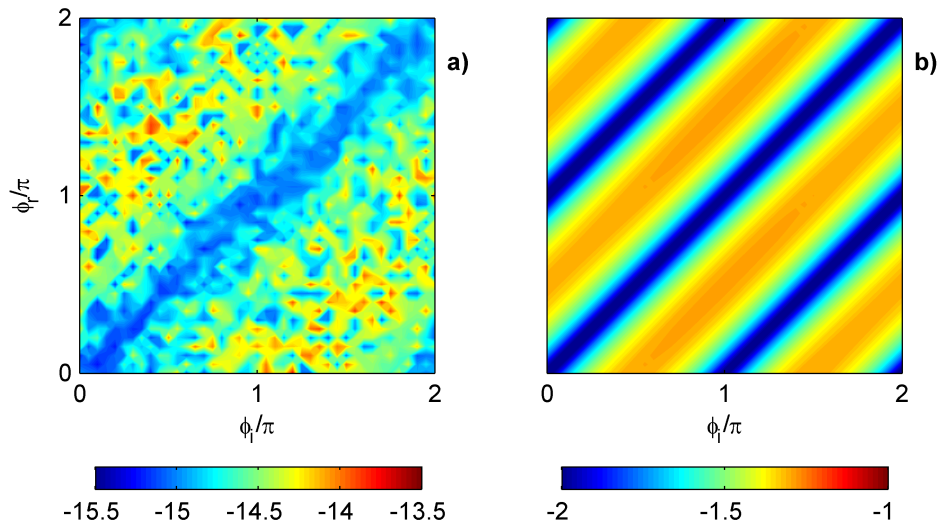


Fig. 6.7 – Log_{10} of error on Stokes 2nd order solution for a) FDKR, b) LS. Results are Hann windowed. Other data: same as Fig. 6.2.

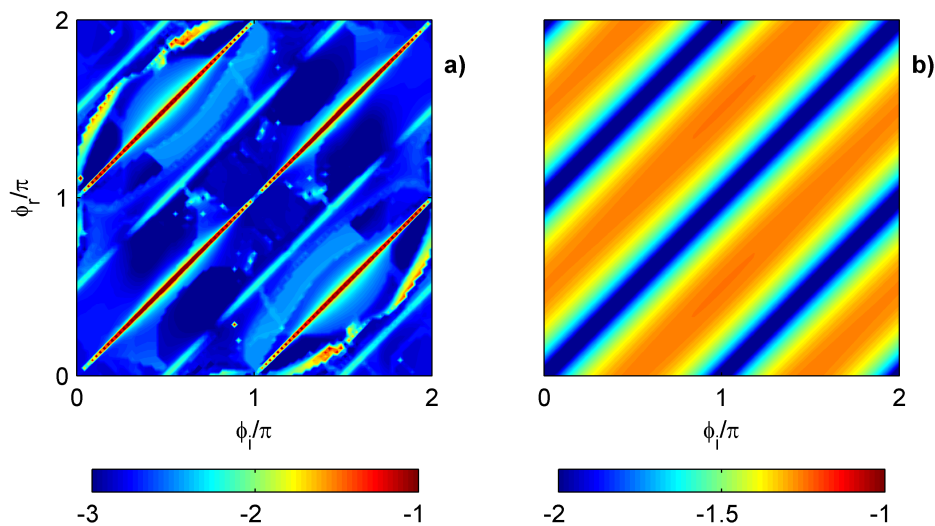


Fig. 6.8 – Same as Fig. 6.7, except for $f = 0.9$ Hz.

depends on the observation point) exactly equal to $q\pi$ ($\forall q \in \mathbb{Z}$) the algorithm converges to wrong amplitudes.

One may fix this *bug* forcing FDKR to the linear solution. But besides a little improvement for the FFT non-sharp resolved cases, it would worsen severely the precision for the rest of the applications. This does remain an open question, thus. Anyhow, note that, in order to invalidate the solution, the phases difference matches ($q\pi$) must be *exact*.

WEAKLY NON-LINEAR LABORATORY WAVES (NUMERICAL) When dealing with laboratory regular waves, and in general, with irregular waves (both field and laboratory events), Stokes solutions predict coexistence of free and bound waves at each frequency band. Linear superposition of these components do not match with local DKR assumptions. In fact, the expression of local amplitude and wave numbers are not stationary in space (according to Stokes). See *e.g.* (4.64).

Consider a simple *quasi*-regular laboratory wave field:

$$\begin{aligned} \eta = & a \cos(\omega t - kx + \phi) + a_F \cos(2\omega t - k_F x + \phi) \\ & + b \cos(\omega t + kx + \phi) + b_F \cos(2\omega t + k_F x + \phi_F) \quad (6.24) \\ & + \text{interactions (4.32)} \end{aligned}$$

with $k = \Omega^{-1}(\omega)$ and $k_F = \Omega^{-1}(2\omega)$ the linear wavenumbers. This is produced generating relatively steep waves with straight Biesel transfer function. But it is also determined by perfect waves interacting with obstacles in the flume. Therefore a frequent case to be dealt with when testing floating structures in relatively steep wave conditions.

Assume that free second order wave is generated at the paddle and let vary the amount of the reflected one. In order to investigate the expected errors, for each case assume the observer phases to be even distributed random variables in the interval $[0; 2\pi]$. In principle the phase of the unwanted outgoing wave can be deterministically evaluated, but let it be an additional unknown variable for general purposes. Results of Monte-Carlo based simulations are reported in Fig. 6.9, where sensitively high wave steepness ($a/L = 0.045$) was considered. Note that, for the last point, $b_F/b = 0.3$. And this is not an infrequent case.

The performance of FDKR is compared with classical LS and with an iterative LS (LS2) which resolves the bounded wave field according to (4.32).

For very small spurious free waves amounts (b_F/a_F) a better behaviour for FDKR was expected (with respect to LS), since the algorithm is able to model exactly the bounded waves phases. The reason for this unexpected discrepancy should be investigated in the future. In general the bigger errors are due

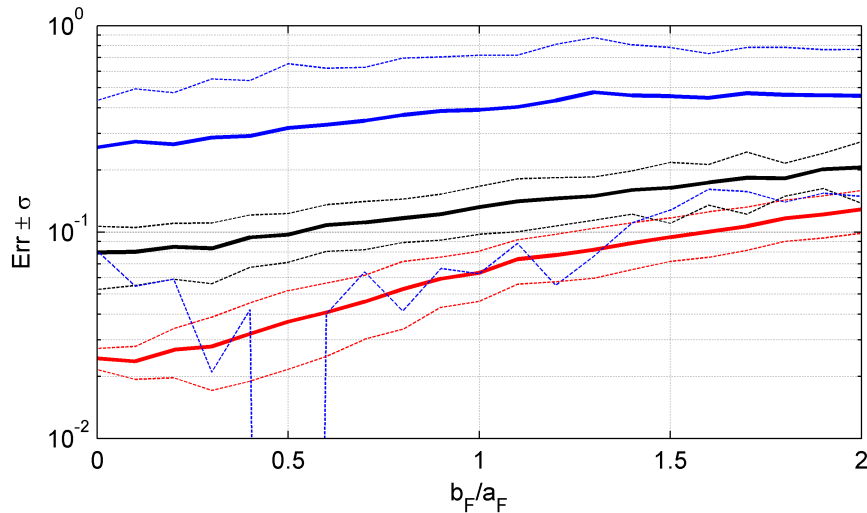


Fig. 6.9 – Error committed by three valuable methods. Black: LS, blue: FDKR, red: LS2 with second order fitting. Thick lines: average errors; dashed lines: confidence interval. Main reflection coefficient is $\rho = 0.5$; $\omega = 1.8\pi \text{rads}^{-1}$, $h = 0.6\text{m}$, a_F is ≈ 0.5 the main bounded component amplitude, $a = 6.9\text{cm}$.

to the fact that the wave field does not match DKR hypotheses. The best results are given by the second order solver.

Comparison of Fig. 6.9 with Fig. 6.8 reveals that the presence of more than one free component (non strictly regular field) dramatically decreases the methods precision. Even if LS2 results were not given before, the reader would trust that its capability is comparable with FDKR, for previous simple wave fields.

6.5.2 WFDKR - FLUME DATA EXAMPLES

This paragraph reports examples of application to extreme cases of wave flume records. A floating breakwater is moored with loose chains in the flume, and gauges are placed in between paddle and FB positions, well away from them. For both examples the gauges spacing is $\mathbf{x} = [00.0850.170.27]$. The reasons for that choice will be described in the next chapter. Waves are generated with piston type paddle with regular monochromatic motion. No correction for spurious waves is adopted.

WFDKR outputs based on the first gauges triplet are compared with other methods. These are the straight LS, based on whole gauges set, a windowed LS (first triplet) and a windowed LS2 (whole set). Windowing and averaging

are done by the same algorithm for the three methods.

EXAMPLE 1 Wave principal frequency is $f = 1.894 \text{ Hz}$, water depth is $h = 0.6 \text{ m}$ and target wave amplitude is $a = 0.65 \text{ cm}$.

Fig. 6.10 shows the outputs of the four mentioned algorithms for a time range where no reflection is expected. WLS2 is the only one which shows almost negligible reflected wave, since it is the only one that captures almost perfectly the phases of the second harmonics. All other suffer a sensible leakage. Airy based LS and WLS2 misinterpret the second harmonics phases. It has been shown that WFDKR is able to exactly reproduce the phases of mono-components. The reason of its failure is then to be considered a confirmation that multiple waves, travelling with different celerities, coexist at each frequency.

For completeness, in Fig. 6.11 attention is paid to time at which FB reflected waves begin passing through the gauges line. In these regions there's no way of distinguishing the better and the worse.

A classical way of evaluating the output of a reflection analysis is to measure the distance between the reconstructed wave $\tilde{\eta} = \eta_i + \eta_r$ (incident+reflected) and the original signal η . A normalized error estimation is here proposed:

$$Err = \frac{(\tilde{\eta} - \eta)}{\max\{|\eta|\}} \quad (6.25)$$

In Fig. 6.12, 6.25 are given for each method, and for the whole data set. The LS method reconstructed wave field is closer to the original than the WLS ones simply because the frequency discretization is more accurate. The better reconstruction is due to WLS2.

The smaller errors are observed for WFDKR in the time range where only incident waves are expected. The reason for the better, even if in cumulative sense, behaviour, is that the phases of the principal component are better estimated by FDKR procedure. At fundamental frequency band, no sensitive bound components are expected, hence the adaptive phase resolution is almost exact. In the reflection zone, the WFDKR errors have the same order of magnitude of Airy based methods.

EXAMPLE 2 Wave principal frequency is $f = 0.812 \text{ Hz}$, water depth is $h = 0.385 \text{ m}$ and target wave amplitude is $a = 9.2 \text{ cm}$.

Fig. 6.13 shows the outputs of the four mentioned algorithms for a time range where no reflection is expected, while Fig. 6.14 for the time range at which FB reflected waves start to reach the gauges.

Again, the best results are due to WLS2. Anyhow, WFDKR outputs are not worse than Airy based methods. This is probably due to the fact that second order phases mismatches are not so big as in the preceding example, *i.e.* wave are less dispersive. Note that relative water depths (kh) are 9.38 and 1.32 for examples 1 and 2 respectively. For that, second order phases are better approximated by FDKR.

Cumulative errors are given in Fig. 6.15. WFDKR ones are lower than the others by an order of magnitude, again for its power of resolving almost exactly the phases of the fundamental components.

6.6 CONCLUDING REMARKS

These few words are meant to close the chapter series spent on research of a valuable reflection analysis method for laboratory waves.

All linear methods do not satisfy the precision need when analysing relative high steep wave conditions, due to their sensitive non-linear characteristic. Even not found in literature, a second order Stokes method was implemented (LS2).

Among all methods DKR seemed a good starting point to be dealt with. Authors report that its performance is limited in case of non strictly speaking narrow band wave spectra. Its precision is related to mismatches between the simplified model quadrature and the one given by its HT. Attempts of ameliorating its capability are done at first by implementing a modified EMD procedure for expanding the wave signals into a set of Bedrosian admitted signals. It was concluded that EMD like utilized procedures are unable to explode the gauges signals into a set of homogeneous basis, useful for reflection analysis. Other DKR problems were recognized and solved by rewriting basic equations and implementing it iteratively. A novel solution (FDKR) was proposed, based

on DKR, but applied to components in the frequency domain, instead of on analytic signals in time domain.

It has been shown that the tool gets rid of FFT frequency discretization and is therefore able of resolving wave phases much better than a linear method. However the application to real data showed that waves interaction are not solved properly. This at least confirms that a number of components with same frequency travelling at different speed co-exist in the observation region.

Wave-wave interactions, at least up to second order, are better detected by LS2. *I.e.* an hydrodynamic model is *really* need, at least up to now.

For these reasons, the final choice is the windowed Stokes second order LS based method. LS2 will be used for separating wave trains from laboratory data collected for the present work.

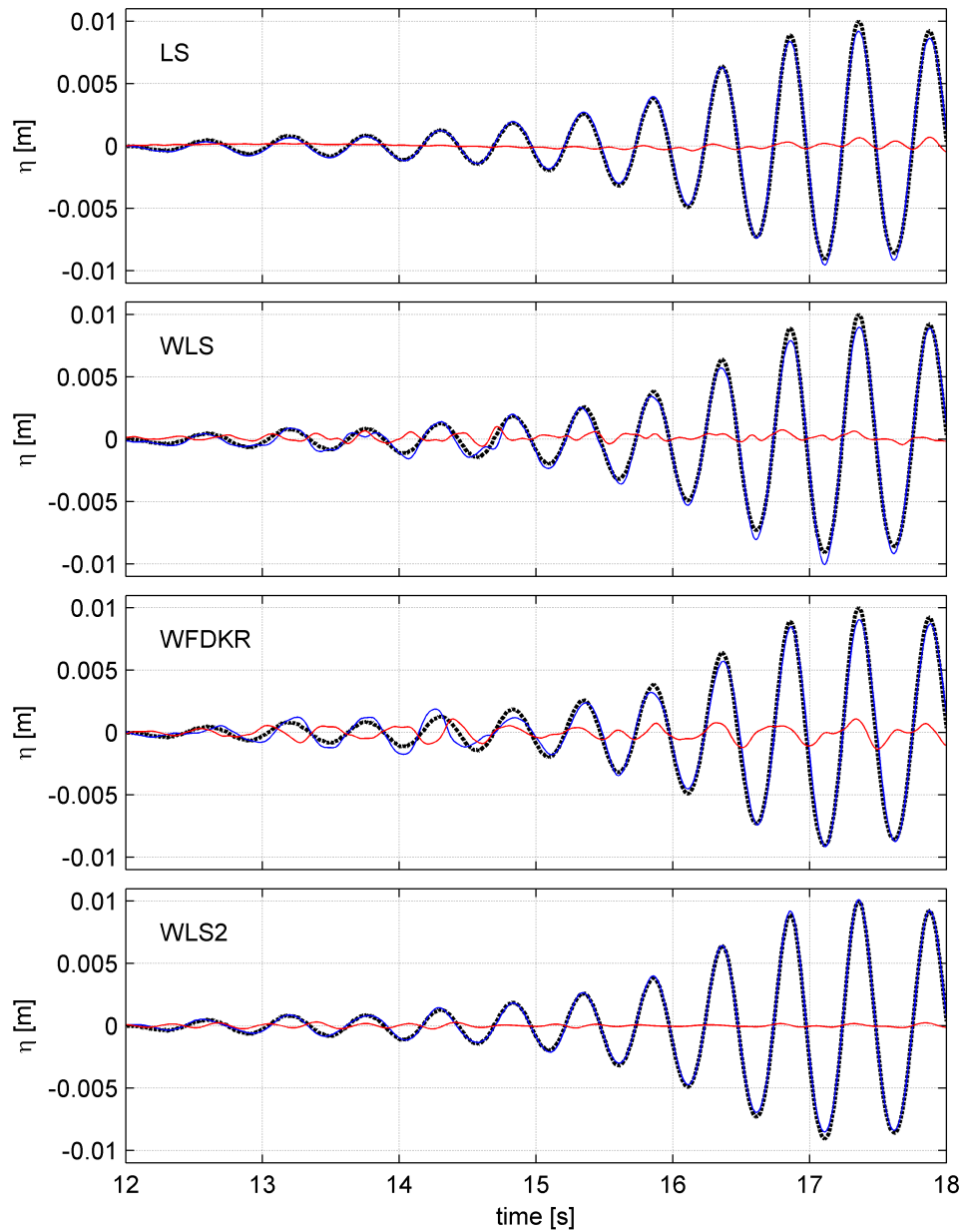


Fig. 6.10 – Example 1. Reflection analysis results where no reflected waves are expected. Outputs of each of considered methods. Black dashed line: original data; blue: incident wave; red: reflected

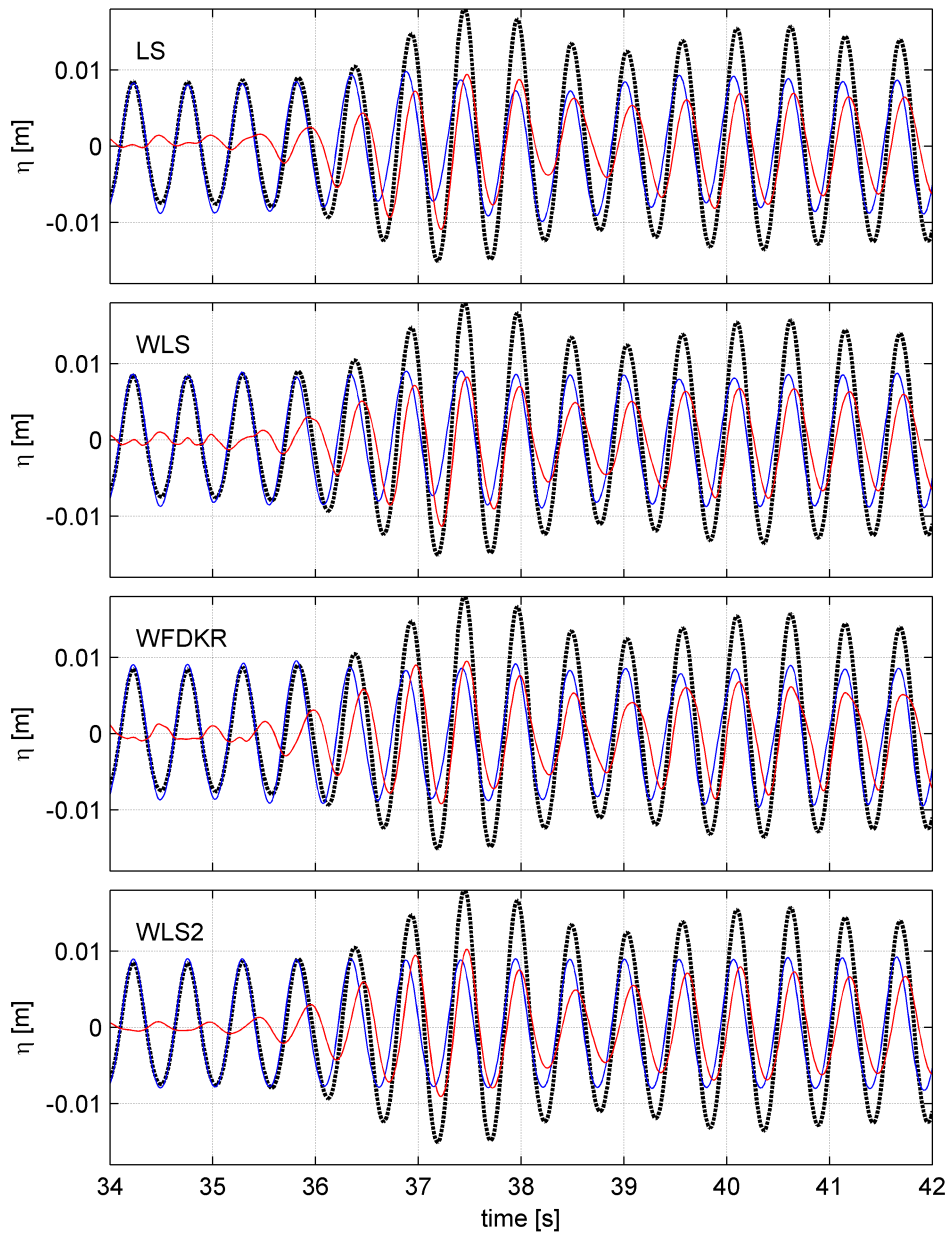


Fig. 6.11 – Example 1. Reflection analysis results where first reflected waves reach the gauges. Outputs of each of considered methods. Black dashed line: original data; blue: incident wave; red: reflected

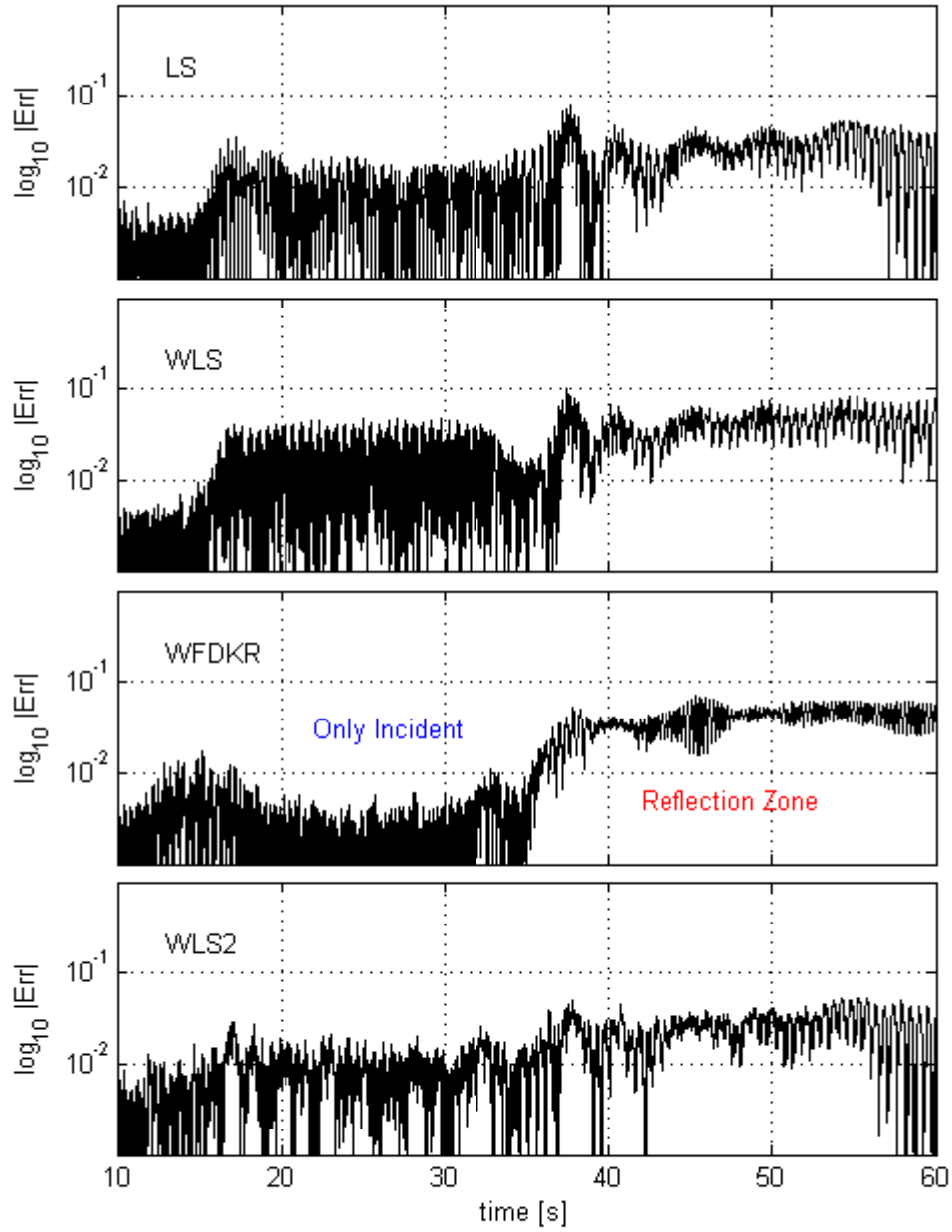


Fig. 6.12 – Example 1. Errors on wave field reconstruction for each of considered methods.

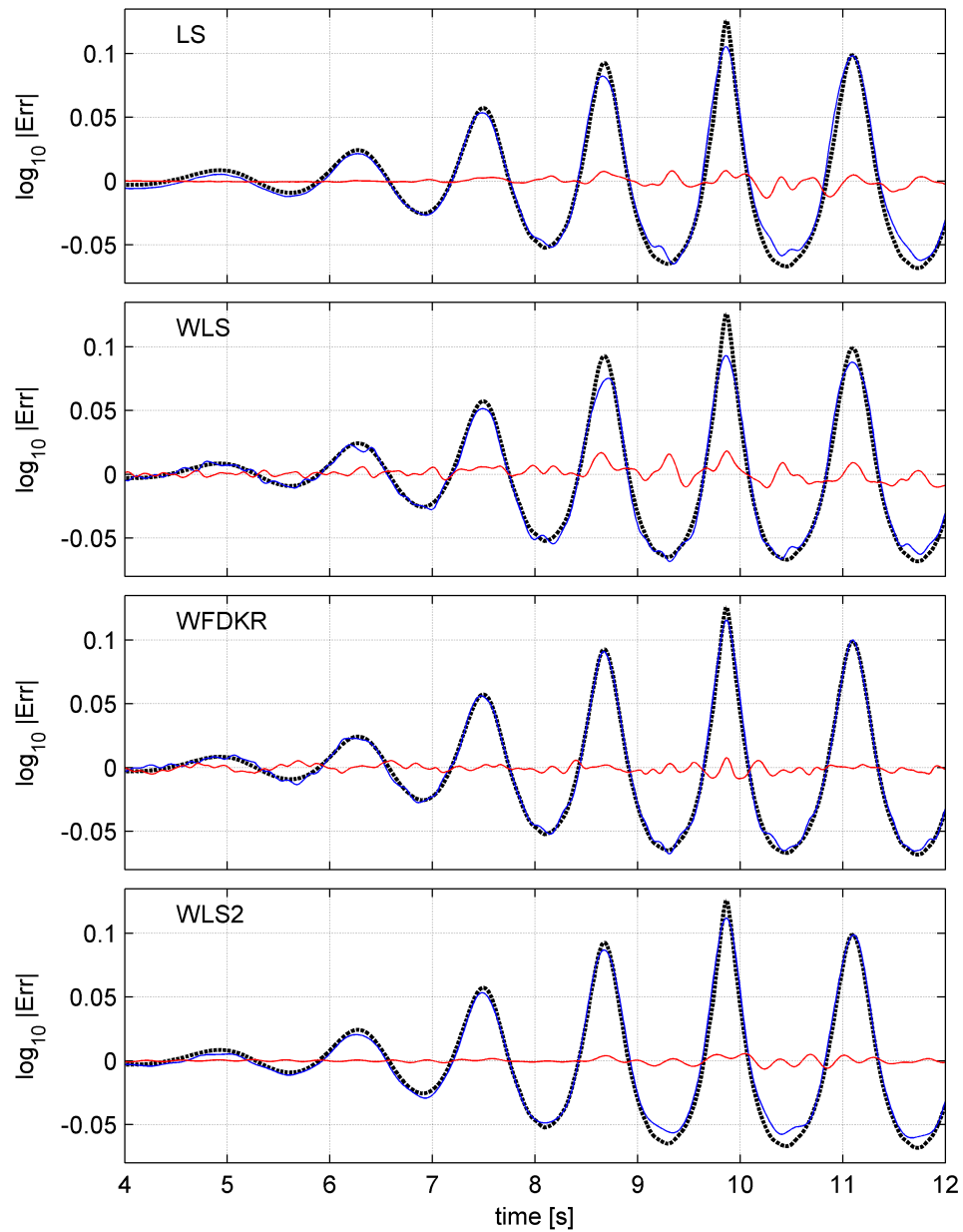


Fig. 6.13 – Example 2. Reflection analysis results where no reflected waves are expected. Outputs of each of considered methods. Black dashed line: original data; blue: incident wave; red: reflected

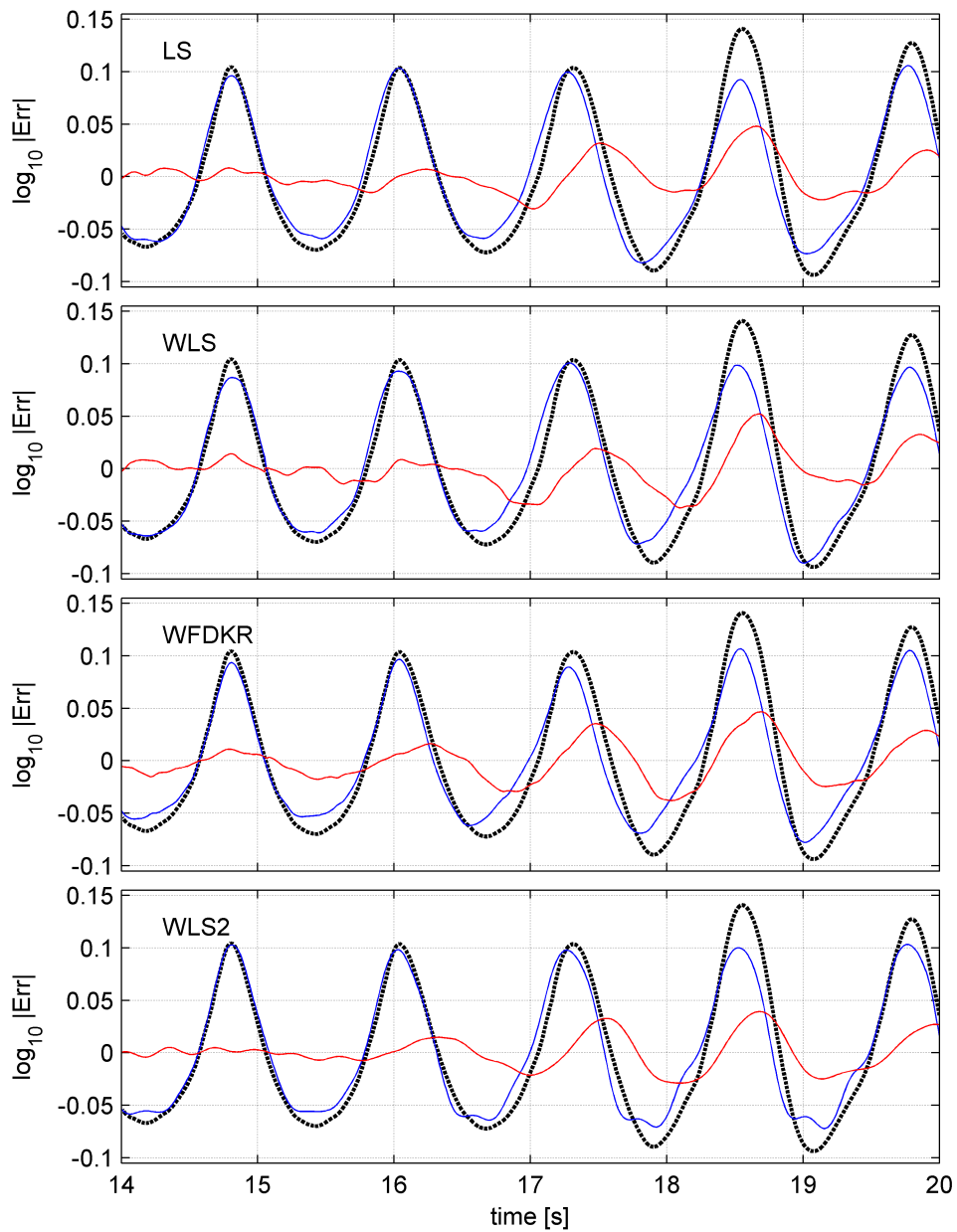


Fig. 6.14 – Example 2. Reflection analysis results where first reflected waves reach the gauges. Outputs of each of considered methods. Black dashed line: original data; blue: incident wave; red: reflected

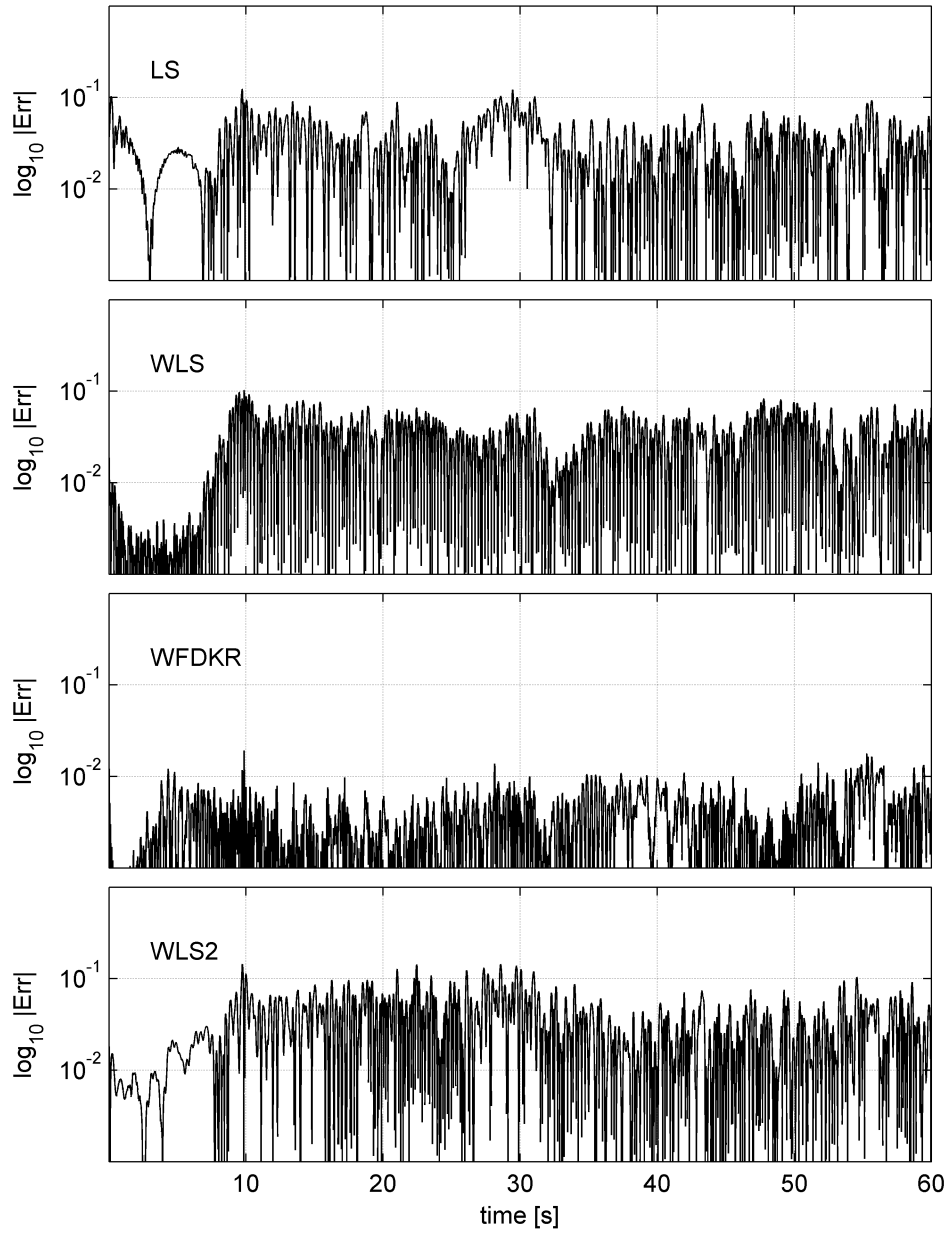


Fig. 6.15 – Example 2. Errors on wave field reconstruction for each of considered methods.

7 EXPERIMENTAL SET-UP

7.1 FACILITIES

Physical model tests have been carried out in the Maritime Laboratory of ICEA Dept. (University of Padova). The wave flume is 36 m long, 1.0 m wide and 1.4 m deep (Fig. 7.1).

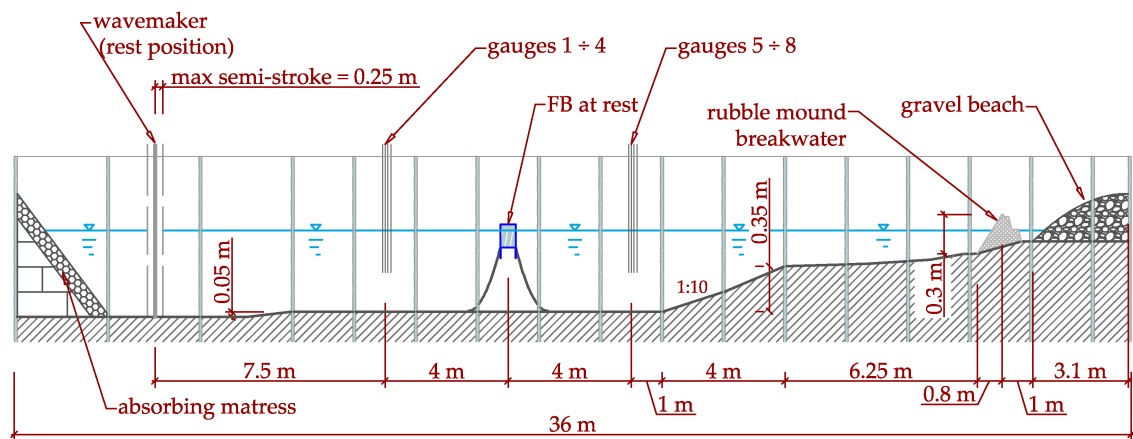


Fig. 7.1 – Wave flume set up. Horizontal scale to vertical scale proportion is 4 : 1.

7.1.1 WAVE GENERATION

The wave generator paddle is a hydraulic servo-controlled roto-translating flap with variable rotation point. It can be set to work as a bottom hinged flap as well as a pure translating piston. All intermediate configurations are possible. For present job the machine motion were set to *piston* mode.

The basic wave generation software is based on *first – order* Biesel technique, allowing both regular motion and irregular JONSWAP and Pierson-Moskowitz like white noise filtered spectra. Other kind of wave conditions can be user de-

fined, imposing needed paddle motion timeseries. The system is equipped with a filter based active absorption system.

Due to the facility complexity, each experimental set-up has to be preceded by an overall paddle transfer function calibration. A set of user friendly VBA based tools has been recently implemented (Pezzutto, 2012) to provide a fast and automatic procedure.

For present job, waves were generated with simple *first – order* technique and active absorption tool was utilized.

7.1.2 WAVE MEASUREMENTS

Water surface time series were sampled with 8 resistive gauges, connected to HRw rack-mounted system. Both gauges calibrations and data sets storage was pursued via rack-USB interface through HRDaq software.

For present job, gauges were divided into two in-line arrays. The first one has been positioned between the paddle and the FB site, and the second between the FB and the beach. Gauges number identifiers are ordered left to right (Fig. 7.1).

The distance of each array from the FB is $4m$ (with reference to gauges 2 and 5), high enough to not capture significant evanescent standing modes.

Each array has been designed to cope with reflection analysis methods enumerated in Sec. 6.5.2. The first three gauges are equally spaced (for DKR use) of an amount of 8.5 cm , and the fourth is positioned 27.1 cm downstream from the first gauge to minimise LS overall singularities.

7.2 MODELS

Two floating breakwater models were utilized for physical tests. General sketch is given in Fig 7.2 and detailed characteristics are summarized in Tab. 7.1. Both models were built using aluminium with a polystyrene core.

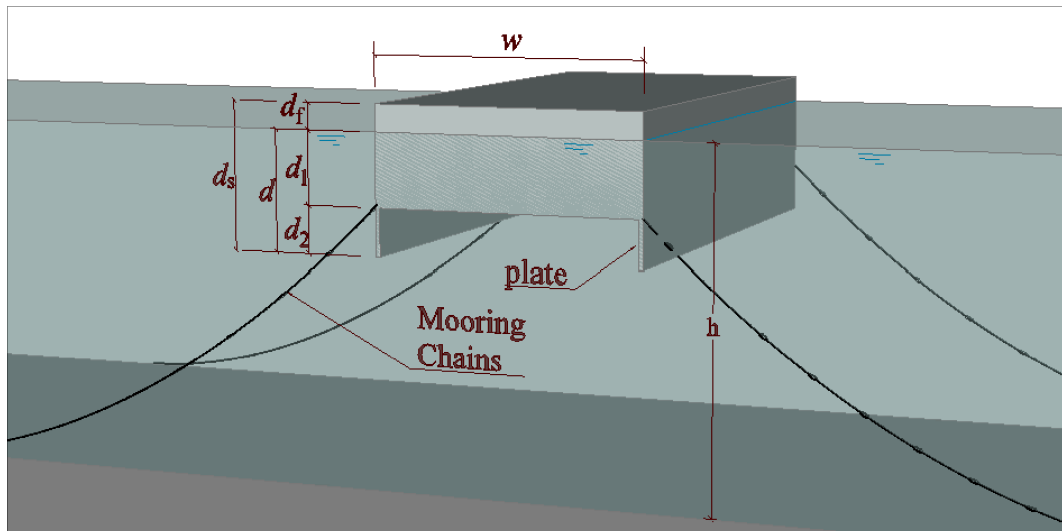


Fig. 7.2 – Sketch of FB models, with indication of 2DV relevant dimension.

Tab. 7.1 – FB models description with reference to Fig. 7.2

FB code	type	mass [kg]	w [m]	d_s [m]	d [m]	d_2 [m]	T_h [s] ^a
S16	single	16.20	0.250	0.150	0.110	0.035	0.88
D56	double	56.30	0.500	0.283	0.178	0.067	1.17

^a heave natural period measured with free decay test on 0.515 m water depth

7.3 TEST CASES

The series of tests has been designed according to the main objective of this job, *i.e.* to investigate the behaviour of some commercial type FBs relative to a set of non dimensional parameters. Some of them have been identified in Ch. 3. These are the ratio of incident wave period over FB heave natural period (evaluated through free decay test), *i.e.* T/T_h , wave steepness kH (or $2\pi H/L$) and relative FB draft d/h .

Due to physical limitation of the wave flume, the small FB has been utilized to investigate relative small d/h conditions, while the bigger one resulted suitable for big d/h ratios. The four setups (series) are here summarized in Tab. 7.2. All waves are regular waves, except where mentioned.

It is worth to mention that some extreme combinations were not investigated due to initial incorrect evaluation of generator limitations, some were excluded

Tab. 7.2 – Test series description. For each series consider all possible combinations with $H/L = [0.03\ 0.05\ 0.09]$.

series	FB	d/h	h [m]	z_c [m] ^a	x_c [m] ^a	T/T_h		
						from	to	step
A	S16	0.183	0.600	0.550	1.400	0.6	1.5	0.1
B	S16	0.286	0.385	0.320	0.900	0.6	1.5	0.1
C	D56	0.286	0.623	0.543	1.520	0.5	1.6	0.1
D	D56	0.396	0.449	0.369	1.100	0.5	1.6	0.1

^a z_c and x_c are vertical and horizontal lengths of chains at rest

for sake of safety, and some others were corrupted for some physical reasons (moorings loosening or breaking, incorrect sampling...). These are here enumerated with notation [*series*, $\langle T/T_h \rangle$, $\langle H/L \rangle$]: [A, 1.5, 0.05], [A, 1.4, 0.09], [A, 1.5, 0.09], [B, 1.5, 0.09], [C, 1.4, 0.05], [C, 1.1~1.4, 0.09], [D, 1.4, 0.05], [D, all, 0.09].

Four additional tests were later included for aesthetic purposes (photos and moovies) and demonstration examples. These are two regular wave tests, namely [D, 0.5, 0.05] and [D, 1.4, 0.02], and two irregular wave runs. The first of these is a narrow banded JONSWAP-type wave series, $\gamma = 3.3$, denoted by J[D, 1, 0.03], where values have to be intended in a *peak* and *significant* terms. The second one is a Pierson-Moskowitz wave series with same modal period of the former, therefore denoted as PM[D, 1, 0.027].

Total number of test cases is then 105. The 103 regular wave tests results will be utilized for FB parametric analysis, while the 2 irregular wave ones are utilized to inspect spectral deformations of waves passing a FB.

7.4 ANALYSIS METHODOLOGIES

7.4.1 PRE-ANALYSIS

REFLECTION	All the results presented in Ch. 8 are derived from least
ANALYSIS	squares frequency domain algorithm LS2 described in 4.1.3.

PRE-TREATMENT LS2 output timeseries have been shortened, eliminating the side end transients. The shortening has been made synchronizing incident, reflected and transmitted waves, accounting for main group celerities and FB and wave gauge positions.

This procedure allowed to retain, case by case, for incident, reflected and transmitted surface elevations, the same series length and the corresponding event representation, in terms of energy flux.

7.4.2 COEFFICIENTS EXPANSION

By pursuing the reflection analyses throughout LS2 method, we achieved an almost second order accuracy on separated time-series. This allows us to evaluate FB process coefficients directly from free waves data. Thus all data presented in the following are to be referred to LS2 reflection analyses.

Gauges arrays have been placed sufficiently far from the floating object, so we can expect that non-linear wave components can be fully described based on primary waves. Denoting the free waves incident signal (complex) amplitude with a_i and the transformed one (reflected, transmitted or dissipated) with a_F , in general we have for a linear process

$$a_F(\omega) = F(\omega) a_i(\omega) \quad (7.1)$$

with $F(\omega)$ a given transfer function. Bounded incident second order spectra are due to primary ones

$$a_i^{II}(\omega_1, \omega_2) = G(\omega_1, \omega_2) a_i(\omega_1) a_i(\omega_2) \quad (7.2)$$

where G are the second order transfer functions. Due to its linearity, the transformed second order spectra are again linear functions of the latter:

$$\begin{aligned} a_F^{II}(\omega_1, \omega_2) &= G(\omega_1, \omega_2) a_F(\omega_1) a_F(\omega_2) \\ &= G(\omega_1, \omega_2) F(\omega_1) a_i(\omega_1) F(\omega_2) a_i(\omega_2) \\ &= F(\omega_1) F(\omega_2) a_i^{II}(\omega_1, \omega_2) \end{aligned} \quad (7.3)$$

If (7.1) holds for reflection, transmission and dissipation of energy for a wave passing an FB, then it is sufficient to evaluate the linear coefficients $F(\omega)$ only.

LINEAR COEFFICIENTS In order to determine (evaluate) $F(\omega)$ from experimental data we first isolate free wave components from second order bounded ones (see Fig. 7.3). Error in pursuing this separation is almost of third order in wave steepness. No additional procedure is needed for that, since, by solving the reflection problem with LS2 method, Fourier components and time series are already available.

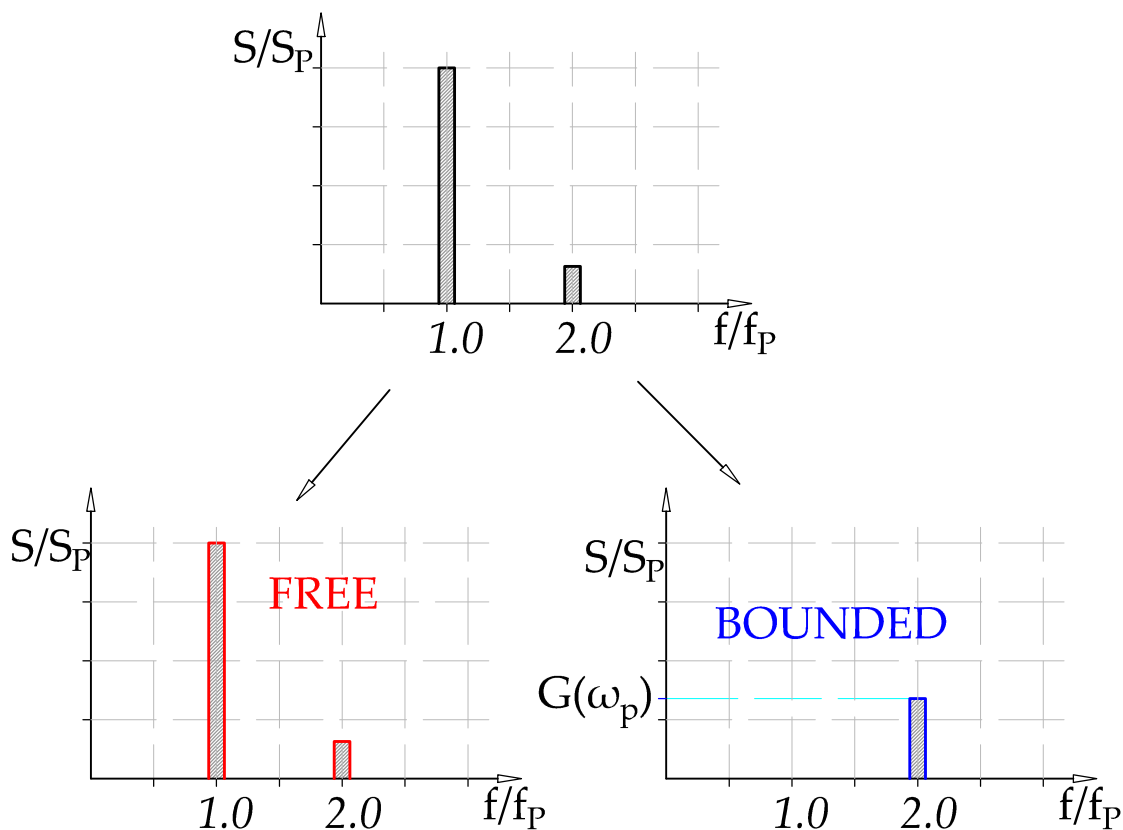


Fig. 7.3 – Refinement of the records, discarding relevant phase-locked components. Ordinate: energy spectral densities, normalized with value at principal frequency.

The whole data set of present job regards laboratory regular waves. Hence, for each record, the most part of energy is concentrated at fundamental frequency (f_p). After the separation (Fig. 7.3), we note that, at double frequency an amount of energy deputed to un-locked waves usually exists for each case. This aspect matches expectations, since it is well known that pure sinusoidal

paddle motion generate unwanted free components, which are second order in wave steepness.

For the same reasons (interaction of a sinusoidal wave with an object) free waves at double frequency ($2 f_p$) are expected to be released by the FB. Therefore, in reflected and transmitted records, we may face $2 f_p$ free components which are partly due to linear reflection (transmission) of incoming components of the same kind, and partly to quadratic transfer from primary f_p components. It is not infrequent then to compute meaningless (bigger than unity) reflection and transmission coefficients at these frequencies bands (Fig. 7.4).

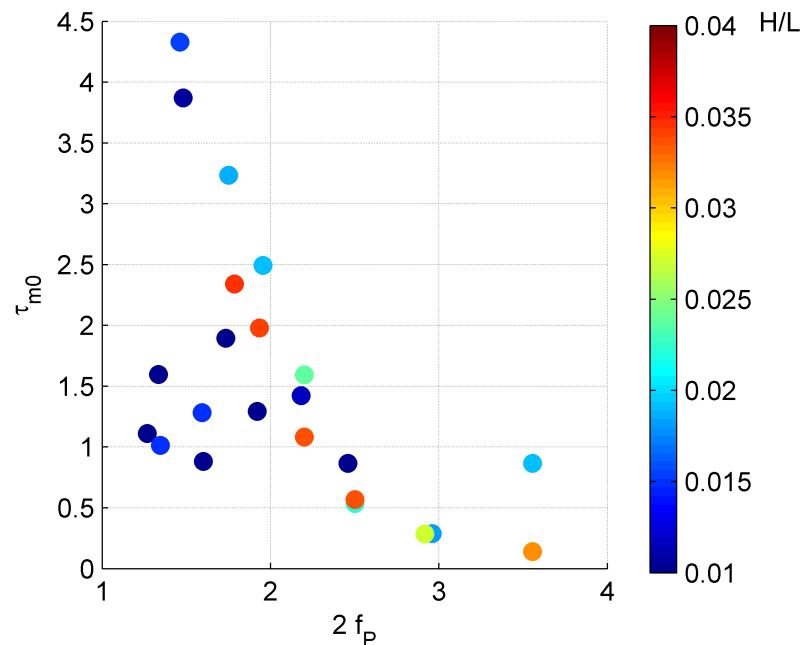


Fig. 7.4 – Transmission coefficients for free second harmonics (series C). Steepness (colorbar) is relative to incident primary component. Coefficients higher than unity reveals that an amount of energy comes from somewhere else in the world.

For these reasons, we will consider only primary waves to interpret linear reflection and transmission coefficients distributions.

NON-LINEAR COEFFICIENTS Once $F(\omega)$ in (7.1) is estimated for reflection and transmission processes, the amount of energy transfer from primary to second harmonics can be depicted. The second harmonic energy increase can be estimated as the difference between measured energy $|a_F(2\omega)|^2$

and its expected linear value:

$$\Delta E_F (2\omega) = |a_F (2\omega)|^2 - F^2 (2\omega) |a_i (2\omega)|^2 \quad (7.4)$$

The coefficient

$$\delta_{F,2}^2 = \frac{|\Delta E_F (2\omega)|}{|a_i (2\omega)|^2} \quad (7.5)$$

does therefore account for second harmonic energy loss, if $\Delta E_F (2\omega)$ is negative, or for an energy increase, if $\Delta E_F (2\omega) > 0$.

Since we are dealing with regular waves only, it is expected that, in the latter case, (7.4) has to be deputed to quadratic transfer from primary component. It is also expected that, at this level, energy flux is conserved:

$$c_g (\omega) \Delta E_F (\omega) = c_g (2\omega) \Delta E_F (2\omega) \quad (7.6)$$

with c_g the group celerity of the free wave at corresponding frequency.

If $\Delta E_F (2\omega) < 0$ such estimation can not be done, because the whole transfer amount results *masked* by second harmonic losses. For these reasons the following coefficient is defined

$$\delta_{F,1}^2 = \max \left\{ 0, \frac{c_g (2\omega) \Delta E_F (2\omega)}{c_g (\omega) |a_i (2\omega)|^2} \right\} \quad (7.7)$$

accounting for additional primary wave loss.

It is worth to notice that, in order to have a complete description for irregular-like waves, second order transfer functions should be estimated throughout bi-chromatic wave fields experiments. This is left for future research.

7.4.3 COEFFICIENTS DEFINITION

Analyses for primary and second harmonics will be separated, and the wave height for the j^{th} harmonic are computed with the proper discrete summation form of following energy integral:

$$H_{m0}^2 (jf_P) = 8 \int_{f_P - \Delta f}^{f_P + \Delta f} E (f) df \quad j = 1, 2 \quad (7.8)$$

where f_p is the frequency of the main wave and $\Delta f \leq f_p/2$.

All transmission (τ_{m0}), reflection (ρ_{m0}) and loss coefficients (δ_{m0}) do refer to spectral analysis, except when differently indicated in text or by subscripts. Squared coefficients do refer to energy ratios, while non squared ones account for amplitudes or heights ratios.

8 RESULTS AND DISCUSSION

8.1 VERIFICATION OF TARGET INCIDENT WAVES

This section is meant to verify experimental magnitudes characteristics and time series regularity. Inspection is made through zero down cross analysis of the incident wave series, previously separated according to the most stable reflection analysis method (LS2).

8.1.1 WAVE PERIODS

Mean period T_m is here defined as the average of all detected zero-cross periods. Figure 8.1 report their deviations from the target periods T , *i.e.*

$$\epsilon(T_{im}) = \frac{T_{im} - T}{T}. \quad (8.1)$$

In all cases T_m deviates from target values less than 1%. By this point of view all data are acceptable.

8.1.2 ROOT MEAN SQUARE HEIGHTS

Root mean square heights is defined as the square root of the average of all zero-cross detected squared wave heights (H_{zc}),

$$H_{rms} = \sqrt{\langle H_{zc}^2 \rangle} \quad (8.2)$$

Figure 8.2 gives the relative errors of LS2 separated incident wave heights (H_{irms}) with respect to the target values (H), *i.e.*

$$\epsilon(H_{irms}) = \frac{H_{irms} - H}{H}. \quad (8.3)$$

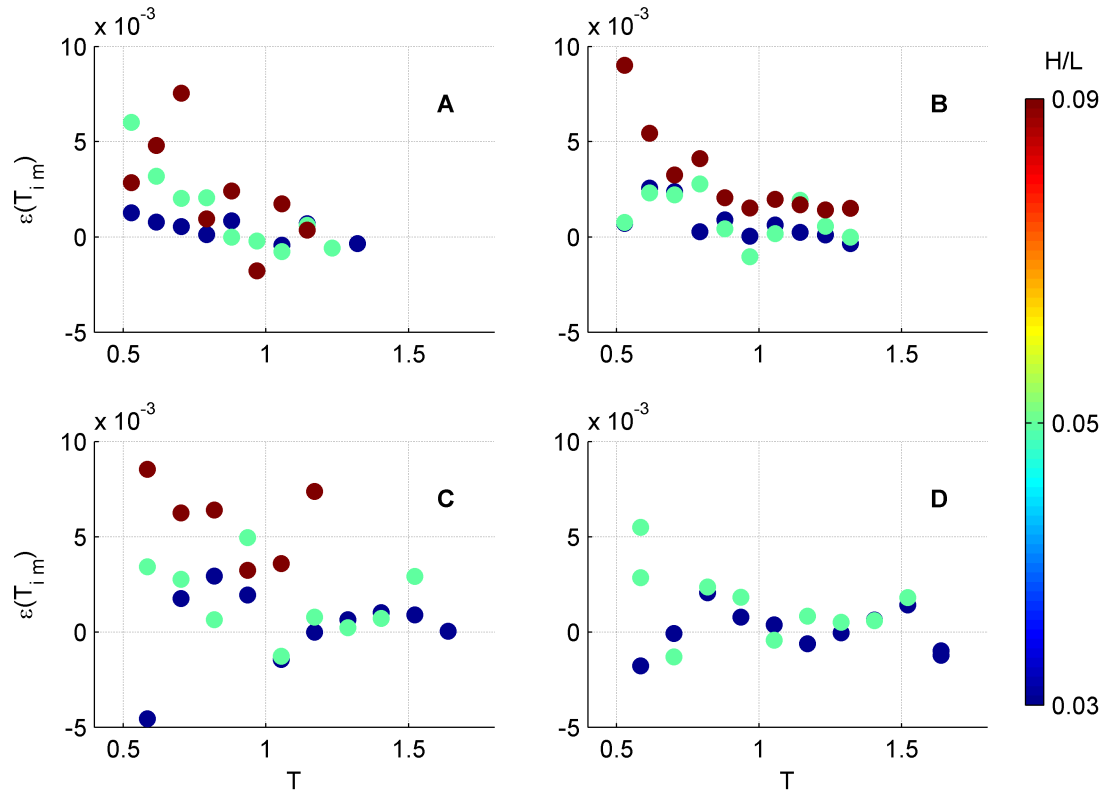


Fig. 8.1 – Relative error on T_m (8.1) of generated waves.
Colorbar: expected wave steepness.

Results are plotted against target wave periods (T) and coloured according to target wave steepness (kH).

There are three recognizable outliers in panel A of Fig. 8.2. Their separation from the main tendency isn't due bad wave data analysis but to wrong user input to the wave generator. These are therefore useful data, and will not be discarded for later manipulations.

The overall behaviour of data states that long waves were generally better reproduced at the wavemaker. Short small waves were usually higher than wanted, while steep short waves turned out to be generally lower. This causes a little compression in the target wave steepness range.

8.1.3 HEIGHTS DISTRIBUTION

Regularity of wave trains is here investigated. In statistical terms, significant wave height is defined as the average of the highest third of H_{zc} set, and is here denoted as $H_{1/3}$. The closer is $H_{1/3}$ to H_{rms} the more regular the wave train.

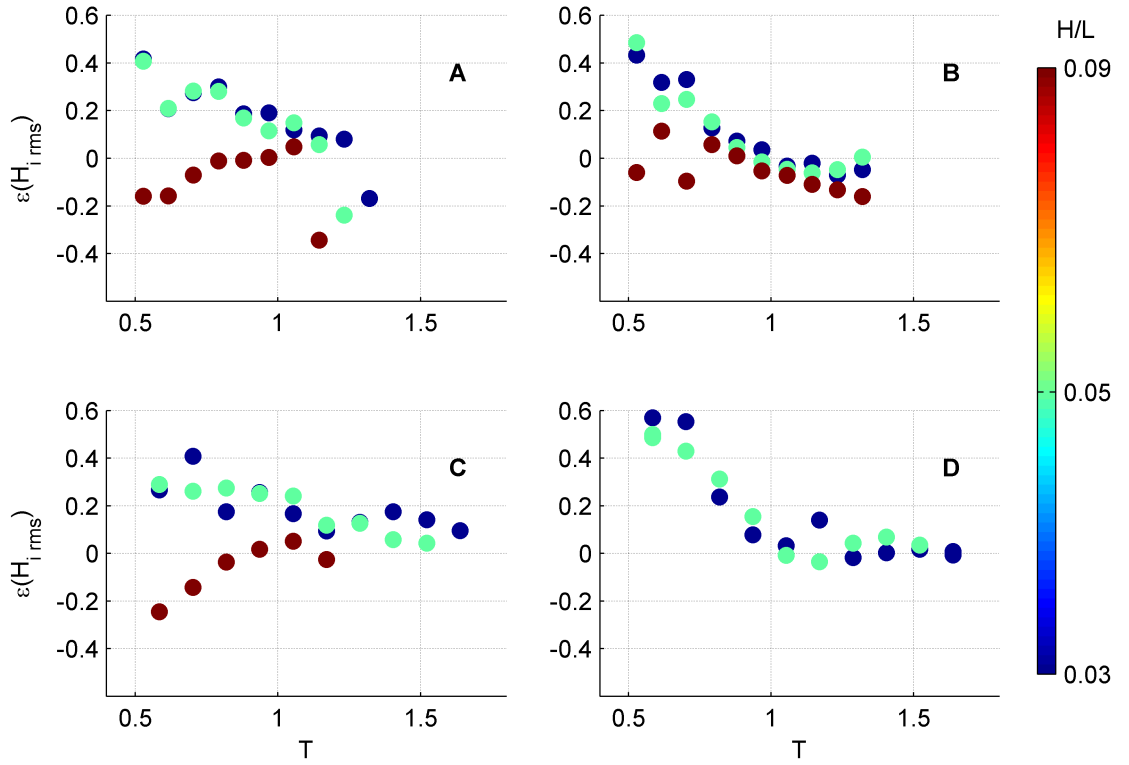


Fig. 8.2 – Relative error on generated H_{rms} . Colorbar: expected wave steepness.

Figure 8.3 reports this deviance, *i.e.*:

$$\epsilon(H_{i1/3}) = \frac{H_{i1/3} - H_{irms}}{H_{irms}}. \quad (8.4)$$

Most deviations are smaller than 0.1, which can be set as the acceptable limit. In fact, in all cases wavemaker rump-up waves are included in the analysis, and these are on the order of 1 over 10.

Relative short waves were very difficult to be generated properly, since transverse oscillation effects appeared very soon, close to the paddle. That was mostly due to the leakage at the wavemaker sides. These effects were more visible in case of steep waves (long and fast paddle motions) and particularly strong after few waves were reflected back from the FBs towards the generation point. All time series were shortened to exclude these phenomena but, in some cases, their early envelope appeared very irregular. The latter are recognizable in the small period regions, namely $0.5 \sim 0.7$ s.

Data presenting a deviation value higher than $\epsilon(H_{i1/3}) = 0.12$ could be ex-

cluded from further investigations. These are [A, 0.6~0.8, 0.09], [B, 0.8, 0.09], and [C, 0.5~0.6, 0.09]. But, in some cases they fit with other data, as it can be verified in next paragraphs.

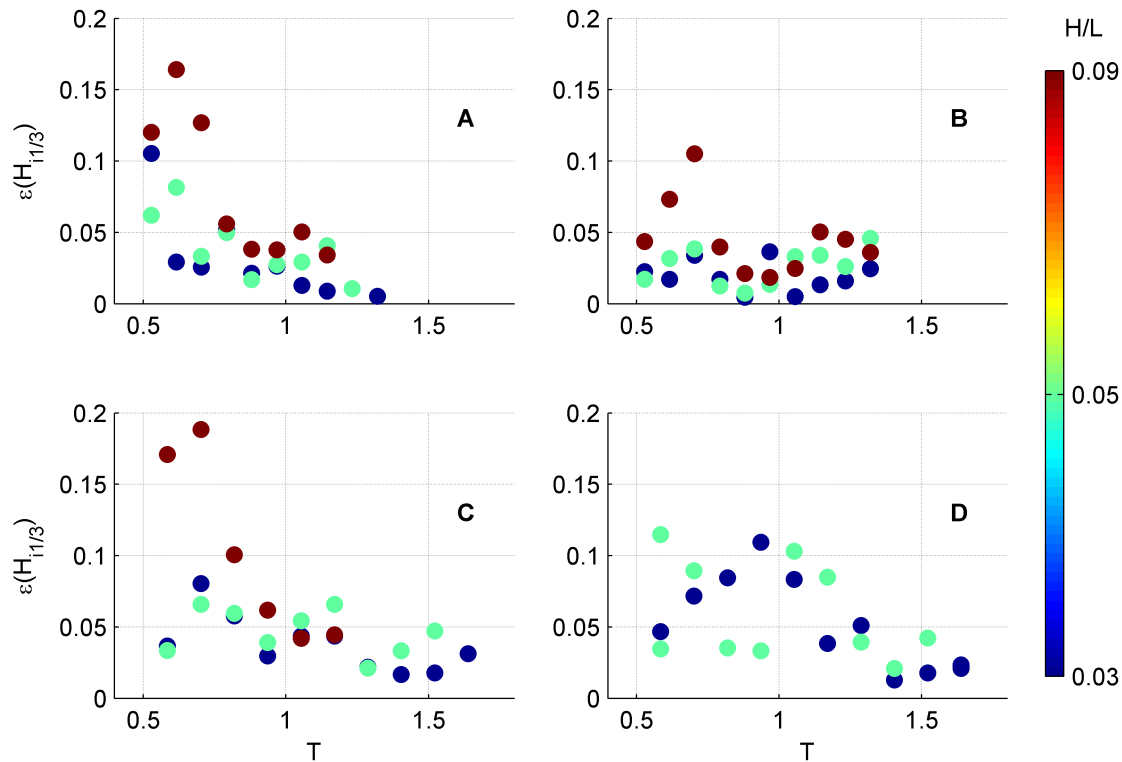


Fig. 8.3 – Regularity of generated wave heights distributions as by (8.4). Colorbar: expected wave steepness.

8.1.4 DISCARDED DATA

In some cases the experiment went corrupted for some reason. Besides the ones already mentioned, a description of the exclusion paradigms and the list of discarded events is hereby described.

In two cases the mooring broke before a significant amount of data was recorded. As these were limit cases (end series, high steepness and very long waves) they were not repeated. These are [B, 0.67, 0.09] and [D, 0.77, 0.05].

In four cases short cross modes (flume lateral near-resonance) developed very soon, thus corrupting the wave field. These are [A, 0.52, 0.09], [B, 1.25, 0.09], [C, 2.00, 0.09] and [C, 1.67, 0.09]. Even capturing the cross modes exactly, data would be unusable. In fact, enhancing dissipative white capping phenomena,

they partially destroy reflected (and incident) wave fields. Thus making the interpretation of the latter a bit cumbersome.

Under particular steep and long waves (thus very far from design conditions) the motion of the FBs suffered of severe mooring snaps. Most of the cases remain included. But a strong deviance from main behaviour was observed for the small FB in cases [B, <0.8, >=0.05] and [B, <0.9, 0.09]. Related data are left for separate extreme cases analysis.

Other four cases are excluded because they reveal (for each reflection analysis method taken into account) that some energy went "created" at main wave frequency, *i.e.* negative energy dissipation coefficients δ^2 were found. Since this coincides with very short waves events, it could be explained by existence of undetected relevant cross modes. These cases are [A, 1.43, 0.05], [A, 1.43, 0.09], [B, 1.67, 0.03] and [B, 1.43, 0.05].

8.2 WAVE TRANSMISSION

8.2.1 LINEAR COEFFICIENTS

In regular wave tests, energy is well concentrated at narrow frequency bands. Since we are analysing here only fundamental components, we commit no substantial error in using τ_{m0} . Fig. 8.4 depicts, series by series, τ_{m0} against the primary waves frequencies f_p . Data are coloured according to estimated wave steepness.

FREQUENCY (TIME) SCALE We recall here the non-dimensional variable introduced in by (3.11), here in terms of frequency:

$$\chi^{-1} = \frac{\omega_P}{\hat{\omega}_h} \quad (8.5)$$

where

$$\hat{\omega}_h = \sqrt{\frac{g}{d + 0.35w}} \quad (8.6)$$

is set on the basis of (3.9). Same data of Fig. 8.4 are given in Fig. 8.5, but plotted against non-dimensional frequencies (8.5). It can be observed that local minima (corresponding to resonance condition) are all located at $\chi \approx 1.2$.

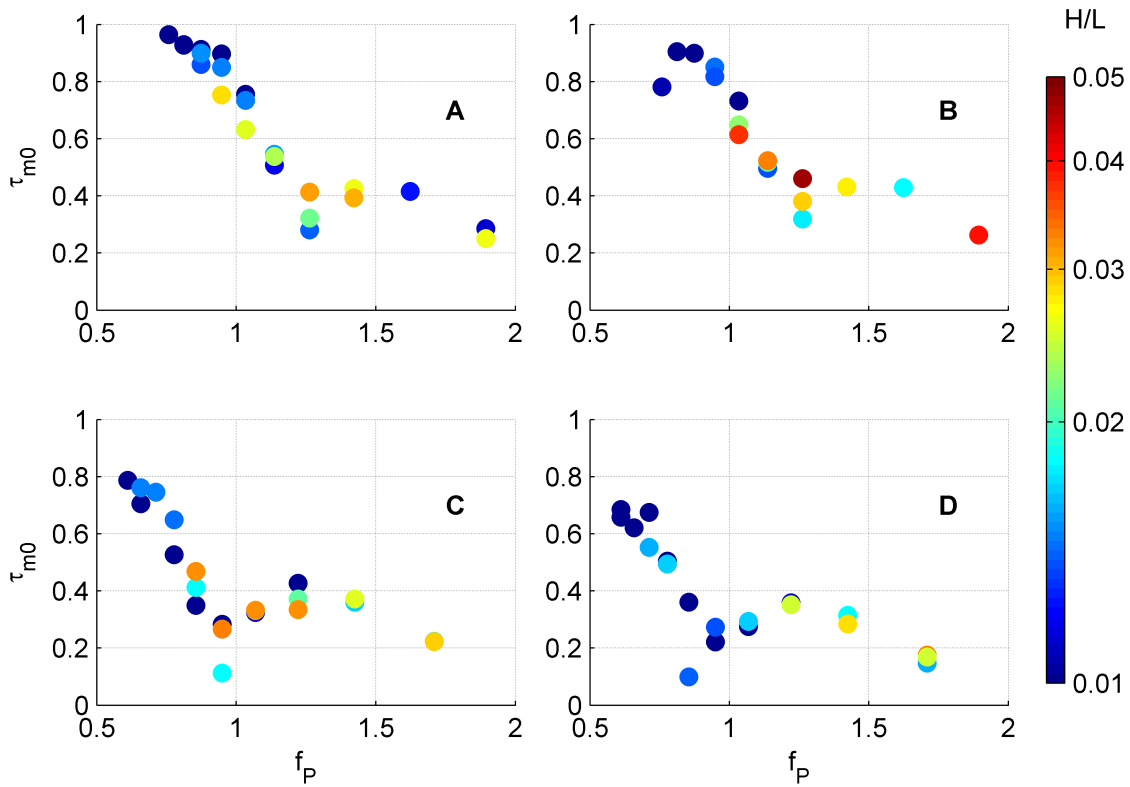


Fig. 8.4 – Transmission coefficients for primary components.

This fact gives more consistency to the choice of geometrical scaling factor for principal wave frequencies.

FREQUENCY	For each case an average frequency response function can
RESPONSE	be extrapolated

$$A_t = T(\chi) A_i \quad (8.7)$$

Where A_i and A_t are the incident and reflected amplitudes. The transfer function T can be expressed as the product of two functions, one describing the general decay of transmission coefficient with respect to (non-dimensional) frequency, and the other the local minimum due to resonance, *i.e.*

$$T(\chi) = T_d(\chi) T_r(\chi) \quad (8.8)$$

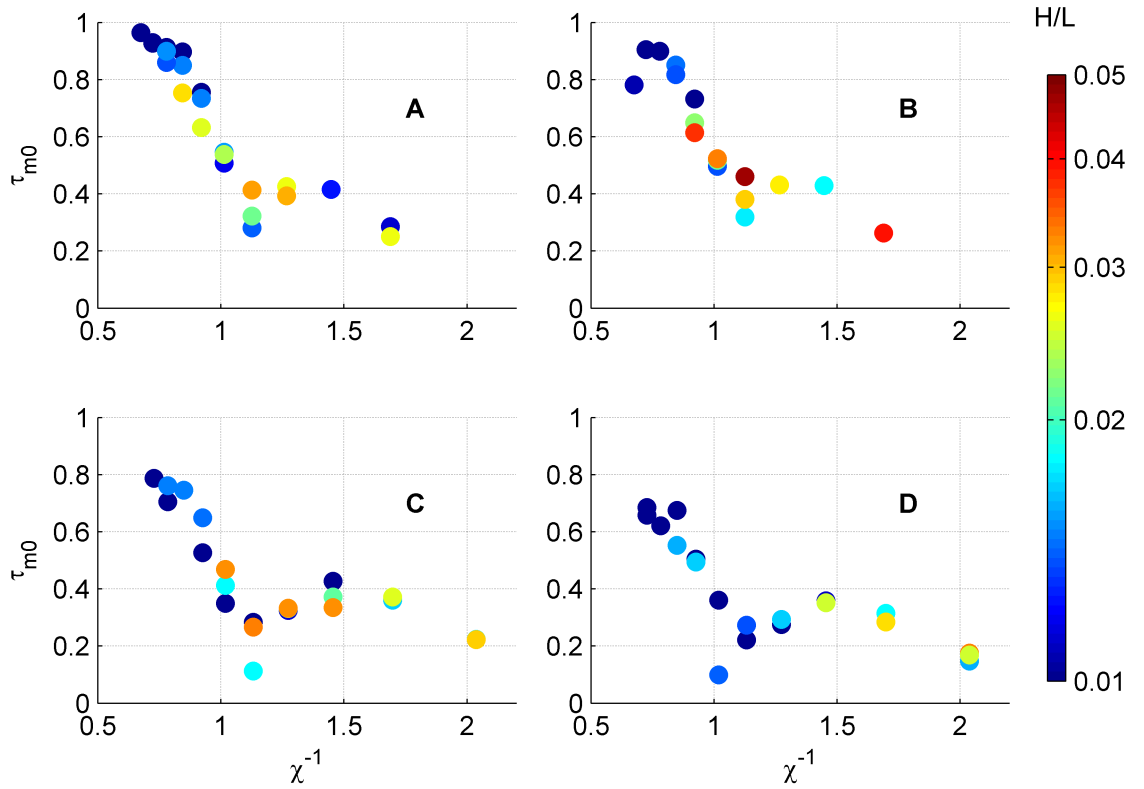


Fig. 8.5 – Transmission coefficients for primary components, with respect to non-dimensional frequency (8.5).

The general decay of transmission coefficient is

$$T_d = 1 - \exp(c_1 \chi^{c_2}) \quad (8.9)$$

and the resonance function

$$T_r = 1 - c_6 y^r \exp[r(1 - y)] \quad (8.10a)$$

$$y = (c_3 \chi)^{-c_5} \quad (8.10b)$$

$$r = \frac{c_4}{c_5} \quad (8.10c)$$

While the former wants to mimic the general low pass behaviour of a floating barrier, the latter is inserted to cope with the local minima, visible in Fig. 8.5 and Fig. 8.4, with local minima of linear mathematical models. In particular, coefficient c_6 govern the height of the minimum, located by c_3 . All the others are shape coefficients.

Other alternatives would have been difficult to control. For example, with an

exponential for low frequencies plus a Rayleigh-Weibull kind for high frequencies, it was somehow difficult to locate the local minima.

With help of Newton-like fitting routine, equations have been fitted to data for each test series. Table 8.1 enumerate the results, while in Fig. 8.6 graphical fits are reported.

Tab. 8.1 – Parameters for (8.9) and (8.10).

coeff.	A	B	C	D
c_1	1.99	2.22	2.75	2.35
c_2	3.54	3.77	3.43	3.64
c_3	1.15	1.13	1.16	1.13
c_4	5.37	4.11	5.02	2.95
c_5	14.70	13.04	5.26	7.21
c_6	0.54	0.50	0.68	0.70

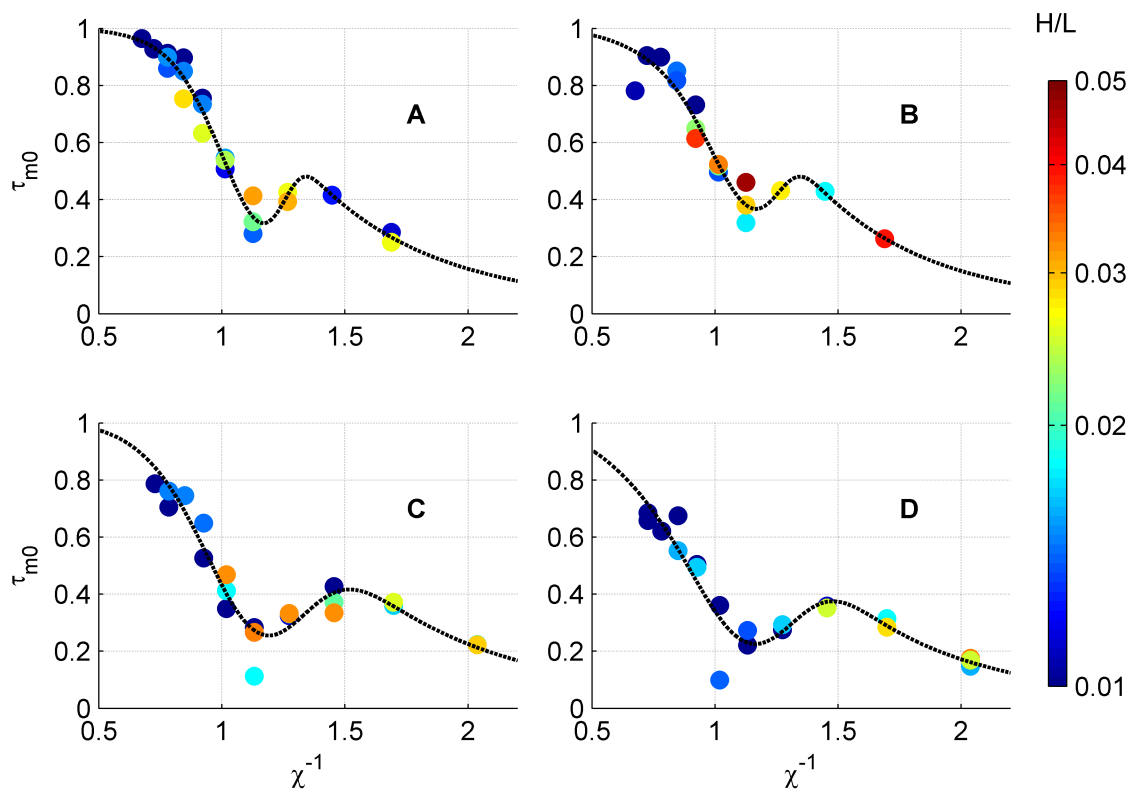


Fig. 8.6 – Fitting functions (8.8) for the transmission coefficients distributions of Fig. 8.5.

WAVE STEEPNESS Very low dependence is observed, in general, with respect to incoming wave height, thus with respect to wave steepness or any other combined parameters.

RELATIVE DEPTH RESPONSE If the second more significant parameter is relative draft d/h , then distributions of panel B and C in Fig. 8.6 should appear very similar, since they represent two cases with same d/h . But it is not. Especially in the region χ^{-1} below resonance zone, C distribution is somewhat lower than B one.

In order to express this secondary variation, an alternative variable might be searched for. Many combinations have been tried, ending up with following (8.11) which satisfy the needs.

$$\zeta = \frac{\tanh \hat{k}_h (h - d)}{\hat{k}_h w} \quad (8.11)$$

where \hat{k}_h is the wavenumber corresponding to heave frequency estimation (8.6) and water depth h .

Note that non physics is involved in last definition. Anyhow it has some meaningful features. The numerator grows from 0 to 1 as draft approaches water depth. Moreover, the wider the FB, the lower the value of ζ . Anyhow, the dimensions must cope with the range of validity of (8.6), which has been verified for compact *box* and π – *type* FB cross sections. As ζ decreases, then lower transmission should be expected.

FIRST ORDER TRANSFER Coefficients for (8.9) and (8.10), which values have been enumerated in Tab. 8.1 are expressed, in this framework, by suitable simple function of ζ . This choice appeared more feasible than searching for a function of ζ that enters 8.7 as a third multiplier.

Simple models, for each coefficient, have been designed based on proper assumptions. These are enumerated in Tab. 8.2, together with respective statistics.

The reasons for such models are readily explained. The first one, governs the strength of the exponential decay, and must have always a positive finite value. Coefficients c_4 and c_5 define the width of (8.10), thus must be positive, but zero

if draft equals water depth, leading to zero transmission. This is enforced by $c_6 = 1$ in the same situation. The other two coefficients (c_2 and c_3) were left to a linear behaviour, even if they are almost the same for each experiment series.

Tab. 8.2 – Parameters for (8.9) and (8.10) as function of ξ .

coeff.	model	a	b	SSE ^a	RMSE ^b	R^{2c}
c_1	$\frac{a}{\xi+1} + b$	1.50	1.22	0.017	0.092	0.566
c_2	$a\xi + b$	0.10	3.46	0.048	0.154	0.014
c_3	$a\xi + b$	0.04	1.12	0.000	0.012	0.233
c_4	$a\xi$	6.70	0.00	0.061	0.143	0.983
c_5	$a\xi$	18.83	0.00	0.889	0.544	0.969
c_6	$\exp a\xi^b$	0.82	1.06	0.002	0.032	0.894

^a residual sum of squares

^b root mean squared error

^c determination coefficient

The function which interpret linear transmission, given graphically in Fig. 8.7, is therefore expressed as

$$T(\chi, \xi) = T_d(\chi, \xi) T_r(\chi, \xi) \quad (8.12)$$

together with (8.9), (8.10) and Tab. 8.2. Verification of data fitting is rendered in Fig. 8.8.

8.2.2 SECOND ORDER COEFFICIENTS

Let trust the linear process described by (8.7), even for what it does predict in the very high frequency region. Second harmonics linear transmission coefficients can thus be compared to what predicted by (8.7). Fig. 8.9 compares the linear interpretation $\tau_{m0}(\chi/2)$ with $T(\chi/2)$.

Second harmonics transmission coefficients are on the order of unity (or higher) and can't thus be described by (8.7). Hence an energy transfer from primary waves has to be admitted. The mount of transfer, with reference to second

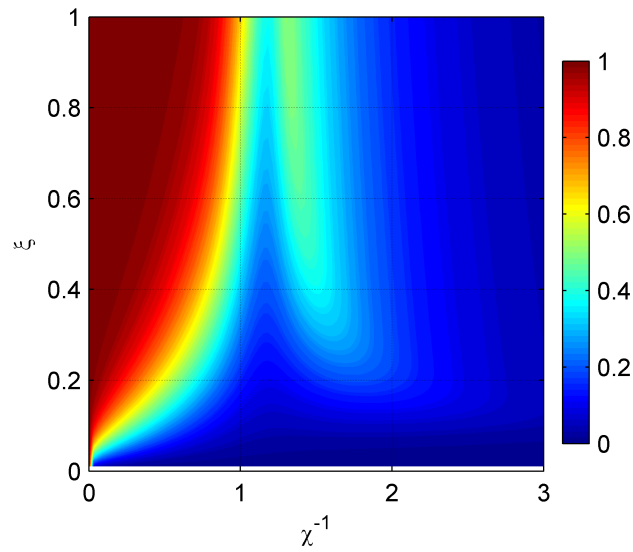


Fig. 8.7 – First order transfer function for transmitted free wave amplitudes.

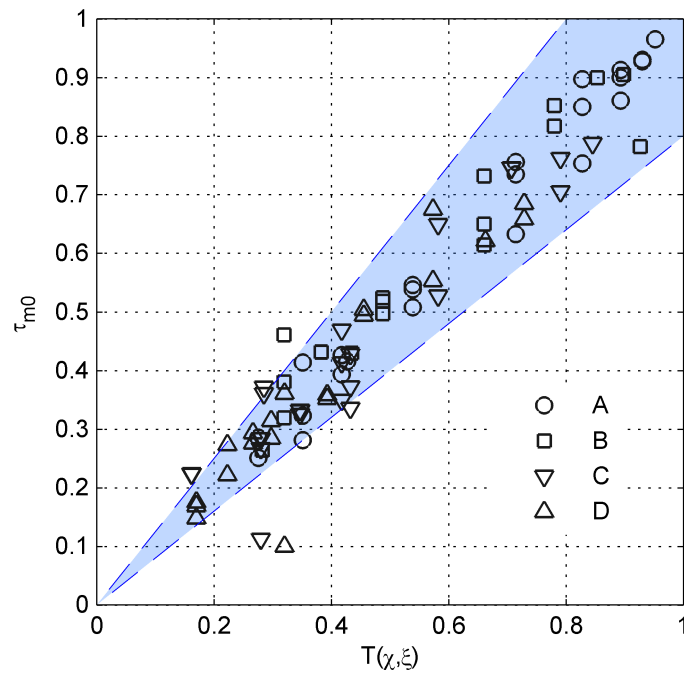


Fig. 8.8 – Principal components transmission coefficients compared to $T(\chi, \xi)$. Shaded area: reversible 20% confidence.

harmonic can be estimated:

$$\Delta E_t(x/2) = |a_t(x/2)|^2 - T^2(x/2, \xi) |a_i(x/2)|^2 \quad (8.13)$$

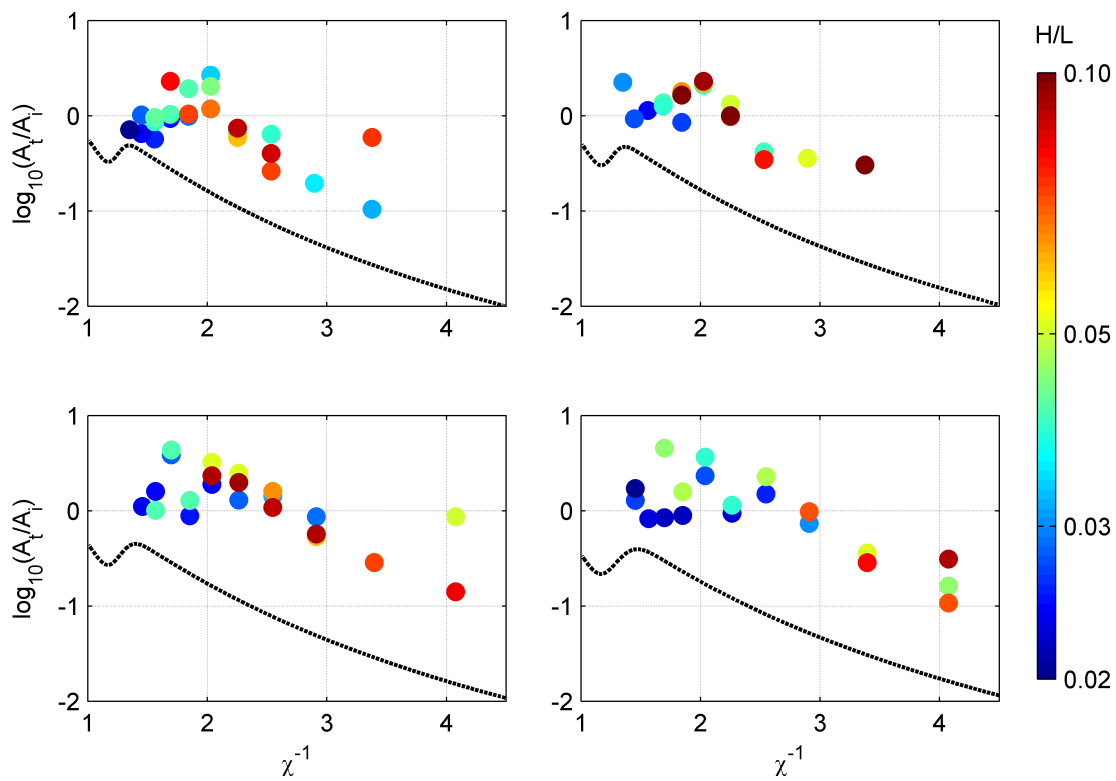


Fig. 8.9 – Comparison of second free harmonics transmission coefficients (scattered data) and what predicted by linear estimation (8.7). Wave steepness refers to primary component.

The energy transfer (loss) coefficients for second harmonic

$$\delta_{t,2}^2 = \frac{|\Delta E_t(\chi/2)|}{|a_i(\chi/2)|^2} \quad (8.14)$$

are given in Fig. 8.10 in logarithmic scale. Abscissa refer to primary frequencies χ^{-1} , which helps the description.

All distributions are very scattered, and may suffer of error estimations of the same order of datum, since the initial measurement error might have spread significantly throughout all computations. Anyhow, some characteristic features can be observed.

In all cases, relative maxima in correspondence of $\chi \approx 1$ appear, which correspond to maxima in energy transfer from primary to second harmonic for waves matching FB resonance frequencies. This is a crucial aspect that linear models are not able to mimic.

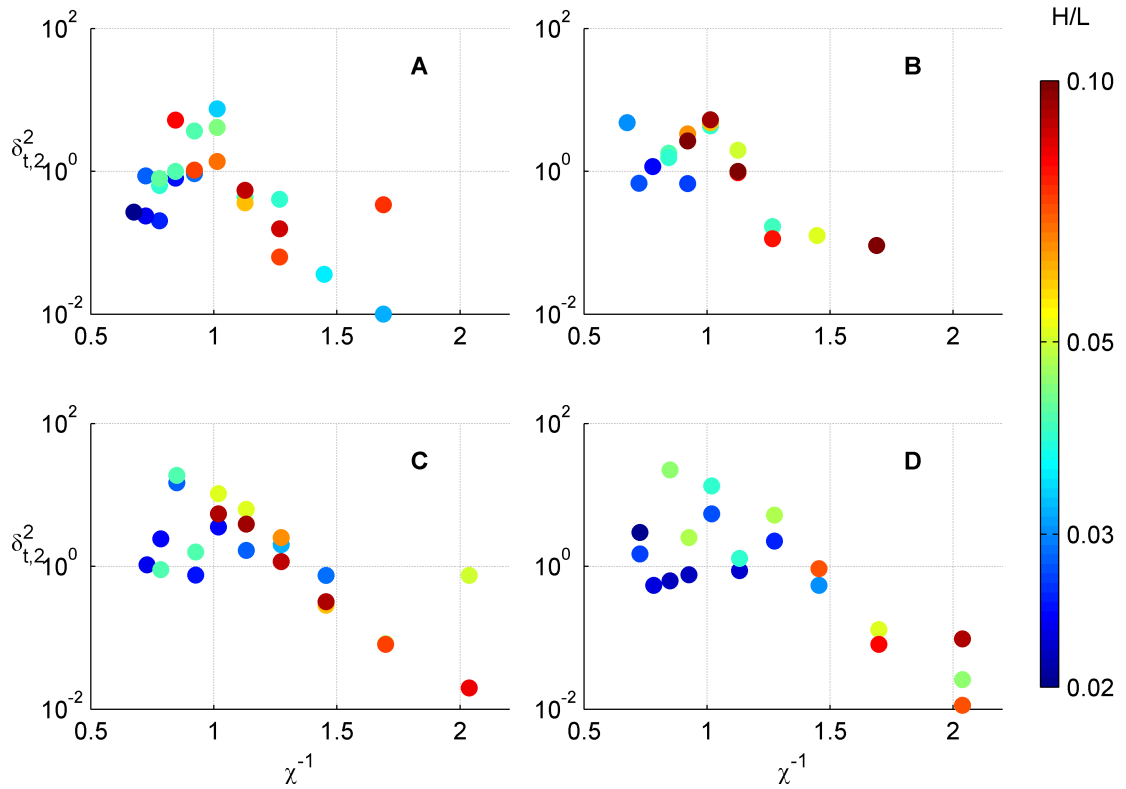


Fig. 8.10 – Energy transfer coefficients (8.14) referred to second harmonic energy variation. Abscissa refers to first order component frequency. Wave steepness refers to primary component.

8.3 WAVE REFLECTION

8.3.1 LINEAR COEFFICIENTS

Reflection coefficients relative to primary frequency band are reported in Fig. 8.11 directly against non dimensional frequency χ^{-1} . The latter confirms as a satisfactory descriptive variable.

DRAFT In the high frequency region ($\chi^{-1} > 1$, plotted data reveals no substantial dependence of ρ_{m0} with respect to any draft/depth combinations. A distinct behaviour is observed in short waves region: higher reflection is found going from case A to D. However, it appears here a negligible aspect and no modelling attempts are pursued.

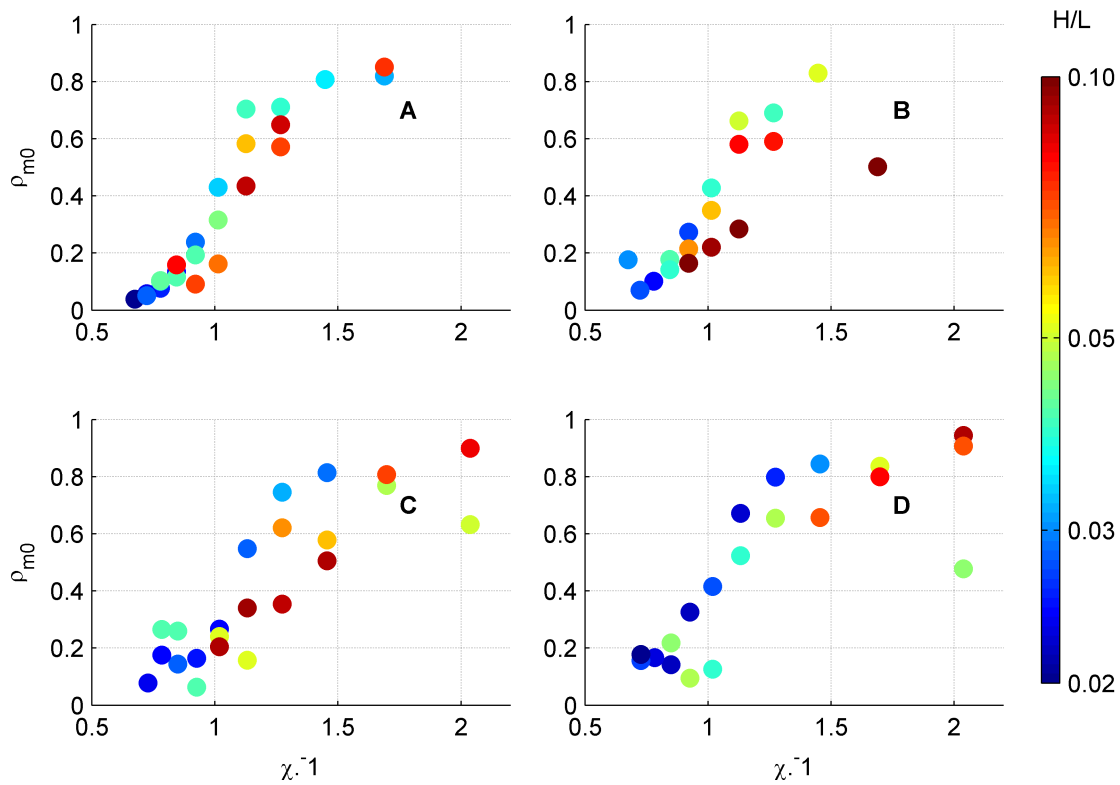


Fig. 8.11 – Reflection coefficients for primary components against normalized frequency. Wave steepness refers to primary incident wave.

WAVE STEEPNESS One can deduce from Fig. 8.11 that the higher the wave steepness of incoming wave, the smaller the reflection coefficient of primary waves. And this enhances as wave frequency grows.

The intervention of H/L on the sea side wave field is thus crucial. This aspect cannot be resolved by any conservative mathematical or numerical model, such as potential eigenfunction expansions, or solutions based on BEM.

FIRST ORDER TRANSFER On the basis of the above observations a simple model has been chosen to mimic the linear reflection process:

$$A_r = R(\chi, H/L) A_i \quad (8.15)$$

The first order transfer function is given as

$$R = 1 - \exp \left[- \left(c_1 \chi^{-1} \right)^{c_2} \right] \quad (8.16)$$

where c_1 and c_2 are steepness dependent functions of the kind:

$$c_j = a_j \exp(-b_j H/L) \quad j = 1, 2 \quad (8.17)$$

The four coefficients have been estimated by non-linear Newton-like fitting, and are resumed in Tab. 8.3.

Tab. 8.3 – Coefficients for (8.17).

a_1	b_1	a_2	b_2
0.93	3.90	5.59	7.80

The shape of the resulting (8.16) is depicted in Fig. 8.12, while its validation against estimated free fundamental components reflection coefficients is given in Fig. 8.13.

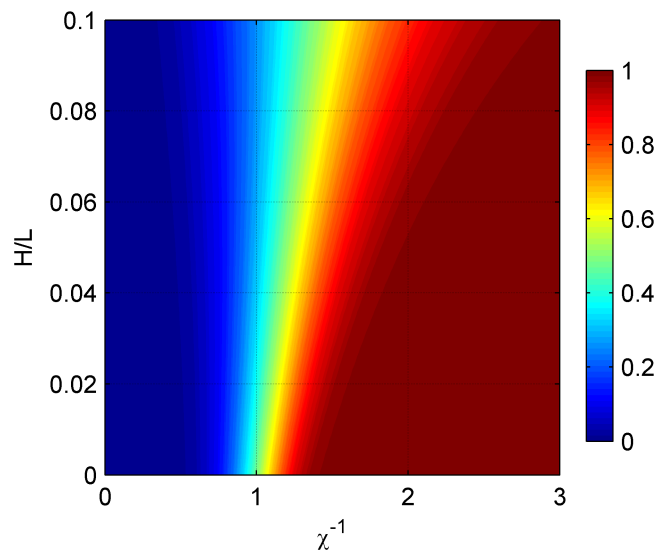


Fig. 8.12 – First order transfer function for reflected free wave amplitudes.

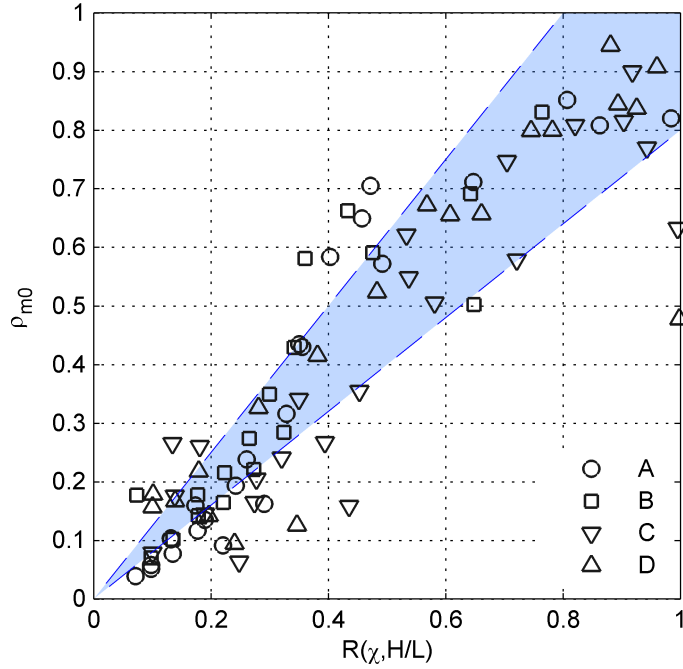


Fig. 8.13 – Principal components reflection coefficients compared to $R(\chi, H/L)$. Shaded area: reversible 20% confidence.

8.3.2 SECOND ORDER COEFFICIENTS

With an expression similar to (8.14), the quadratic energy transfer coefficient (loss) for reflected second harmonics can be estimated as:

$$\delta_{r,2}^2 = \frac{|\Delta E_r(\chi/2)|}{|a_i(\chi/2)|^2} \quad (8.18)$$

with

$$\Delta E_r(\chi/2) = |a_r(\chi/2)|^2 - R^2(\chi/2, \zeta) |a_i(\chi/2)|^2 \quad (8.19)$$

Results are given in Fig. 8.14. Note that in many cases the second order transfer appears negative, down to values of -1 . This could be due to the fact that R (8.16) overestimates the linear reflection coefficients ρ_{m0} (see Fig. 8.13). Under such assumption, (8.18) have been re-evaluated admitting a 20% overestimation (Fig. 8.15).

Unfortunately, even with this correction, data appear very scattered, and no physical meanings can be deduced. Most probably the scattering is due to huge error spreading. A secondary maximum appears at resonance conditions

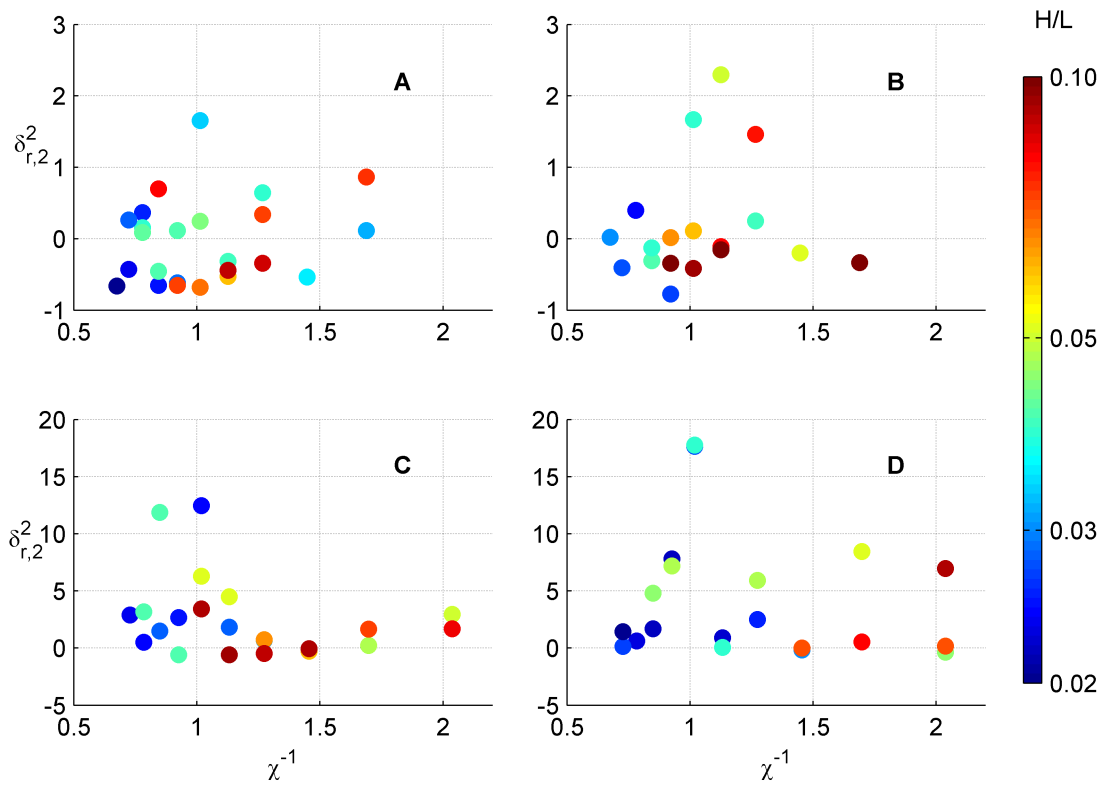


Fig. 8.14 – Energy transfer coefficients (8.18) for reflected second harmonics. Abscissa refers to first order component frequency. Wave steepness refers to primary component.

in panel D, but it might be a fake.

Moreover the energy transfers could be severely masked by dissipating processes, occurring at small scales. For this reason, the coefficients hereby derived can not be distinguished by energy losses, could thus be cast as *net* energy transfer coefficients.

8.4 WAVE ENERGY DISSIPATION

8.4.1 PRIMARY WAVE ENERGY LOSSES

Energy loss coefficients relative to primary frequency band are reported in Fig. 8.16 directly against non dimensional frequency χ^{-1} .

Evident maxima in correspondence of unitary relative frequency do reveal that the most energy is lost by primary waves in near-resonant conditions.

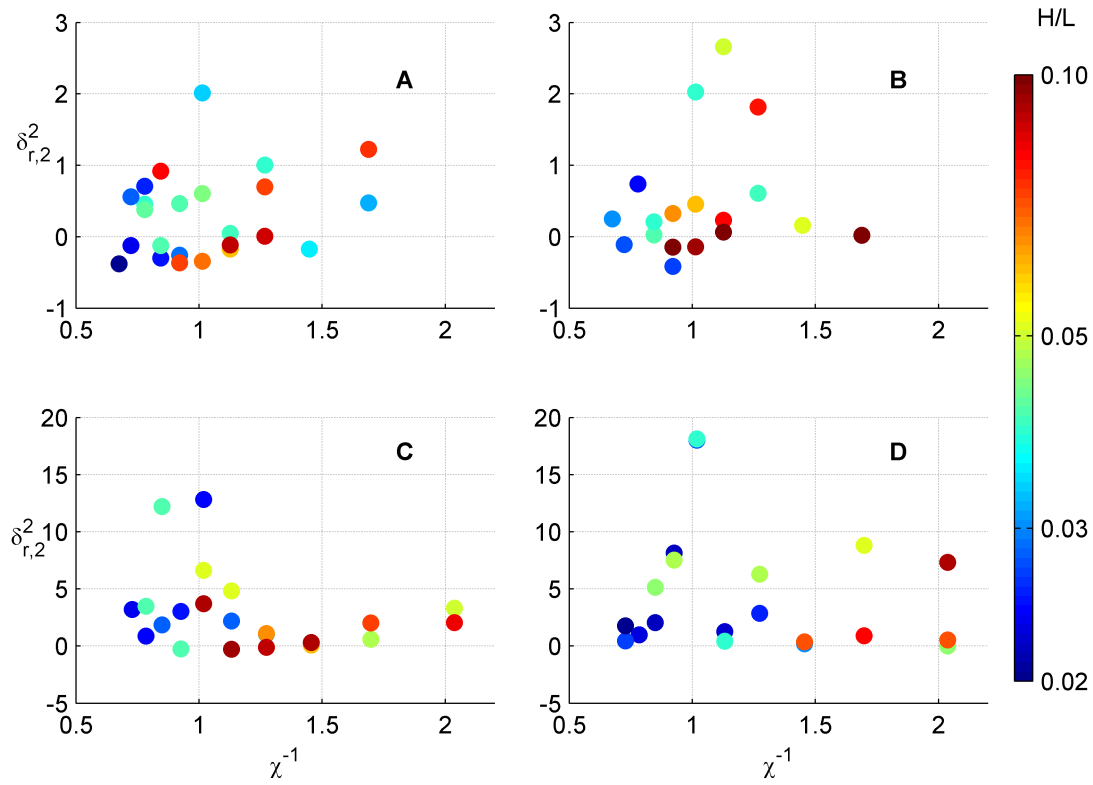


Fig. 8.15 – Same as Fig. 8.14 but admitting a 20% overestimation for R .

The analysis related to steepness and draft parameters is left to following 8.4.2 where net losses are treated.

EXPRESSION FOR PRIMARY LOSSES The total energy loss of fundamental components can be approximated by D (8.20), a function of the three parameters identified in this job: scaled period χ (frequency χ^{-1} , relative draft parameter ξ and wave steepness H/L , with wave quantities referred to the incident wave field.

$$D = 1 - R^2(\chi, H/L) - T^2(\chi, \xi) \quad (8.20)$$

Comparison with data δ_{m0}^2 is given in Fig. 8.17. D evaluations are based on expected generated waves features (rather than estimated ones). Therefore, the very outsiders do not conflict with general behaviour.

Note that the match of (8.20) is not perfect, since for very small H/L , it defines a small region where D is little negative. All formula derived so far proceed from fitting of estimated coefficients, which are error affected. Moreover, they

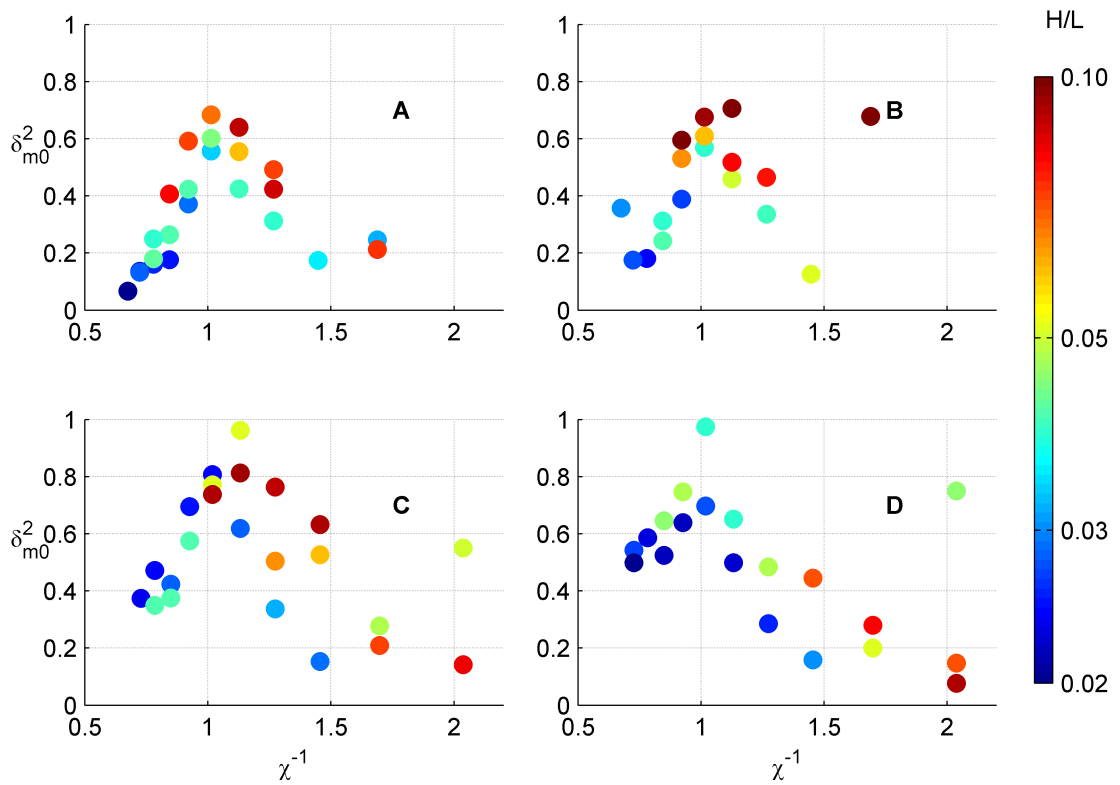


Fig. 8.16 – Energy loss coefficients for primary components against normalized frequency. Wave steepness refers to estimated primary incident wave.

do not exactly reproduce the results. Anyhow, since errors are not systematic, these relationships are based on evident data physical meanings, reproducing them qualitatively, and, with some confidence interval, also quantitatively.

8.4.2 NET ENERGY LOSSES

It is worth to notice that part of this energy loss does not leave the system. It feeds transmitted and reflected secondary components, in the sense of (8.14) and (8.18), as revealed by Figs. 8.10 and 8.14.

Energy balance for primary waves must then be rewritten as:

$$\tau^2 + \rho^2 + \delta_L^2 = 1 - \delta_T^2 \quad (8.21)$$

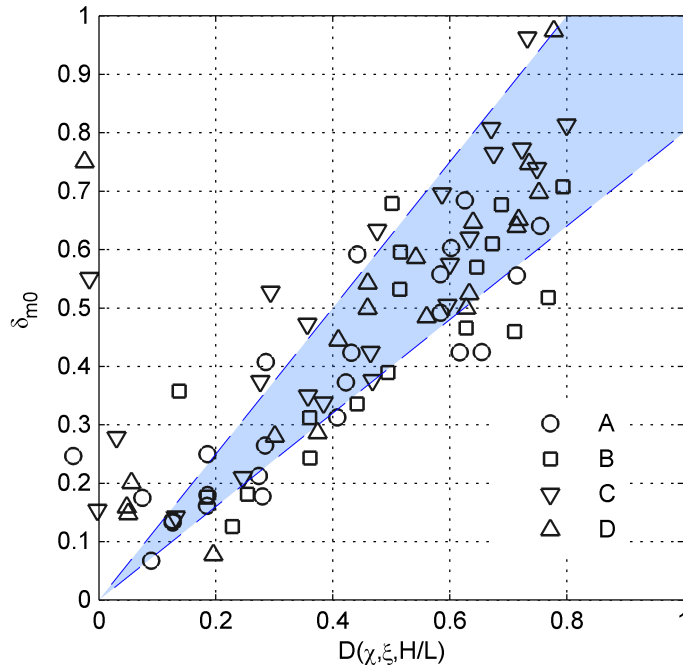


Fig. 8.17 – Principal components energy loss coefficients compared to $D(\chi, \zeta, H/L)$. Shaded area: reversible 20% confidence.

where, up to second order precision, δ_L^2 (Fig. 8.20) can be cast as the system energy loss coefficient (referred to primary amplitude), while

$$\delta_T^2 = \delta_{t,1}^2 + \delta_{r,1}^2 \quad (8.22)$$

is the amount of energy transfer (relative to primary energy) from primary incident component to reflected and transmitted second harmonics (Fig. 8.18). For the definition of $\delta_{t,1}^2$ and $\delta_{r,1}^2$ see Par. 7.4.2, in particular (7.7). These affects the estimation of energy loss through direct energy balance of at most 15%, as showed in 8.19, in which

$$\epsilon(\delta) = \frac{\delta_{T,m0}^2}{\delta_{m0}^2} \quad (8.23)$$

with

$$\delta_{m0}^2 = \delta_{T,m0}^2 + \delta_{L,m0}^2. \quad (8.24)$$

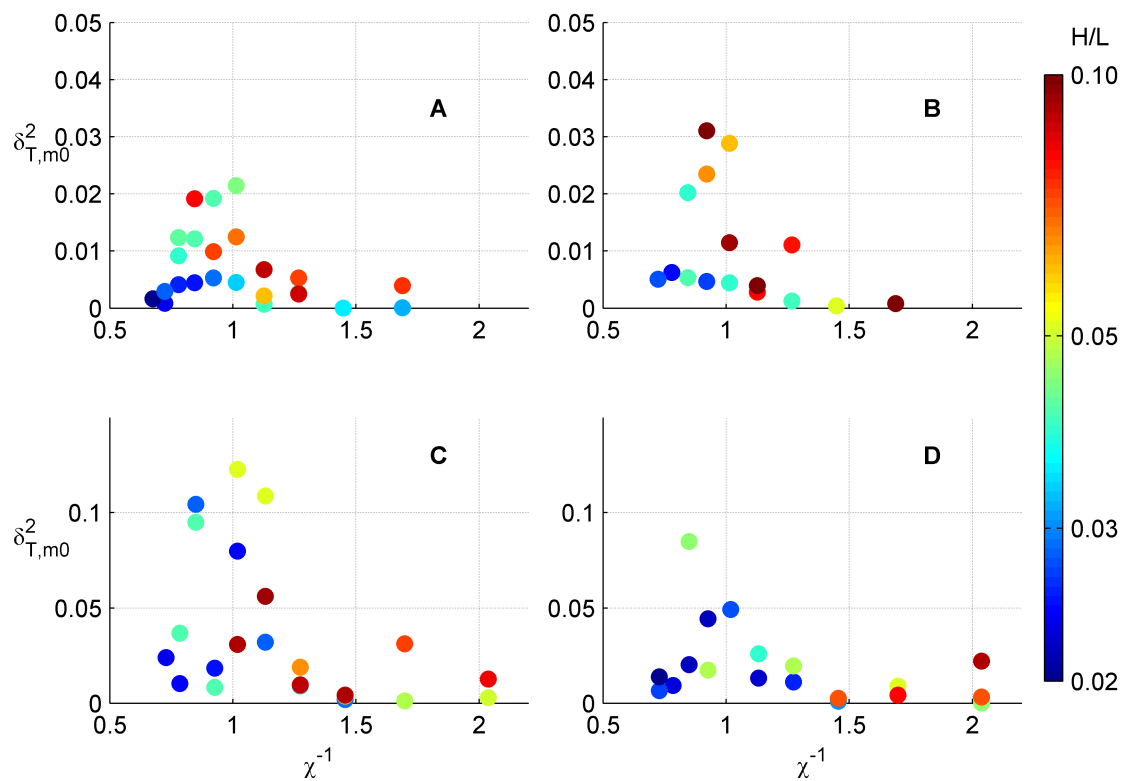


Fig. 8.18 – Coefficients for primary component energy loss due to transfer to second harmonics. Wave steepness refers to estimated primary incident wave.

PARAMETERS Finally Fig. 8.20 reports primary component net losses
 SENSITIVITY $\delta_{L,m0}^2$. Relative maxima at near resonant frequency are conserved.

As expected, steeper waves do lose higher amount of energy. This mostly corresponds to lower reflection coefficients.

As water depth parameter decreases, a little increase in local maxima is observed. The distributions do also broaden, with higher energy losses both at low and high frequencies.

8.5 SPECTRA RECONSTRUCTION

The last two experimental runs were based on irregular wave fields. This brief section aims at evaluating reconstruction of transmitted and reflected spectra based on linear hypotheses, throughout the proposed formula (8.12) and (8.16). Energy losses distributions are also compared to what predicted by (8.20). All

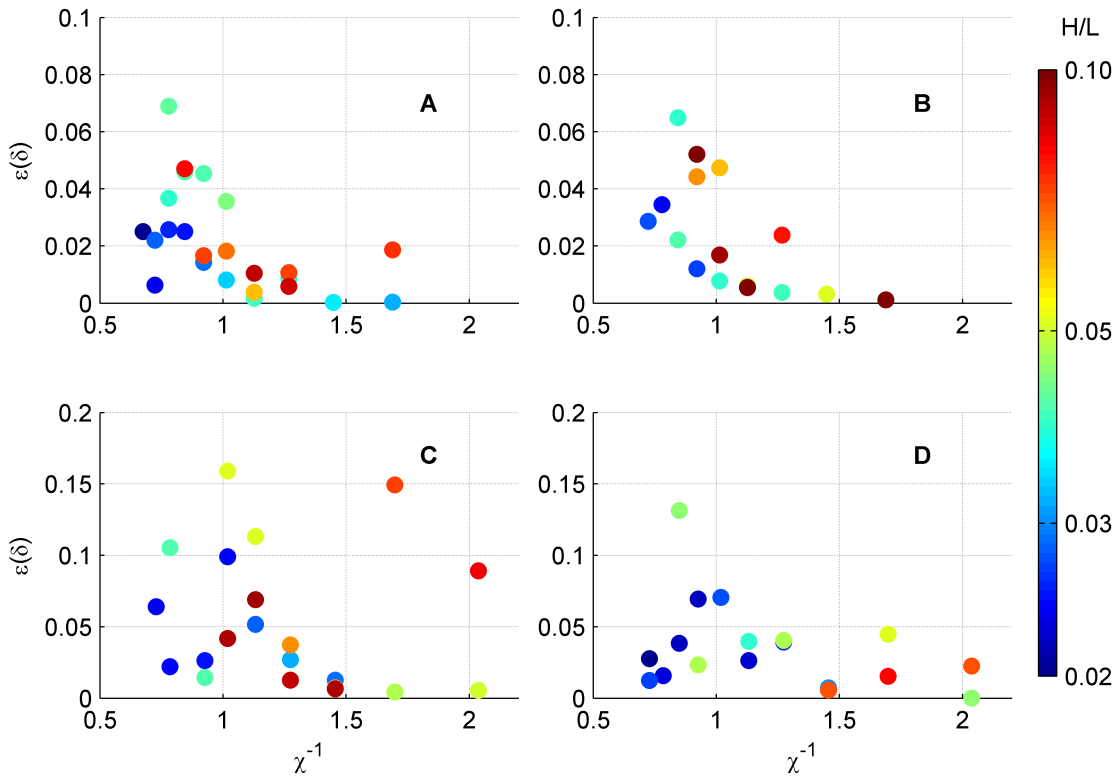


Fig. 8.19 – Incidence of energy transfer from primary to second harmonic on total loss.

predictions are generated starting from the expected incident spectra, which are also compared to measured ones.

Figs. 8.21 and 8.22 summarize the results for the JONSWAP and the Piersom-Moskowitz cases, respectively. Distributions, given with respect to non dimensional frequency χ^{-1} , are normalized with respect to peak value of predicted curves. Incident wave spectra are very well described, therefore the analyses of the other distributions can be easily uncoupled.

In both cases the peak of transmitted spectrum is slightly underestimated, while the shape is well reproduced. On the contrary, energy losses are slightly overestimated close to the peak, while the high frequencies energies are underestimated. Second order energy transfers from peak to high harmonics should be then taken into account.

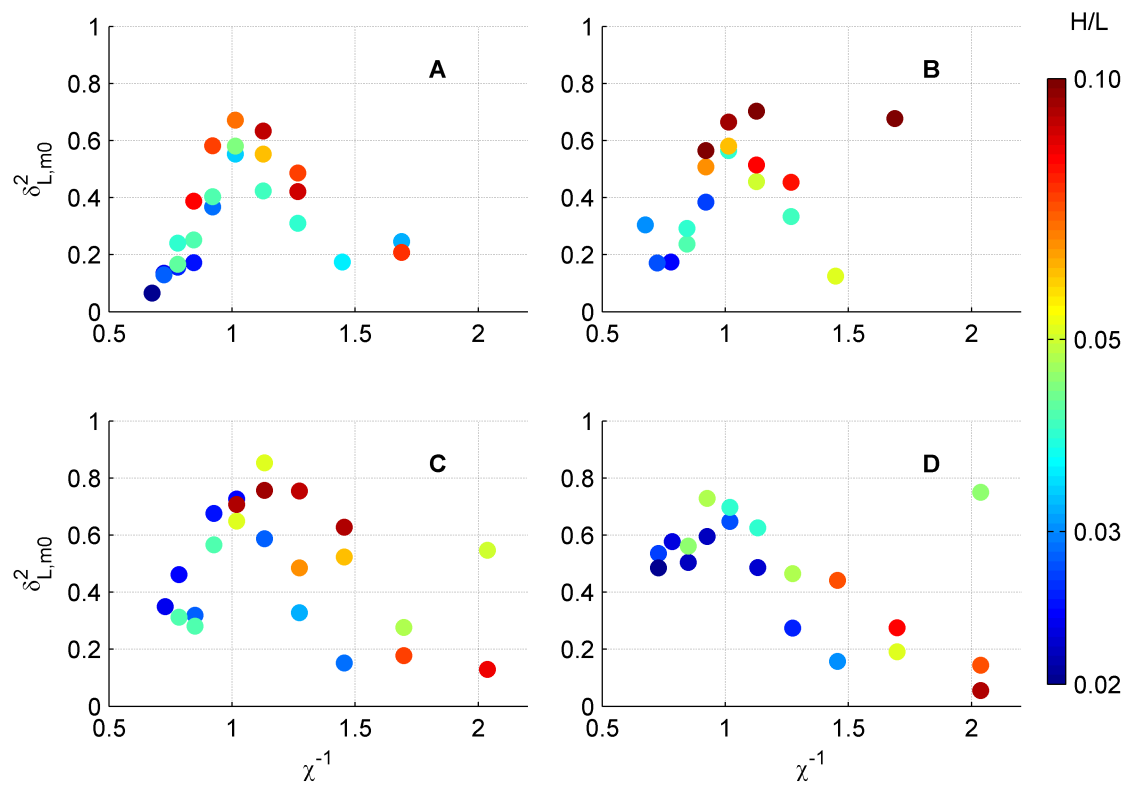


Fig. 8.20 – Coefficients for net primary components energy loss. Wave steepness refers to estimated primary incident wave.

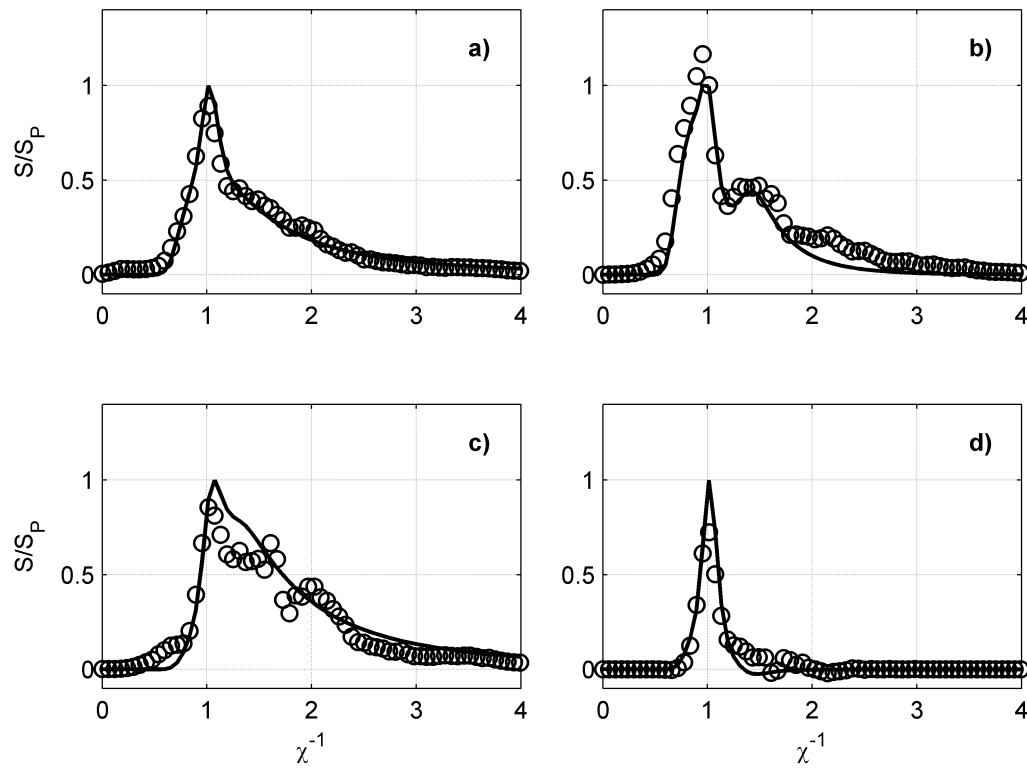


Fig. 8.21 – Predicted spectra (symbols) Vs measurements (curves) for the JONSWAP case. a) incident, b) transmitted, c) reflected, d) energy loss

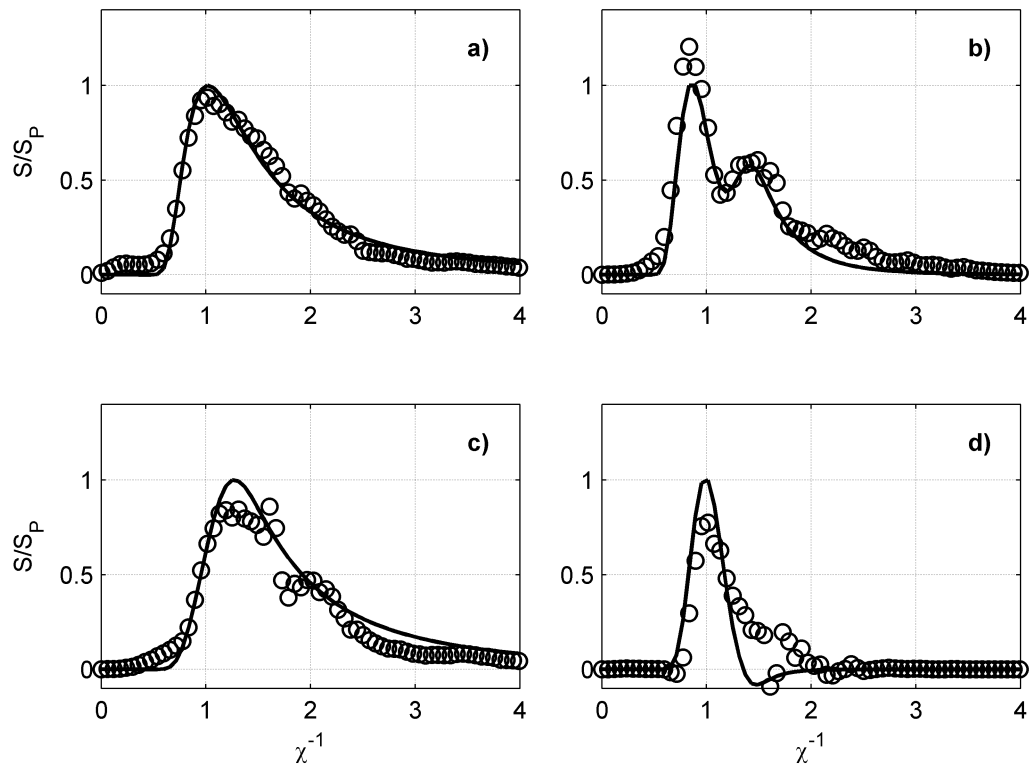


Fig. 8.22 – Predicted spectra (symbols) Vs measurements (curves) for the Pierson-Moskowitz case. a) incident, b) transmitted, c) reflected, d) energy loss

9 CONCLUSIONS

Floating breakwaters (FB) have been increasingly used, during the last decades, to protect marinas or small craft harbours. Related scientific publications has followed this trend. These devices present an alternative solution to conventional fixed breakwaters and can be effective in coastal areas with mild wave environment conditions. Recently, the search for innovative approaches aiming at flood risk mitigation in coastal areas, deltas, estuaries of large rivers and shoreline protection has drawn attention to the potentialities of floating breakwaters.

Much of the effort has been drawn to investigate on increasing FB efficiency, in terms of wave height reduction and in increasing energy dissipation capabilities. This shares many common topics with floating wave energy converters (WEC) world. In fact, a WEC is nevertheless than an FB which harvest energy, instead of dissipating it. A growing number of studies provides specific analysis on the wake wave field of a WEC, and discuss on the possibility of matching the two targets of wave climate mitigation and energy harvesting.

Numerical models used to describe the long term evolution of a shoreline are based on spectral (wave action propagation) equations, or rather on depth-averaged equations (*e.g.* Bousinnesq). The interactions of a floating barrier with the wave field is then deputed to some parametrized transfer functions, which mimic wave energy transmission and dissipation in the frequency domain.

The first part of this thesis has been focused on the research of a small significant number of non-dimensional parameters which govern the 2DV process of a wave passing an FB.

Three main parameters have been identified. The first one (χ) is the ratio between the incoming wave frequency and an approximation of FB heave natural frequency, based on principal FB cross section dimensions. Wave steepness

has been considered to be the second variable which helps in describing the amount of dissipated energy. A FB draft to water depth ratio has been identified.

Available algorithms for the decomposition into incident and reflected waves of flume records are mostly Stokes-FFT based. It has been shown that they suffer some limitations for relatively high wave steepness. Since the latter is considered as a crucial parameter, a lot of effort has been drawn in solving some conundrums of actual methods.

Two algorithms have been proposed. The first one, based on empirical mode decomposition, did not give satisfactory results. The second one is based on linear waves superposition, but, getting rid of linear dispersion relation, detects automatically each phase celerity. The proposed algorithm appears to be effective for relatively shallow water waves, for which the phase modulation approach is more consistent than Stokes formulations. A Stokes 2nd order algorithm has also been implemented.

An extensive set of wave flume tests have been planned accordingly to the proposed set of parameters. is also introduced.

Results are given (and discussed) in Ch. 8. Linear transmission and reflection transfer functions are derived, based on experimental data fitting. These are validated with irregular wave experimental data.

It was observed, by the linear point of view, that the transmission process mainly depends on incoming wave frequency (χ) and on FB relative draft. The last parameter does not enter the reflection process, which is basically described by χ and wave steepness. In particular, steeper waves loose more energy, and are less reflected.

Throughout a second order analysis of transmission and reflection processes, it was also found that, for transmitted waves only, a significant amount of energy transfer from primary to secondary harmonics is observed.

This leads to the observation that second order energy transfers should be detected in order to have a sufficiently detailed description of the phenomena. Non-linear interactions evaluation for irregular wave fields can be pursued throughout experimental data retrieved from simple bi-chromatic tests.

A UNCERTAINTIES EVALUATION

A.1 MONTE CARLO UNCERTAINTIES EVALUATION

Dissipation coefficients are determined via energy balance:

$$\delta^2 = 1 - \rho^2 - \tau^2 \quad (\text{A.1})$$

And uncertainties do spread according to

$$\sigma^2(\delta^2) = \sigma^2(\rho^2) + \sigma^2(\tau^2) + 2cov(\rho^2, \tau^2) \quad (\text{A.2})$$

It is hereby described an MC method based on expectable FB flume tests Stokes 2nd order wave fields. It has been utilized to evaluate dissipation coefficient uncertainties by Pezzutto et al. (2012).

A.1.1 PSEUDO-REGULAR WAVES IN A FLUME

Second order quasi-regular wave fields interacting with structures it is therefore common to sample, at the n^{th} gauge, a signal of the form:

$$\begin{aligned} \eta_n = & a \cos \theta_{i,n} + a_2 \cos 2\theta_{i,n} + b_2 \cos \vartheta_{i,n} \\ & \rho_1 a \cos \theta_{r,n} + \rho_1 a_2 \cos 2\theta_{r,n} + \rho_2 b_2 \cos \vartheta_{r,n} \end{aligned} \quad (\text{A.3})$$

where the phases of the non-harmonic component with amplitude b_2 are defined as follows

$$\theta_{i,n} = \omega t - kx_n + \phi_{i,n} \quad (\text{A.4a})$$

$$\theta_{r,n} = \omega t + kx_n + \phi_{r,n} \quad (\text{A.4b})$$

$$\vartheta_{i,n} = 2\omega t - k_F x_n + \varphi_{i,n} \quad (\text{A.4c})$$

$$\vartheta_{i,n} = 2\omega t - k_F x_n + \varphi_{i,n} \quad (\text{A.4d})$$

phase shifts (φ_{in} and φ_{rn}) differs from the harmonic component ones, and ρ_2 is the reflection coefficient associated to the free component.

We must add that in an unreliable wave field, in which a_2 is set equal to zero, *i.e.* no bounded components are travelling in any direction, LS is able to detect exactly incident and reflected waves. This comes out from the linearity hypotheses of the method, that is to say that LS considers each perturbation as a free wave.

When attempting the generation of pseudo-regular waves the release of these free components can be avoided, thus generating more-regular waves (see e.g. Schaffer, 1996). On the other hand, as we mentioned before, the general process around the reflecting obstacle is such that non-harmonic waves, travelling backwards, are liberated from that region. This occurs especially (but not only) in the case of waves interacting with floating bodies.

The method proposed by Zelt and Skjelbreia (1992) was used to separate incident from reflected waves. This method will be hereafter referred as LS.

Moreover, the uncertainty on τ depends on the coupling of two distinct LS procedures. The first one, LS1, is used to separate incident and reflected wave field at the first gauges array, thus getting an estimation of ρ . The second, LS2, is used to separate the incident (transmitted with respect to the FB) and the beach reflected wave field. Only the combination of the two results allows evaluation of τ as ratio between the two detected incident wave heights.

We compute reflection and transmission coefficients as ratios of 0^{th} order spectral moments (m) of the LS separated signals:

$$\rho^2 = \frac{m_r}{m_i} \quad \tau^2 = \frac{\bar{m}_i}{m_i} \quad (\text{A.5})$$

where subscripts *i* and *r* stand for incident and reflected wave spectra, while \bar{m}_i identifies the incident signal on LS2, namely the transmitted wave spectral moment, which is detected through the application of LS to the wake-side gauges recordings (gauges 5 to 8). The first two moments (m_i and m_r) are evaluated with LS1 applied to gauges 1 to 4.

In the following subsections we discuss the main phenomena related to a wave flume pseudo-regular wave field which may lead to errors when analysing them through the single LS procedure.

Filtering the signals passing only a narrow band centred at the principal component frequency ω , as proposed before, would not be a correct procedure. Therefore, being aware that some energy is carried back from the reflecting obstacle by the non-harmonic component (2ω), we have processed signals which have the form of (A.3). This procedure is a source of errors due to the presence of bounded harmonics which travels at the same carrier celerity.

A.1.2 COMBINED APPROACH

We performed Monte-Carlo (MC) simulations based on (A.3), considering the following 6 parameters: a , ρ_1 , ϕ_{i1} , ϕ_{r1} , φ_{i1} and φ_{r1} . An amount of energy is supposed to be carried back by the non-harmonic component, but this value is limited by fixing a coefficient β such that ρ_1 is a uniformly distributed random variable in the interval:

$$\rho_1 \in [(1 - \beta)\rho; \rho] \in \mathbb{R} \quad (\text{A.6})$$

being ρ the total reflection coefficient. For the free component, ρ_2 is a function of ρ and ρ_1 , satisfying the following condition:

$$\rho^2 = \frac{\rho_1^2 (a^2 + a_2^2) + \rho_2^2 a_{2F}^2}{a^2 + a_2^2 + a_{2F}^2} \quad (\text{A.7})$$

Second order amplitudes are known on the basis of Stokes-like solutions, provided that a is fixed. The latter is a uniformly distributed random variable in the interval $[a_{min}; a_{max}]$ which is defined for each case on the basis of the sampled time-series. We report in Fig.A.1 a typical distribution of the MC output.

Results of this procedure are used to estimate errors and uncertainties of the LS detected values in processing laboratory data.

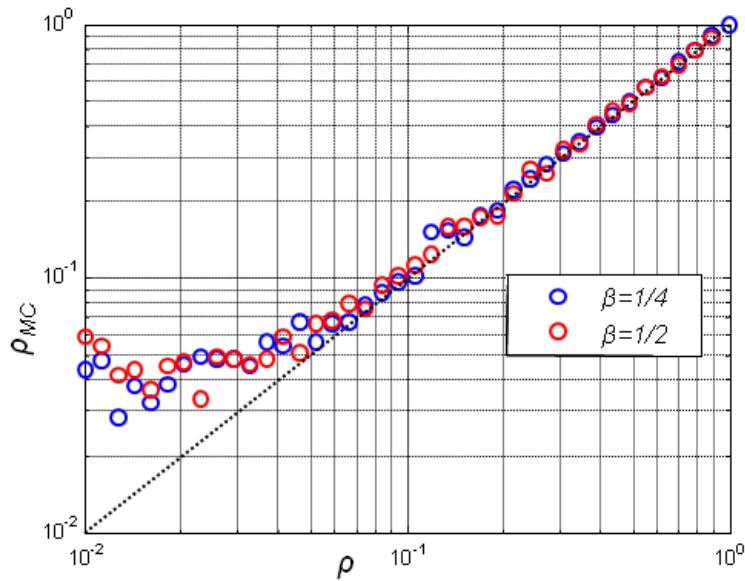


Fig. A.1 – Expected LS values for reflection coefficient ρ_{MC} based on MC simulations with time-series of the kind Eq.(7). Fundamental frequency is $f = 1$ Hz. β accounts for ρ_2 magnitude providing that $\rho = m_r/m_i$.

The evaluation of ρ and τ will be done, for each test, in the following way. We process first gauges array samples, obtaining an initial value for the reflection coefficient:

$$DATA\{1 : 4\} \xrightarrow{IN} LS1 \xrightarrow{OUT} \rho_{LS1} \quad (A.8)$$

With this estimation we enter a curve of the kind depicted in Fig.A.1, *i.e.* we perform a series of MC simulations, looking for the best match between ρ_{MC} and ρ_{LS1} , obtaining the most probable true value of ρ and the associated distributions of the incident and reflected spectral moments:

$$\rho_{LS1} \xrightarrow{IN} MC \xrightarrow{OUT} \left\{ \rho, \sigma^2(\rho), m_i, m_r \right\} \quad (A.9)$$

Afterwards we do the same with respect to the second gauges array:

$$DATA\{5 : 8\} \xrightarrow{IN} LS2 \xrightarrow{OUT} \rho_{LS2} \quad (A.10)$$

In this case we are interested in storing the distribution of the incident 0 – th spectral moment only:

$$\rho_{LS1} \xrightarrow{IN} MC \xrightarrow{OUT} \bar{m}_i \quad (\text{A.11})$$

We can then compute the transmission coefficient:

$$\tau^2 = \frac{E(\bar{m}_i)}{E(m_i)} \quad (\text{A.12})$$

where $E(X)$ stands for the expected value of variable X . Its variance can be estimated as:

$$\sigma^2(\tau^2) = \tau^4 \left[\frac{\sigma^2(\bar{m}_i)}{\bar{m}_i^2} + \frac{\sigma^2(m_i)}{m_i^2} - 2 \frac{E(m_i \bar{m}_i)}{m_i \bar{m}_i} + 2 \right] \quad (\text{A.13})$$

The covariance associated to transmission and reflection coefficients is:

$$cov(\rho^2, \tau^2) = 2 \left[E\left(\frac{\bar{m}_i m_r}{m_i^2}\right) - E\left(\frac{\bar{m}_i}{m_i}\right) E\left(\frac{m_r}{m_i}\right) \right] \quad (\text{A.14})$$

Finally, the uncertainty on the dissipation coefficient is evaluated with (A.2).

REFERENCES

- Abdolali, A., Franco, L., Bellotti, G., Kolahdoozan, M., 2012. Hydraulic and numerical modeling of the performance of π -type floating breakwaters. In: The 10th International Conference on Coasts, Ports and Marine Structures.
- Ajiwibowo, H., Yuanita, N., November 2009. Transmission coefficient on pontoon for damping the short waves. In: Proc. Int. Conf. on Sustainable Infrastructure and Built Environment in Developing Countries. Bandung, West Java, Indonesia.
- Atzeni, A., Balzano, A., Montaldo, N., 1998. Frangiflutti galleggiante zavorrato con acqua sottoposto a moto ondoso irregolare. In: Atti del XXVI Convegno di Idraulica e Costruzioni Idrauliche. pp. 181–192.
- Ayenu-Prah, A., Attoh-Okine, N., 2010. A criterion for selecting relevant intrinsic modes functions in empirical mode decomposition. *Adv. Adapt. Data Anal.* 2 (01), 1–24.
- Azzellino, A., Contestabile, P., Ferrante, V., Lanfredi, C., Vicinanza, D., 2011. Strategic environmental assessment to evaluate wec projects in the perspective of the environmental cost-benefit analysis. In: Proceedings of the International Offshore and Polar Engineering Conference. pp. 709–715.
- Bakkenes, H. J., 2002. Observation and separation of bound and free low-frequency waves in the nearshore zone. Master's thesis, Delft University of Technology.
- Bedrosian, E., 1963. A product theorem for hilbert transforms. *Proceedings of the IEEE* 51 (5), 868–869.
URL http://www.rand.org/pubs/research_memoranda/2008/RM3439.pdf

- Beels, C., Troch, P., Backer, G. D., Vantorre, M., Rouck, J. D., 2010. Numerical implementation and sensitivity analysis of a wave energy converter in a time-dependent mild-slope equation model. *Coastal Engineering* 57 (5), 471–492.
- URL <http://www.sciencedirect.com/science/article/pii/S0378383909001823>
- Blumberg, G., Cox, R., 1988. Floating breakwater physical model testing for marina applications. *Bulletin 63, PIANC - AIPCN*.
- Booij, N., Ris, R. C., Holthuijsen, L. H., 1999. A third-generation wave model for coastal regions: 1. model description and validation. *Journal of Geophysical Research* 104, 7649–7666.
- Burcharth, H. F., Andersen, T. L., Zanuttigh, B., Nørgaard, J. H., Ruol, P., Martinelli, L., Angelelli, E., Mendoza-Baldwin, E., Silva-Casarín, R., Enriquez-Ortiz, C., Koftis, T., Prinos, P., Galiatsatou, P., Chávez-Cárdenas, X., Hoil-Baeza, J., Bustos-Lira, A., Pinedo-González, J., Kuznetsov, S., Saprykina, Y., Lara, J. L., Steendam, G. J., Pezzutto, P., Sergent, P., Prevot, G., 2012a. Theseus deliverable id2. 5: Report on physical tests on innovative coastal structures, final version. *Tech. rep., European Commission*.
- Burcharth, H. F., Zanuttigh, B., Nørgaard, J. H., Andersen, T. L., Raosa, A. N., Higuera, P., Maza, M., Barajas, G., Lara, J. L., Prinos, P., Tsakiri, M., Ruol, P., Martinelli, L., Pezzutto, P., Koftis, T., Kuznetsov, S., Saprykina, Y., Bevilacqua, G., Sergent, P., Prevot, G., Kergadallan, X., Ostrowski, R., Pruszek, Z., Szmytkiewicz, M., Galiatsatou, P., 2012b. Theseus deliverable id2. 4: Report on numerical modelling tests on innovative coastal structures, preliminary version. *Tech. rep., European Commission*.
- Chakrabarti, S. K., 1987. *Hydrodynamics of off-shore structures*. WIT Press.
- Cox, R., Coghlan, I., Kerry, C., 2007. Floating breakwater performance in irregular waves with particular emphasis on wave transmission and reflection, energy dissipation, motion and restraining forces. In: *International Conference on Coastal Structures*. Vol. 1. pp. 351–362.

- Dätig, M., Schlurmann, T., 2004. Performance and limitations of the hilbert-huang transformation (hht) with an application to irregular water waves. *Ocean Engineering* 31 (14-15), 1783–1834.
- Deng, Y., Wang, W., Qian, C., Wang, Z., Dai, D., 2001. Boundary-processing-technique in emd method and hilbert transform. *Chinese Science Bulletin* 46, 954–960.
URL <http://dx.doi.org/10.1007/BF02900475>
- Dong, G., Zheng, Y., Li, Y., Teng, B., Guan, C., Lin, D., 2008. Experiments on wave transmission coefficients of floating breakwaters. *Ocean Engineering* 35 (8Ú9), 931 – 938.
URL <http://www.sciencedirect.com/science/article/pii/S0029801808000140>
- Fousert, M. W., 2006. Floating breakwater: Theoretical study of a dynamic wave attenuating system. Master's thesis.
URL <http://repository.tudelft.nl/assets/uuid:87d7e889-8aaf-410b-9502-495412c59308/2007Foustert.pdf>
- Frigaard, P., Brorsen, M., 1995. A time-domain method for separating incident and reflected irregular waves. *Coastal Engineering* 24, 205–215.
- Frigaard, P., Christensen, M., 1995. An absorbing wave-maker based on digital filters. In: *International Conference on Coastal Engineering*. Vol. 1. ASCE, pp. 168–168.
URL <http://journals.tdl.org/ICCE/article/viewFile/4954/4634>
- Fugazza, M., Natale, L., 1988. Energy losses and floating breakwater response. *Journal of Waterway, Port, Coastal and Ocean Engineering* 114 (2), 191–205.
- Gesraha, M., 2006. Analysis of π shaped floating breakwater in oblique waves: I. impervious rigid wave boards. *Applied Ocean Research* 28 (5), 327–338.
- Goda, Y., Suzuki, Y., 1976. Estimation of incident and reflected waves in random wave experiments. In: *Proceedings of 15th International Conference on Coastal Engineering*. Vol. 1. Hawaii, pp. 828–845.
URL <http://journals.tdl.org/ICCE/article/view/3096/2761>

- Grønbech, J., Jensen, T., Andersen, H., 1996. Reflection analysis with separation of cross modes. In: Proceedings of 25th Conference on Coastal Engineering. pp. 968–980.
URL <http://journals.tdl.org/ICCE/article/view/5280/4958>
- Hayes, W. D., December 1970. Conservation of action and modal wave action. Proceedings of the Royal Society of London. Series A, Mathematical and Physical Sciences 320 (1541), 187–208.
URL <http://www.jstor.org/stable/77799>
- He, F., Huang, Z., Law, A. W.-K., 2012. Hydrodynamic performance of a rectangular floating breakwater with and without pneumatic chambers: An experimental study. Ocean Engineering 51 (0), 16–27.
URL <http://www.sciencedirect.com/science/article/pii/S0029801812001692>
- Headland, J. R., 1995. Marine Structures Engineering: specialised applications. International Thomson Publishing Inc., Ch. Floating breakwaters, pp. 367 – 411.
- Huang, N., Shen, S. S. P., 2005. Hilbert-Huang Transform and Its Applications. World Scientific.
- Huang, N., Shen, Z., Long, S., 1999. A new view of nonlinear water waves: The hilbert spectrum 1. Annual Review of Fluid Mechanics 31 (1), 417–457.
- Huang, N., Shen, Z., Long, S., Wu, M., Shih, H., Zheng, Q., Yen, N., Tung, C., Liu, H., 1998. The empirical mode decomposition and the hilbert spectrum for nonlinear and non-stationary time series analysis. Proceedings of the Royal Society of London. Series A: Mathematical, Physical and Engineering Sciences 454 (1971), 903–995.
- Huang, N., Wu, Z., Long, S., Arnold, K., Chen, X., Blank, K., 2009. On instantaneous frequency. Adv. Adapt. Data Anal 1 (2), 177–229.
- Jung, K. H., Chang, K. A., Huang, E., 2004. Two-dimensional flow characteristics of wave interactions with a fixed rectangular structure. Ocean Engineering 31, 975–998.

- Jung, K. H., Chang, K. A., Huang, E., 2005. Two-dimensional flow characteristics of wave interactions with a free-rolling rectangular structure. *Ocean Engineering* 32, 1–20.
- King, F., 2009a. Hilbert transforms, Volume 1. Vol. 124 of *Encyclopedia of Mathematics and its Applications*. Cambridge University Press.
- King, F., 2009b. Hilbert transforms, Volume 2. Vol. 125 of *Encyclopedia of Mathematics and its Applications*. Cambridge University Press.
- Kitano, T., Mase, H., Kioka, W., 2002. Time domain decomposition of incident and reflected waves. In: *International Conference on Coastal Engineering*. ASCE, pp. 1697–1708.
- Koftis, T., Prinos, P., 2011. Floating breakwaters: Parametric analysis and functional design. In: *Proc. 5th Pan-Hellenic Conference for Coastal Zone Management and Improvement NTUA*. Long abstract in English.
- Koftis, T., Prinos, P., Koutandos, E., 2006. 2d-v hydrodynamics of wave-floating breakwater interaction. *Journal of Hydraulic Research* 44 (4), 451–469.
URL <http://www.tandfonline.com/doi/abs/10.1080/00221686.2006.9521697>
- Koutandos, E., Prinos, P., Gironella, X., 2005. Floating breakwaters under regular and irregular wave forcing: reflection and transmission characteristics. *Journal of Hydraulic Research* 43 (2), 174–188.
URL <http://www.tandfonline.com/doi/abs/10.1080/00221686.2005.9641234>
- Lin, C., Huang, C., 2004. Decomposition of incident and reflected higher harmonic waves using four wave gauges. *Coastal engineering* 51 (5), 395–406.
- Longuet-Higgins, M., 1987. The propagation of short surface waves on longer gravity waves. *Journal of Fluid Mechanics* 177, 293–306.
- Longuet-Higgins, M., Stewart, R., 1960. Changes in the form of short gravity waves on long waves and tidal currents. *Journal of Fluid Mechanics* 8 (04), 565–583.

- Mansard, E. P. D., Funke, E., 1980. The measurement of incident and reflected spectra using a least squares method. In: ASCE (Ed.), Proceedings of 17th International Conference on Coastal Engineering. Vol. 1. New York, pp. 154–172.
URL <http://journals.tdl.org/ICCE/article/viewFile/3432/3112>
- Martinelli, L., Pezzutto, P., Ruol, P., 2012. Formula sperimentale per la stima dell'efficienza di frangiflutti galleggianti di tipo π . In: Atti XXXIII Convegno Nazionale di Idraulica e Costruzioni Idrauliche.
- Martinelli, L., Ruol, P., Zanuttigh, B., 2008. Wave basin experiments on floating breakwaters with different layouts. Applied Ocean Research 30 (3), 199–207.
- Mays, T. W., 1997. Three-dimensional analysis of moored cylinders used as breakwaters. Master's thesis.
- McCartney, B., 1985. Floating breakwater design. Journal of Waterway, Port, Coastal and Ocean Engineering 111, 304 – 318.
- Medina, J. R., 2001. Estimation of incident and reflected waves using simulated annealing. Journal of Waterway, Port, Coastal, and Ocean Engineering 127, 213–221.
URL [http://ascelibrary.org/doi/pdf/10.1061/\(ASCE\)0733-950X\(2001\)127%3A4\(213\)](http://ascelibrary.org/doi/pdf/10.1061/(ASCE)0733-950X(2001)127%3A4(213))
- Melville, W., 1983. Wave modulation and breakdown. Journal of Fluid Mechanics 128 (03), 489–506.
- Nece, R. E., Richey, E. P., 1972. Wave transmission tests of floating breakwater for oak harbour. Water Resources Series Tech. Report 32, Dep. of Civil and Env. Eng. - Univ. of Washington.
- Neelamani, S., Rajendran, R., 2002a. Wave interaction with \perp -type breakwaters. Ocean Engineering 29 (5), 561 – 589.
URL <http://www.sciencedirect.com/science/article/pii/S0029801801000300>

- Neelamani, S., Rajendran, R., 2002b. Wave interaction with t-type breakwaters. *Ocean Engineering* 29 (2), 151–175.
URL <http://www.sciencedirect.com/science/article/pii/S0029801800000603>
- Newman, J. N., 1977. *Marine hydrodynamics*. MIT Press.
- Nørgaard, J. H., Andersen, T. L., 2012. Investigation of wave transmission from a floating wave dragon wave energy converter. In: *Twenty-second (2012) International Offshore and Polar Engineering Conference*.
- Nuttall, A. H., oct. 1966. On the quadrature approximation to the hilbert transform of modulated signals. *Proceedings of the IEEE* 54 (10), 1458 – 1459.
URL <http://ieeexplore.ieee.org/stamp/stamp.jsp?tp=&arnumber=1447068>
- Pezzutto, P., 2012. Nuovi strumenti per il laboratorio marittimo del dip. icea. Internal tech. report, ICEA Department - University of Padova, in preparation.
- Pezzutto, P., Ruol, P., Martinelli, L., 2012. A parametric analysis of dissipation capacity for Π -type floating breakwaters. In: *The Proceedings of the 22nd (2012) International Offshore and Polar Engineering Conference*. pp. 1294–1300.
- Phillips, O., 1981. Dispersion of short wavelets in the presence of a dominant long wave. *Journal of Fluid Mechanics* 107, 465–485.
- Prislin, I., Zhang, J., Seymour, R. J., 1997. Deterministic decomposition of deep water short-crested irregular gravity waves. *Journal of Geophysical Research* 102, 667 – 688.
URL <http://www.agu.org/journals/jc/v102/iC06/97JC00791/97JC00791.pdf>
- Qingjie, Z., Huayong, Z., Lincheng, S., 2010. A new method for mitigation of end effect in empirical mode decomposition. In: *Informatics in Control*,

- Automation and Robotics (CAR), 2010 2nd International Asia Conference on. Vol. 1. IEEE, pp. 400–403.
- Rahman, M. A., Mizutani, N., Kawasaki, K., 2006. Numerical modeling of dynamic responses and mooring forces of submerged floating breakwater. *Coastal Engineering* 53 (10), 799 – 815.
URL <http://www.sciencedirect.com/science/article/pii/S0378383906000639>
- Reilly, A., Frazer, G., Boashash, B., nov 1994. Analytic signal generation-tips and traps. *Signal Processing, IEEE Transactions on* 42 (11), 3241–3245.
- Ruol, P., 1984. Floating breakwaters in small basins. In: *Int. Symp. on Maritime Structures in the Mediterranean Sea*.
- Ruol, P., Martinelli, L., 2007. Wave flume investigation on different mooring systems for floating breakwaters. In: *International Conference on Coastal Structures*. No. 1. pp. 327–338.
- Ruol, P., Martinelli, L., Pezzutto, P., June 2011. Multi-chamber owc devices to reduce and convert wave energy in harbour entrance and inner channels. In: *The Proceedings of the 21st (2011) International Offshore and Polar Engineering Conference*. pp. –.
- Ruol, P., Martinelli, L., Pezzutto, P., 2012a. Experimental and numerical investigation of the effect of mooring stiffness on the behaviour of p-type floating breakwaters. In: *The Proceedings of the 22nd (2012) International Offshore and Polar Engineering Conference*. pp. 1301–1308.
- Ruol, P., Martinelli, L., Pezzutto, P., 2012b. Limits of the new transmission formula for π -type floating breakwaters. In: *International Conference on Coastal Engineering*.
- Ruol, P., Martinelli, L., Pezzutto, P., 2013. A formula to predict transmission for p-type floating breakwaters. *JOURNAL OF WATERWAY PORT COASTAL AND OCEAN ENGINEERING-ASCE* 139 (1), 1–8.

- Ruol, P., Pezzutto, P., Martinelli, L., 2010a. Analisi sperimentale sulla risposta 2d di molteplici frangiflutti galleggianti. In: Atti del XXXII convegno nazionale di idraulica e costruzioni idrauliche.
- Ruol, P., Zanuttigh, B., Martinelli, L., Kofoed, J. P., , Frigaard, P., 2010b. Near-shore floating wave energy converters: Applications for coastal protection. In: 32nd International Conference on Coastal Engineering.
URL http://vbn.aau.dk/files/47412328/Near_Shore_Floating_Wave_Energy_Converters.pdf
- Sanchez, M., Chevalier, C., 2006. A linear method to evaluate energy fluxes in a wave flume. *Journal of Hydraulic Research* 44 (1), 107–114.
- Sannasiraj, S., Sundar, V., Sundaravadivelu, R., 1998. Mooring forces and motion responses of pontoon-type floating breakwaters. *Ocean Engineering* 25 (1), 27–48.
URL <http://www.sciencedirect.com/science/article/pii/S0029801896000443>
- Sarpkaya, T., Isaacson, M., 1981. *Mechanics of wave forces on off-shore structures*. Van Nostrand-Reinhold.
- Schäffer, H., Steenberg, C., 2003. Second-order wavemaker theory for multidirectional waves. *Ocean Engineering* 30 (10), 1203–1231.
URL <http://www.sciencedirect.com/science/article/pii/S0029801802001002>
- Senjanovič, I., Šime Malenica, Tomašević, S., 2008. Investigation of ship hydroelasticity. *Ocean Engineering* 35 (5–6), 523 – 535.
URL <http://www.sciencedirect.com/science/article/pii/S0029801807002545>
- Sharma, J., Dean, R., February 1981. Second-order directional seas and associated wave forces. *SPE Journal* 21 (1), 129–140.
- Smith, H. C., Pearce, C., Millar, D. L., 2012. Further analysis of change in nearshore wave climate due to an offshore wave farm: An enhanced case study for the wave hub site. *Renewable Energy* 40 (1), 51–64.

- URL <http://www.sciencedirect.com/science/article/pii/S0960148111005210>
- Sumer, B. M., Fredsøe, J., 1997. Hydrodynamics around cylindrical structures. In: *Advanced Series on Ocean Engineering*. Vol. 12. World Scientific.
- Tang, B., Dong, S., Song, T., 2012. Method for eliminating mode mixing of empirical mode decomposition based on the revised blind source separation. *Signal Processing* 92 (1), 248 – 258.
- URL <http://www.sciencedirect.com/science/article/pii/S0165168411002477>
- Torres, M., Colominas, M., Schlotthauer, G., Flandrin, P., may 2011. A complete ensemble empirical mode decomposition with adaptive noise. In: *Acoustics, Speech and Signal Processing (ICASSP), 2011 IEEE International Conference on*. pp. 4144 –4147.
- Tsinker, G. P., 1994. *Marine structure engineering: specialized application*. International Thomson Publishing Inc.
- Uzaki, K., Ikehata, Y., Matsunaga, N., 2011. Performance of the wave energy dissipation of a floating breakwater with truss structures and the quantification of transmission coefficients. *Journal of Coastal Research* 27 (4), 687–697.
- Wang, W., 2005. *The Hilbert-Huang Transform in Engineering*. Taylor & Francis Group. London: CRC Press, Ch. 12: Decomposition of Wave Groups with EMD Method, pp. 267–280.
- Williams, K. J., 1988. An experimental study of wave-obstacle interaction in a two-dimensional domain. *Journal of Hydraulic Research* 26, 463–482.
- Wu, F., Qu, L., 2008. An improved method for restraining the end effect in empirical mode decomposition and its applications to the fault diagnosis of large rotating machinery. *Journal of Sound and Vibration* 314 (3), 586–602.
- Wu, S.-D., Chiou, J.-C., Goldman, E., aug. 2010. Solution for mode mixing phenomenon of the empirical mode decomposition. In: *Advanced Computer Theory and Engineering (ICACTE), 2010 3rd International Conference on*. Vol. 2. pp. V2–500 –V2–504.

- Wu, Z., Huang, N., 2009. Ensemble empirical mode decomposition: A noise-assisted data analysis method. *Advances in Adaptive Data Analysis* 1 (1), 1–41.
- Zanuttigh, B., Martinelli, L., Castagnetti, M., Ruol, P., Kofoed, J. P., Frigaard, P., 2010. Integration of wave energy converters into coastal protection schemes. In: *3rd International Conference on Ocean Energy*.
URL http://www.image.unipd.it/p.ruol/pubblications/87_ZanuttighMCPKF_ICOE%202010_Bilbao.pdf
- Zelt, J., Skjelbreia, J., 1992. Estimating incident and reflected wave fields using an arbitrary number of wave gauges. In: ASCE (Ed.), *Proceedings of 23rd International Conference Coastal Engineering*. Vol. 1. New York, pp. 777–789.
URL <http://journals.tdl.org/ICCE/article/view/4736/4417>
- Zhang, J., Chen, L., Ye, M., Randall, R. E., 1996. Hybrid wave model for unidirectional irregular waves-part i. theory and numerical scheme. *Applied Ocean Research* 18, 77–92.
- Zhang, J., Melville, W., 1990. Evolution of weakly nonlinear short waves riding on long gravity waves. *Journal of Fluid Mechanics* 214 (1), 321–346.
URL <http://airsea.ucsd.edu/papers/ZHANG%20J,%20MELVILLE%20WK%20-%20JOURNAL%20OF%20FLUID%20MECHANICS%20214%20-%201990.pdf>
- Zhang, J., Yang, J., Wen, J., Prislun, I., Hong, K., 1999. Deterministic wave model for short-crested ocean waves: Part i. theory and numerical scheme. *Applied Ocean Research* 21, 167–188.
- Zhidong, Z., Yang, W., July 2007. A new method for processing end effect in empirical mode decomposition. In: *Communications, Circuits and Systems, 2007. ICCAS 2007. International Conference on*. pp. 841–845.
URL <http://ieeexplore.ieee.org/stamp/stamp.jsp?tp=&arnumber=4348181>
- Zhidong, Z., Yi, L., Qing, L., 2011. Adaptive Filtering Applications. InTech, Ch. 5: Adaptive Noise Removal of ECG Signal Based On Ensemble Empirical

Mode Decomposition, pp. 123–140.

URL <http://cdn.intechweb.org/pdfs/16116.pdf>